NASA Technical Paper 2681

May 1987

Experimental Evaluation of Turning Vane Designs for High-Speed and Coupled Fan-Drive Corners of 0.1-Scale Model of NASA Lewis Research Center's Proposed Altitude Wind Tunnel

Thomas F. Gelder,
Royce D. Moore,
Rickey J. Shyne,
and Donald R. Boldman

NASA

NASA Technical Paper 2681

1987

Experimental Evaluation of Turning Vane Designs for High-Speed and Coupled Fan-Drive Corners of 0.1-Scale Model of NASA Lewis Research Center's Proposed Altitude Wind Tunnel

Thomas F. Gelder,
Royce D. Moore,
Rickey J. Shyne,
and Donald R. Boldman

Lewis Research Center
Cleveland, Ohio

National Aeronautics and Space Administration

Scientific and Technical Information Branch

Summary

Two turning vane designs were experimentally evaluated for the fan-drive corner (corner 2) coupled to an upstream diffuser and the high-speed corner (corner 1) of the 0.1-scale model of NASA Lewis's proposed Altitude Wind Tunnel. For corner 2 both a controlled-diffusion vane design (vane A4) and a circular-arc vane design (vane B) were studied. Corner 2 also contained a simulated shaft fairing for the fan-drive system. The corner 1 configuration was the best of several tested earlier as an isolated element. It consisted of a controlled-diffusion turning vane (vane A10) and a simulated scoop to remove exhaust from the tunnel test section. Both uniform and screen-induced distorted inflow to corner 1 were studied at inlet Mach numbers from about 0.18 to 0.46. Detailed static pressure patterns on the corner walls and on the turning vane surfaces are reported along with detailed total pressure profiles at the corner inlets and outlets.

Near design inlet conditions the corner 1 total pressure loss coefficient was about 0.16, the same value as when tested as an isolated element, as expected. The corner 2 loss coefficient was about 0.12 with either the controlled-diffusion or the circular-arc vane design. This loss was about 25 percent less than when corner 2 was tested alone instead of coupled to corner 1. The controlled-diffusion vane design (A4) has the advantage of 20 percent fewer vanes than the circular-arc vane design (B). Only 22 A4 vanes are required in contrast to 28 B vanes; however, the A4 vane shape is more complex. The effects of simulated inlet flow distortion on the overall losses for corner 1 or 2 were small with little difference due to vane design.

Introduction

It has been proposed that the inactive Altitude Wind Tunnel (AWT) at the NASA Lewis Research Center be rehabilitated to meet the aeropropulsion needs of the future. The proposed program would extend the capabilities of the tunnel to permit testing at Mach numbers up to 0.92. The tunnel would accommodate tests involving fuel-burning engines, adverse weather conditions, and acoustic evaluations. The tunnel internal components were removed when it was converted to altitude test chambers for space research in the late 1950's and early 1960's. Therefore the proposed AWT (fig. 1) would require all new internal components but retain the original tunnel shell. In addition to a new test section and heat exchanger, four new sets of turning vanes and a new two-stage fan-drive system would be required. The high-speed corner (corner 1, downstream of the test section) would have an engine exhaust removal scoop extending through the center of the turning vanes. The fan-drive corner (corner 2) would have a drive-shaft fairing extending through the center of its turning vanes. Corners 3 and 4 turning vanes would be clean (i.e., no other parts would pass through these corners). The tunnel components are described in detail in references 1 to 3.

Because of the magnitude of the proposed AWT rehabilitation, including the much higher than usual inlet Mach numbers required for corners 1 and 2, a modeling effort was undertaken to ensure the technical soundness of the new component designs. A 0.1 scale was chosen as the common size for the various components partly because it represented the upper limit of the NASA Lewis exhauster flow capabilities. After the individual components have been tested, various subassemblies could also be tested to evaluate the interactions of the various tunnel loop components.

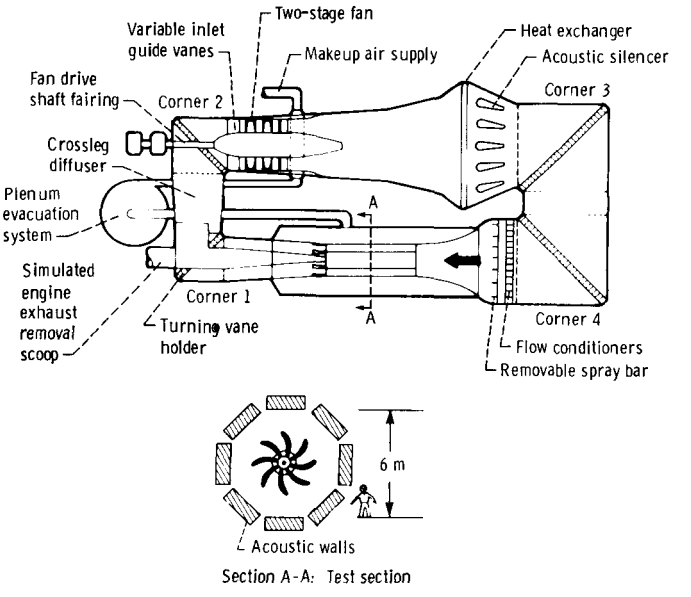

Mach number	0 to 0.9+
Altitude, m	0 to 17 000+
Total temperature, ^{o}C	-40 to 15
Test-section acoustic level, dB (OASPL)	120

Figure 1.—Capabilities of modified and rehabilitated AWT.

The results from the corner 1 turning vane studies are presented in references 4 and 5 and include configurations with and without the simulated exhaust removal scoop in place. Results from the corner 2 studies are given in reference 6. This configuration consisted of a crossleg diffuser, the corner turning vanes, the simulated fan drive-shaft fairing, and the fan variable inlet guide vanes (VIGV's). Except for corner 1 with the scoop, all the configurations were tested with two turning vane designs. The A vanes were controlled-diffusion-shaped airfoils; the B vanes were circular-arc-shaped airfoils. The B vane shapes and spacings were identical for both corners 1 and 2. The A vane shapes and spacings, although not identical for both corners because of different design inlet Mach numbers, were essentially the same (i.e., within typical machining tolerances).

To determine the interaction effects, if any, corner 1 with its simulated scoop was connected to the crossleg diffuser and the corner 2 configuration. This report presents and discusses the results obtained with this combination of corners. The discussion includes comparisons with the isolated-corner results previously published (refs. 4 to 6). Also, both uniform inlet flow and distorted inlet flow (generated by screens) were considered.

Because the results from the corner 1 studies (ref. 4) indicated that vanes A10 (controlled-diffusion airfoils reset $-5°$ from design) gave the lowest loss, that vane set was the only one used for corner 1 in the present investigation. Both a controlled-diffusion airfoil (vane A4) and the circular-arc airfoil (vane B) were used for corner 2 because corner 2 studies (ref. 6) did not favor a particular vane design.

Data were obtained at corner 1 inlet Mach numbers from about 0.18 to 0.46, which corresponded (approximately) to tunnel test-section Mach numbers from about 0.3 to 0.92. Total pressure distributions at the corner 1 inlet, the diffuser exit, downstream of the corner 2 vanes (VIGV inlet), and downstream of the VIGV's were obtained from rakes. Axial wall static pressure and vane surface pressure measurements were also obtained. All the pressure data are presented in tabular form for all configurations tested. Only the tables for overall performance are shown full size in this report; all others are available in microfiche supplement at the end of the report.

Apparatus and Procedure

Test Apparatus

In the combined corner 1–corner 2 test rig (figs. 2 and 3) room air entered a bellmouth and passed through a honeycomb flow straightener and two 1-diameter-long (D = 82.296 cm) spool pieces before reaching corner 1 with the simulated scoop. The air was then turned by the vanes and flowed through the crossleg diffuser to corner 2. After the corner 2 turn the air flowed through the inlet guide vanes and three spool pieces before exhausting through a choke-plate assembly to the central altitude exhauster system. The individual components were the same as those described in references 4 and 6, but they were combined in the manner shown in figure 3.

The choke-plate assembly was used for flow control. It consisted of a series of six removable plates plus one fixed plate arranged in the form of a converging nozzle. This

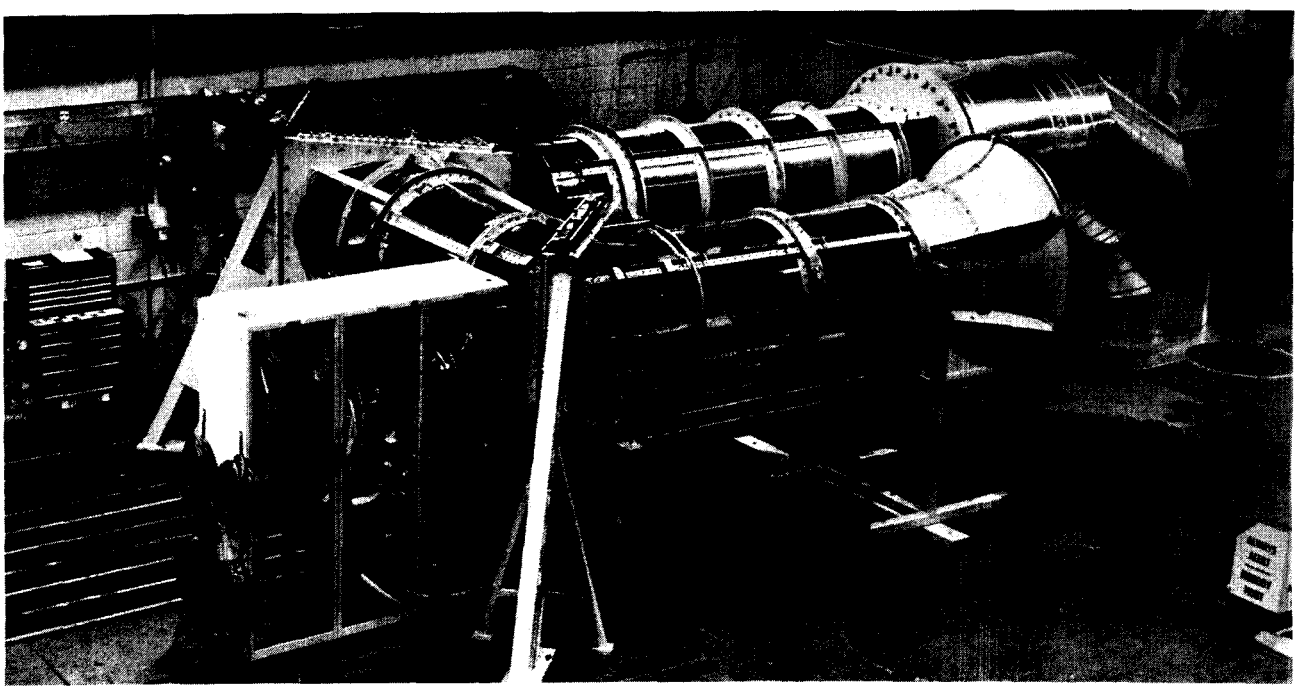

Figure 2.—Overall view of 0.1-scale corner 1–corner 2 test configuration.

Axial station	X/82.296	Axial station	Y/82.296	Axial station	Z/82.296
1	−2.04	34	0.075	54	−1.21
2	−1.84	35	.10	55	−1.10
3	−1.64	36	.14	56	−.98
4	−1.44	37	.18	57	−.86
5	−1.24	38	.22	58	−.75
6	−.95	39	.265	59	−.63
7	−.75	40	.31	60	−.52
8	−.55	41	.43	61	−.40
9	−.35	42	.55	62	−.29
10	−.15	43	.65	63	−.26
12	0	44	.80	64	−.23
13	.05	45	.92	65	−.20
14	.15	46	1.05	66	−.17
15	.25	47	1.10	67	−.14
16	.35	48	1.33	68	−.10
17	.45	49	1.45	69	−.07
18	.55	50	1.56	70	−.04
19	.65	51	1.68	71	−.01
20	.75	52	1.79	72	.02
		53	2.37	73	.05
				74	.08
				75	.11
				76	.14
				77	.17
				78	.20
				79	.24

See table 6(a) for circumferential locations.

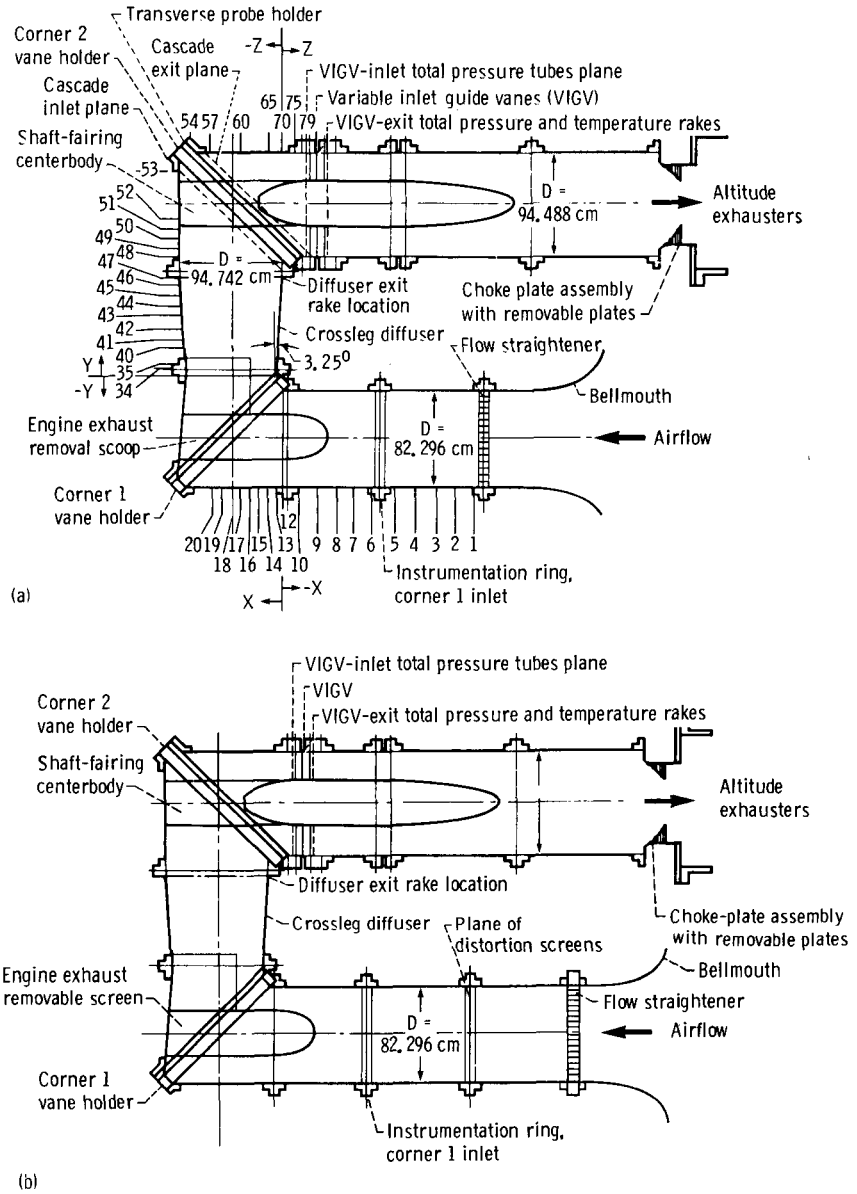

(a) With uniform inflow.
(b) With distorted inflow.

Figure 3.—Schematic of corner 1-corner 2 test apparatus.

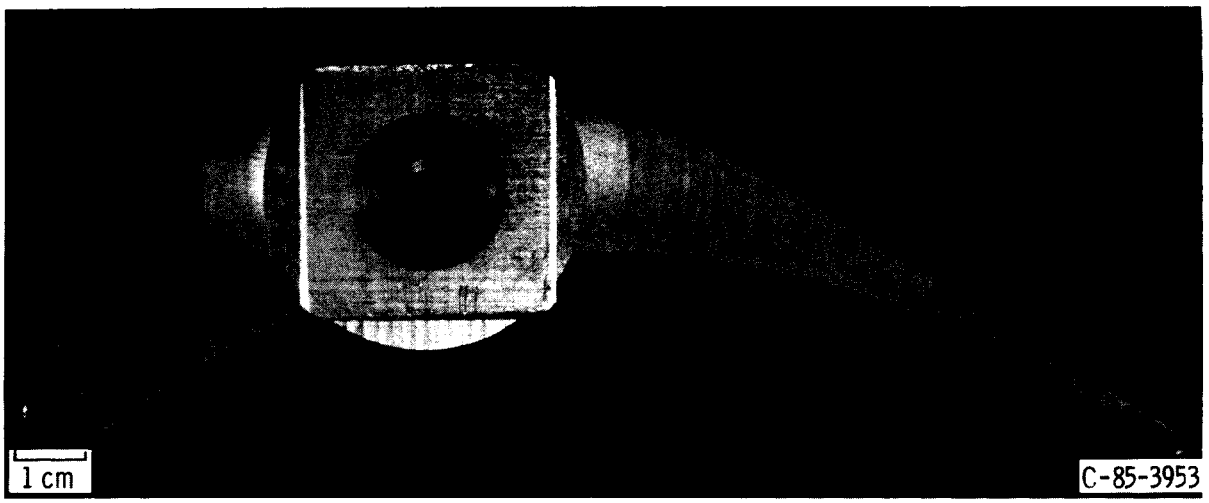

Figure 4.—End view of corner 1 vane A10.

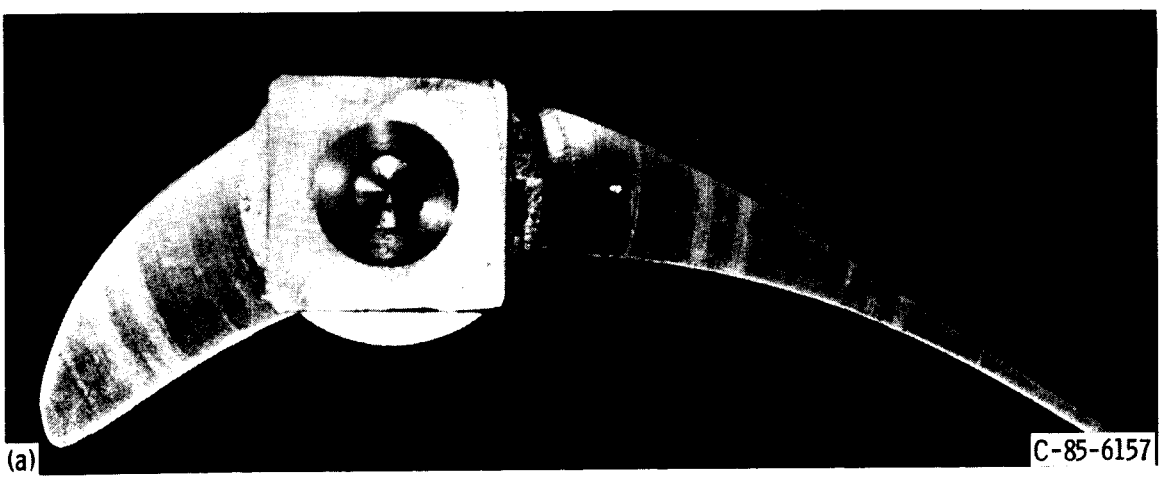

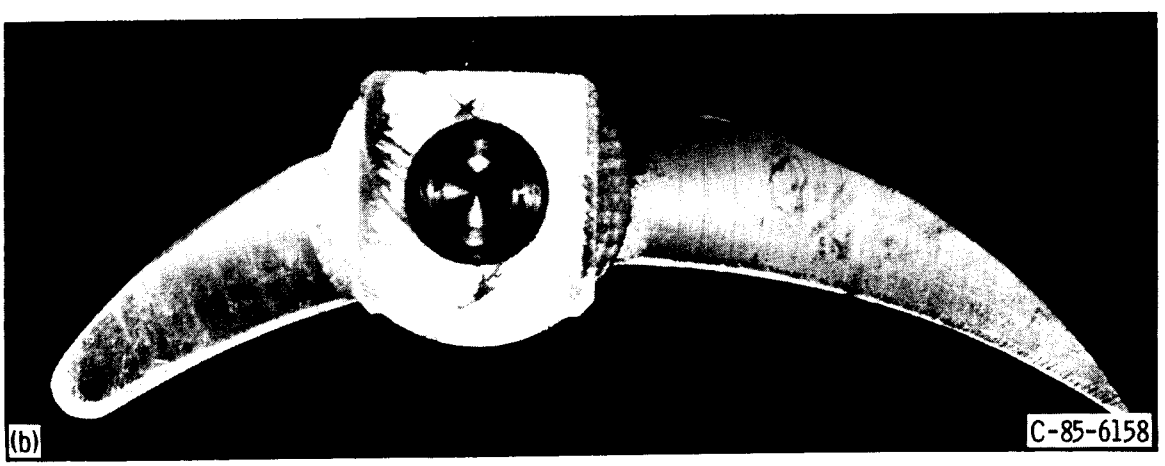

(a) Vane A4. (b) Vane B.

Figure 5.—End views of corner 2 vanes.

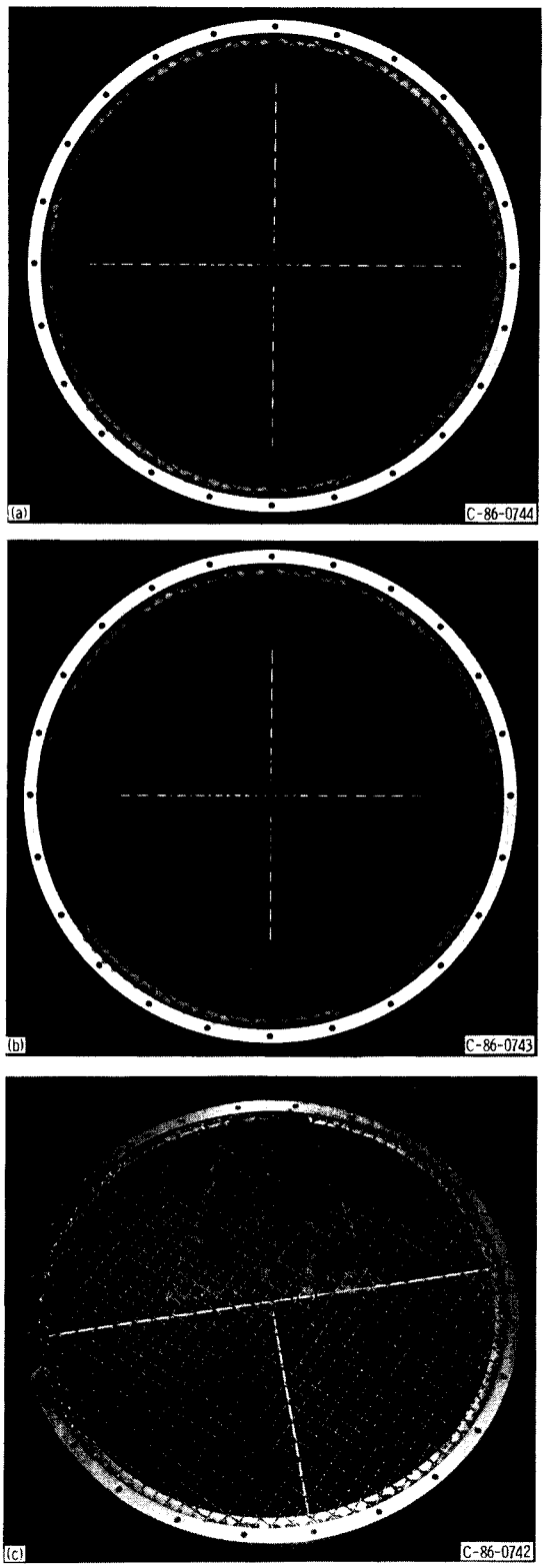

(a) 6.35-cm (~15-percent radius) tip radial distortion screen.
(b) 12.70-cm (~30-percent radius) tip radial distortion screen.
(c) Approximately 50° sector circumferential distortion screen.

Figure 6.—Inlet distortion screens mounted on backup screen and rods.

assembly of plates provided seven specific flow rates between about 35 and 82 kg/sec. The inlet flow straightener was an aluminum honeycomb with a hexagonal cell pattern (0.95 cm across flats by 7.08 cm long).

The turning vane designs are described in detail (including vane coordinates) in references 4 and 6. For the present study vane A10 (controlled-diffusion airfoil reset −5° from design) of figure 4 was used exclusively for corner 1. Two vane shapes (fig. 5) were used for corner 2: vane A4 (controlled-diffusion airfoil reset −5° from design with outside vane of cascade removed), and vane B (circular-arc airfoil).

To simulate distorted inflow patterns, screens were installed 2 diameters ahead of corner 1 (fig. 3(b)). Two tip radial profiles were tested. As illustrated in figures 6(a) and (b), one had a fine screen (12 mesh; 0.07-cm-diam wire) that extended 6.35 cm from the outer wall; the other had a fine screen that extended 12.70 cm. These fine screens were mounted on a coarse backup screen (1 mesh; 0.32-cm-diam wire). The circumferential distortion was generated from a fine-screen sector of about 50° (fig. 6(c)). This pattern was chosen to simulate the effect of the exhaust removal scoop pivoted to its highest expected angle of attack. The radial screen patterns were to simulate the effect of wall boundary layers from the high-speed diffuser between the test section and corner 1 (fig. 1).

Instrumentation

The airflow was determined from measurements on the choke-plate nozzle previously described. To determine the overall performance of corner 1 including the diffuser, diametrical rakes (fig. 7) were used upstream of corner 1 and at the diffuser exit (corner 2 inlet) as indicated in figure 3(a). These rakes could be moved to four positions around the circumference (45° spacing). The rakes contained 16 elements for total pressure measurement and 6 elements for total temperature measurement. Boundary layer rakes (fig. 8) were also installed at the same stations as the diametrical rakes. Outer wall static pressure taps were located at approximately the same axial planes as the rakes.

The overall performance of corner 2 was determined from the diffuser exit diametrical rakes and the total pressure probes mounted on the VIGV leading edge (fig. 9). Each of the 12 VIGV's had five total pressure probes. Downstream of the VIGV's in the flow region outside the guide vane wakes, four radial rakes were mounted (see one in fig. 9). These rakes could be moved to three other circumferential locations, which provided data every 30° of circumference. These VIGV exit rakes furnished additional detail on the total pressure patterns downstream of corner 2. For example (as indicated in table 3(a)), the exit rakes surveyed 12 more circumferential locations and 3 more spanwise locations than the inlet rakes.

Other wall static pressure taps were installed in the spool pieces, the diffuser, the shaft fairing, and the corner. The axial locations of these wall taps are given in figure 3 and their circumferential locations in table 6(a).

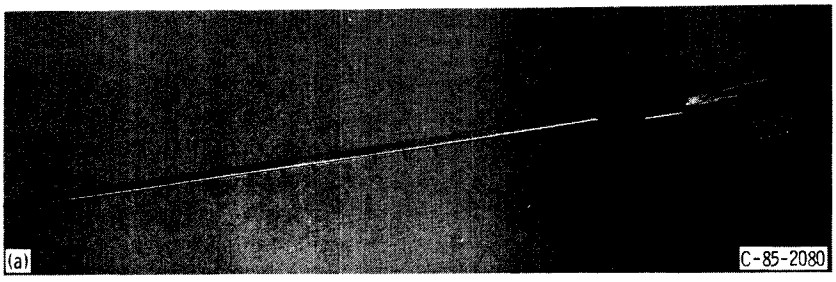

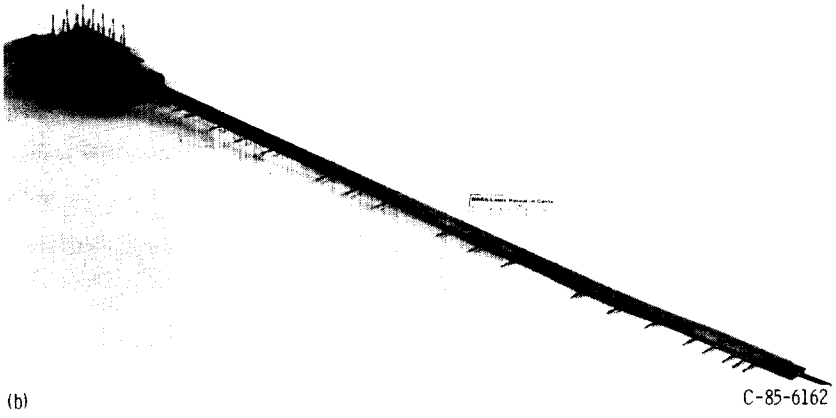

Element	Type (a)	Distance from outer wall to centerline, percent of span	Distance from outer wall, cm	
			Inlet	Exit
1	P	5.0	2.057	2.314
2	T	7.5	3.086	3.470
3	P	10.0	4.115	4.028
4	↓	15.0	6.172	6.139
5	↓	20.0	8.230	9.253
6	↓	30.0	12.344	13.881
7	T	40.0	16.459	18.506
8	P	50.0	20.574	23.134
9	P	70.0	28.804	32.388
10	T	80.0	32.918	37.013
11	P	90.0	37.033	41.641
12	P	90.0	45.263	50.891
13	T	80.0	49.378	55.519
14	P	70.0	53.492	60.144
15	P	50.0	61.722	69.395
16	T	40.0	65.837	74.026
17	P	30.0	69.952	78.651
18	↓	20.0	74.066	83.273
19	↓	15.0	76.124	85.593
20	↓	10.0	78.181	87.904
21	T	7.5	79.210	89.065
22	P	5.0	80.239	90.216

[a]P denotes pressure; T denotes temperature.

(a) Corner 1 inlet. (b) Diffuser exit.

Figure 7.—Diametrical rakes for measuring total pressure and temperature.

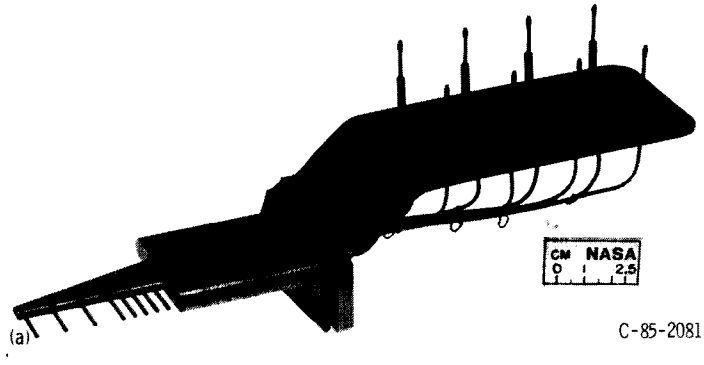

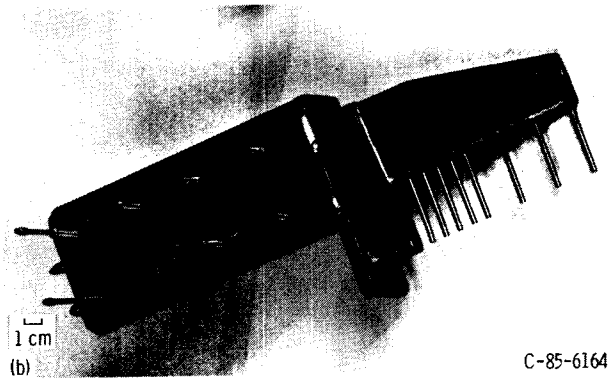

Element	Distance from outer wall to centerline, percent of span	Distance from outer wall, cm	
		Inlet	Exit
1	1.0	0.411	0.462
2	2.0	.823	.925
3	3.0	1.234	1.387
4	4.0	1.646	1.852
5	5.0	2.057	2.314
6	7.5	3.086	3.470
7	10.0	4.115	4.628
8	12.5	5.144	5.784

(a) Corner 1 inlet. (b) Diffuser exit.

Figure 8.—Boundary layer rakes for measuring total pressure.

Element	Distance from outer wall to inner wall, percent of span	Distance from outer wall, cm
1	10.0	3.785
2	30.0	8.966
3	50.0	14.148
4	70.0	19.329
5	90.0	24.511

(a)

Element	Type (a)	Distance from outer wall to inner wall, percent of span	Distance from from outer wall, cm
1	P	5.0	1.295
2	T	7.5	1.943
3	P	10.0	2.591
4	↓	15.0	3.886
5	↓	20.0	5.207
6	↓	30.0	7.772
7	T	40.0	10.363
8	P	50.0	12.954
9	P	70.0	18.136
10	T	80.0	20.726
11	P	90.0	23.317

[a]P denotes pressure and T denotes temperature.
(b)

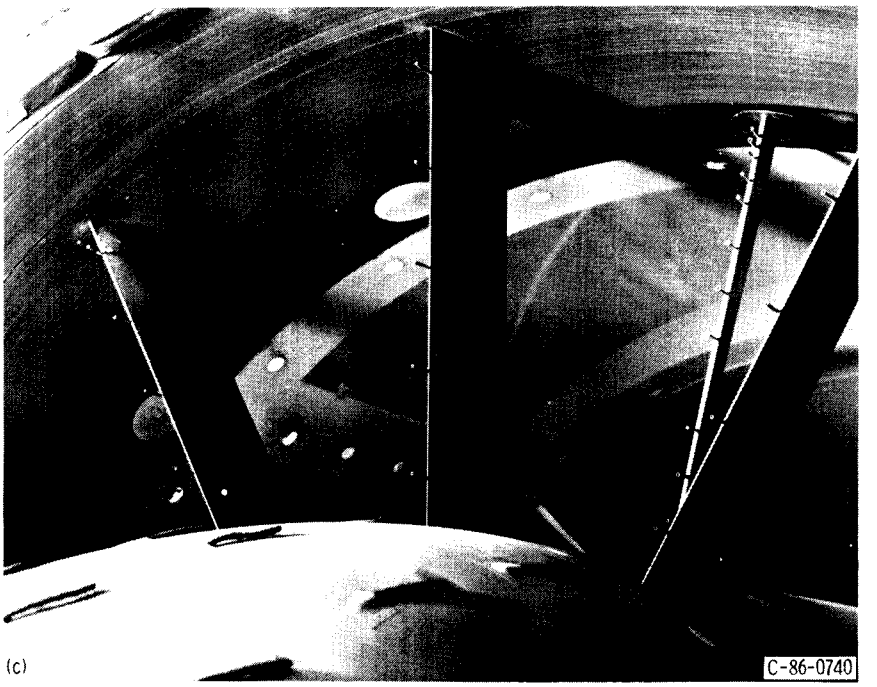

(a) VIGV inlet locations.
(b) VIGV exit locations.
(c) VIGV instrumentation.

Figure 9.—Instrumentation at inlet and exit of variable inlet guide vanes (VIGV's).

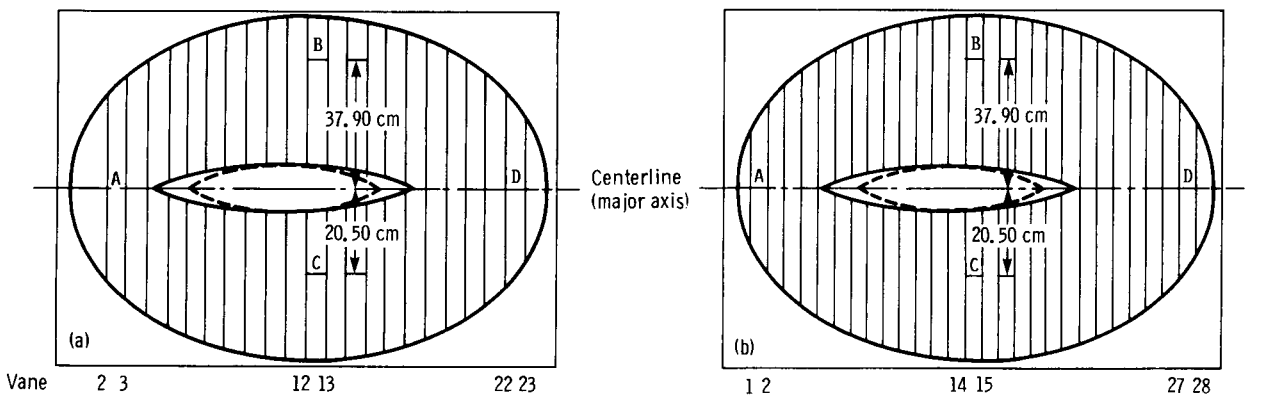

(a) Vane A4.
(b) Vane B.

Figure 10.—Location of vane surface static pressure taps (looking downstream).

Corner 2 vane performance was evaluated in part from surface static pressures obtained from taps on adjacent vanes in four passages (fig. 10). Two of the passages were along the major axis near the outside and inside corners (labeled locations A and D in fig. 10). The other two locations were in the central passage (B above the centerbody and C below).

To visually illustrate the flow conditions, tufts were taped to the walls and centerbodies.

All the rake total pressure and static pressure measurements were recorded on individual transducers that were calibrated just before each reading. The temperatures were determined from Chromel-constantan thermocouples by using a floating-point temperature reference.

Test Procedure

For a given vane configuration a particular choke-plate assembly was installed to set the desired airflow. The corner 1 inlet diametrical rake was positioned in the instrumentation ring (fig. 3) at either 0° or 225° (clockwise looking downstream). The inlet boundary layer rakes were positioned 90° from the large inlet rake. The diffuser exit (corner 2 inlet) diametrical rake was positioned at either 225° or 0° (opposite the upstream rake position). The outlet boundary layer rakes were also positioned 90° from the large diffuser exit rake. The four VIGV exit rakes were positioned 90° apart. Data were recorded with this particular rake arrangement. The facility was then shut down and all rakes except those at the VIGV exit were manually indexed 45°. The VIGV exit rakes were manually indexed 30°. The flow point was reestablished and data were then recorded at the next position. This procedure was repeated until data were recorded at the four diametrical and boundary layer rake positions and the three VIGV exit rake positions. The upstream and downstream rakes were rotated in opposite directions to minimize the effect of the upstream rake wake on the downstream pressure measurement. All the static pressures as well as the VIGV leading-edge total pressures were recorded at each rake position.

Calculation Procedure

The VIGV leading-edge total pressures and all static pressures recorded at the four rake positions were arithmetically averaged and corrected to standard-day conditions at the VIGV inlet plane to obtain the tabulated data presented in this report.

The total pressure measurements from the rakes were arranged for a given flow point to form the tabulated arrays of total pressure at a given circumferential location θ (in degrees from top dead center, clockwise looking downstream) and given percent of span (from the outer wall). Table 2(a) shows the typical array. The total pressures from the diametrical rakes were area averaged at each station to obtain the overall performance values presented in tables 1, 8, 15, and 22.

The airflow was calculated from Fliegner's formula (ref. 9) for a choked flow by using measured values of nozzle total pressure and total temperature. This calculated airflow agreed within 2 percent with the mass-averaged airflow calculated from several cases in which very detailed flow surveys were made. The velocity head (dynamic pressure) and the average corner inlet and exit Mach numbers were based on the calculated airflow. Total pressure, static pressure (including room pressure), total temperature, velocity head, and airflow were all corrected to standard-day conditions based on the VIGV inlet condition.

The symbols and equations used in the calculations are presented in appendixes A and B, respectively.

Results and Discussion

The effects of inlet Mach number (flow rate), vane design, inlet distortion, coupling of corners 1 and 2, and circumferential location on corner performance are evaluated in this section. Corner 1 used vane A10 and included the simulated exhaust scoop throughout this study unless otherwise noted. Corner 2 used either vane A4 (controlled-diffusion type) or vane B (circular-arc type) and included a simulated drive-shaft fairing. Most of this section concerns overall corner performance in terms of total pressure at various stations. Then the static pressure distributions on the ducting walls and fairings are examined. Finally vane surface pressure profiles are considered.

Presentation of Results

Tables. – All of the data from the corner 1–corner 2 studies are presented in tables. Absolute pressures are in newtons per square centimeter (corrected to standard-day conditions at the VIGV inlet) unless otherwise noted. The total array of data tables is as follows:

Content of table	Inflow			
	Uniform		Distorted	
	Vane configuration in corner 2			
	B	A4	B	A4
	Table numbers			
Overall performance for each flow rate	1	8	15	22
Distributions for each flow rate:[a]				
P_t across corner	2	9	16	23
P_t across VIGV	3	10	17	24
P_s at VIGV exit	4	11	18	25
P_s at vane inlet and exit	5	12	19	26
P_s throughout corner	6	13	20	27
P_s on vane surfaces	7	14	21	28

[a]These tables are presented as microfiche.

Plots. – To illustrate and thus clarify the effects of the many different variables involved in these studies, selected data from the tables were plotted. When total or static pressure was the dependent variable, it was made dimensionless for all plots by dividing by the pressure in the room (corrected to standard-day conditions at the VIGV inlet) from which the air was drawn into the bellmouth (fig. 2). These room, or reservoir, pressures are listed for all conditions in tables 1, 8, 15, and 22. Dimensionless ratios were used to avoid the possible unfamiliarity with the pressure units of newtons per square centimeter used in the tables. Pressures ratioed to room values also provide a numerical value the reader can relate to.

In the tables total pressures are listed as a function of percent of span from the tip (outer wall). In the plots, however, a uniform scale of percent of total flow area was selected as the independent variable (abscissa). This was done to reveal the effect of area weighting or area averaging on the pressures, which was to give more weight to regions near the outer wall than did radius or span averaging. It is area-averaged pressures that are required for determining the corner loss coefficient (defined in appendix B). For convenient reference, however, percent-of-span scales (nonuniformly spaced of course) are also indicated along the abscissa for the total pressure plots.

Corner Losses with Uniform Inflow

As expected the corner 2 vane design had no effect on the corner 1 losses (fig. 11). With the tunnel test-section Mach number at its design value of 0.8 the inlet Mach numbers to corners 1 and 2 were estimated to be nominally 0.4 and 0.26, respectively. Thus at design the corner 1 loss coefficient was about 0.16. Corner 1 loss coefficients increased from about 0.14 to 0.17 as the inlet Mach number increased from about 0.2 to 0.45.

At its design inlet Mach number corner 2, when operating downstream of corner 1 and the crossleg diffuser, had a loss coefficient with either vanes A4 or vanes B of about 0.12. Also, there was essentially no change in loss coefficient as the inlet Mach number was varied from about 0.1 to 0.3. When corner 2 was operating with a bellmouth instead of corner 1 upstream (results from ref. 6), the loss coefficient was about 0.165 irrespective of vane design or inlet Mach number. The reasons for lower corner 2 losses when operating downstream of corner 1 than when operating alone are explained immediately after the discussion of inlet distortion effects.

Inlet Distortion Effects

Two radial patterns and one circumferential pattern of inlet flow distortion were imposed on the corner 1–corner 2 configurations. These distortions were generated by screens as previously discussed (fig. 6). The resulting levels and patterns of inlet distortion for the design flow rate are shown by the total pressure contours in figure 12. The radial distortions (figs. 12(a) and (b)) were intended to cover the range of those expected from the boundary layer growth on the walls of the high-speed diffuser upstream of corner 1 (fig. 1). The local to room total pressure ratios ranged from about 0.90 to 0.96 near the outer wall for these radial inflow distortions. (The backing screen across the entire duct (fig. 6) limited the maximum pressure recovery to about 0.96.) The total pressure disturbances caused by the radial screens extended nearly twice

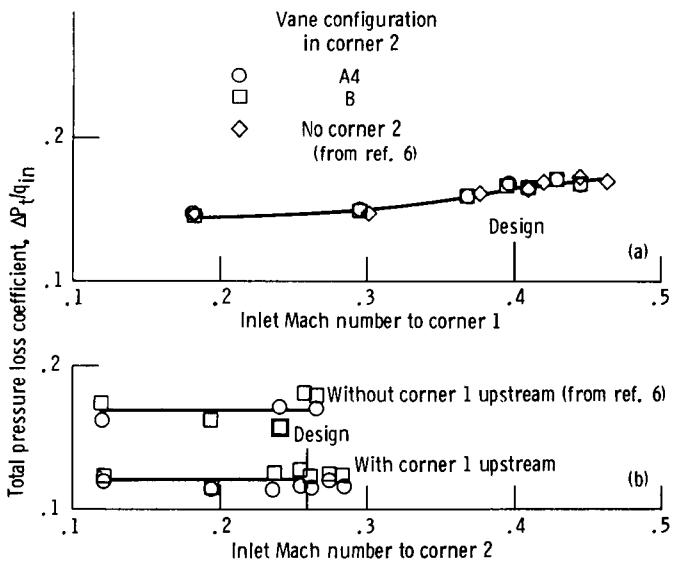

(a) Corner 1 with vanes A10, scoop, and diffuser.
(b) Corner 2.

Figure 11.—Comparison of corner loss coefficients.

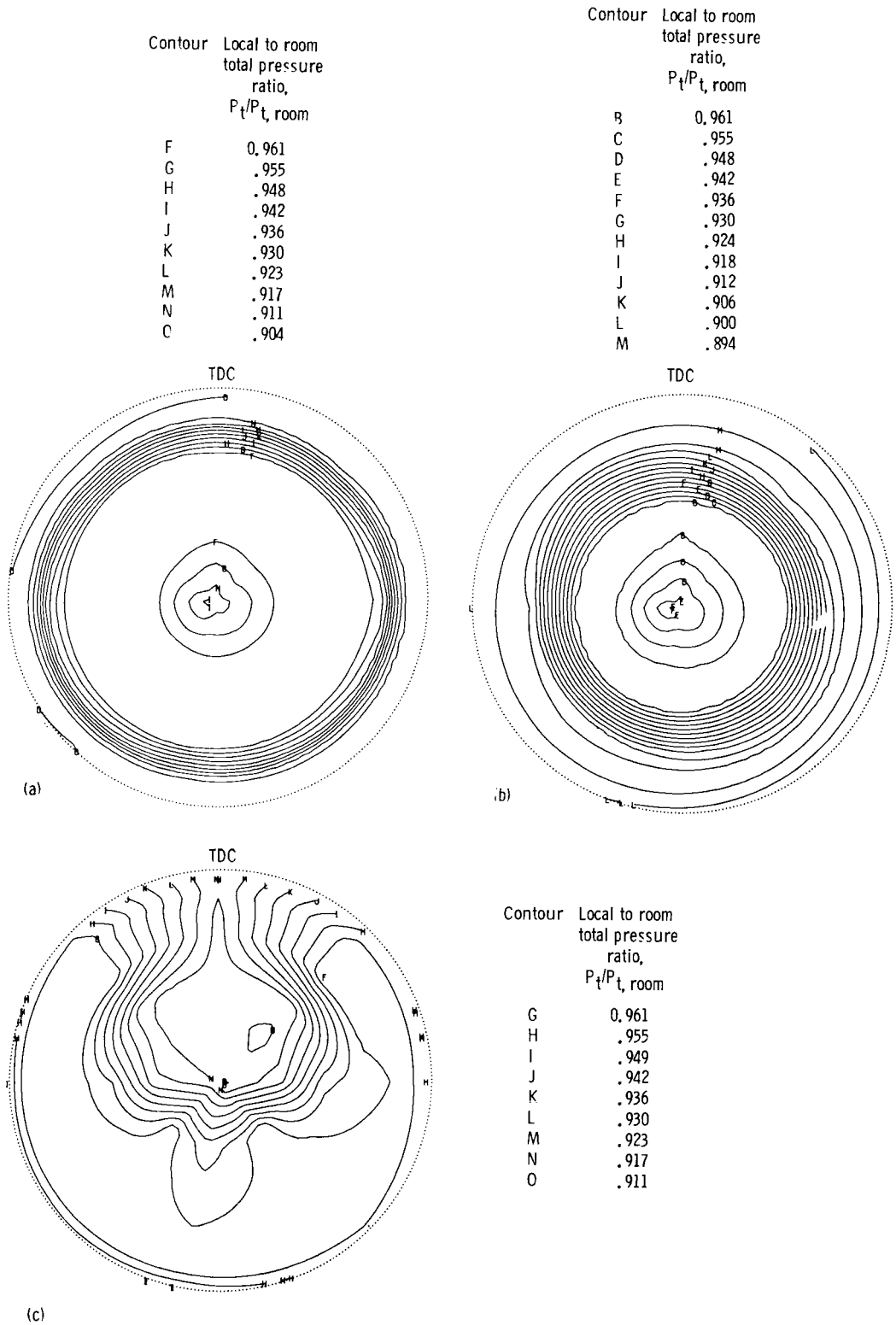

(a) With 6.35-cm (~15-percent radius) tip radial distortion screen. Readings 1241 to 1244.
(b) With 12.70-cm (~30-percent radius) tip radial distortion screen. Readings 1224 to 1227.
(c) With ~50° sector circumferential distortion screen. Readings 1258 to 1261.

Figure 12.—Contour plots of corner 1 inlet local to room total pressure ratios for imposed inlet distortions. Looking downstream; nominal airflow, 72.8 kg/sec; nominal corner 1 inlet Mach number, 0.395.

as far from the wall as the radial extent of the screen. For example, in figure 12(a) the total pressure falloff extended to about 30 percent of radius from a screen that extended about 15 percent (6.35 cm from wall). In figure 12(b) the pressure falloff extended to about 50 percent of radius from a screen that extended about 30 percent (12.70 cm from wall).

The circumferential distortion in figure 12(c) was intended to simulate the exhaust removal scoop (fig. 1) at its maximum expected angle of attack. The local to room total pressure ratios ranged from about 0.91 to 0.96 in an 80° (approximately) sector centered along a line from the top dead center of the duct (TDC, $\theta = 0°$) to its centerline. This circumferential distortion resulted from a screen sector of about 50° (fig. 6(c)).

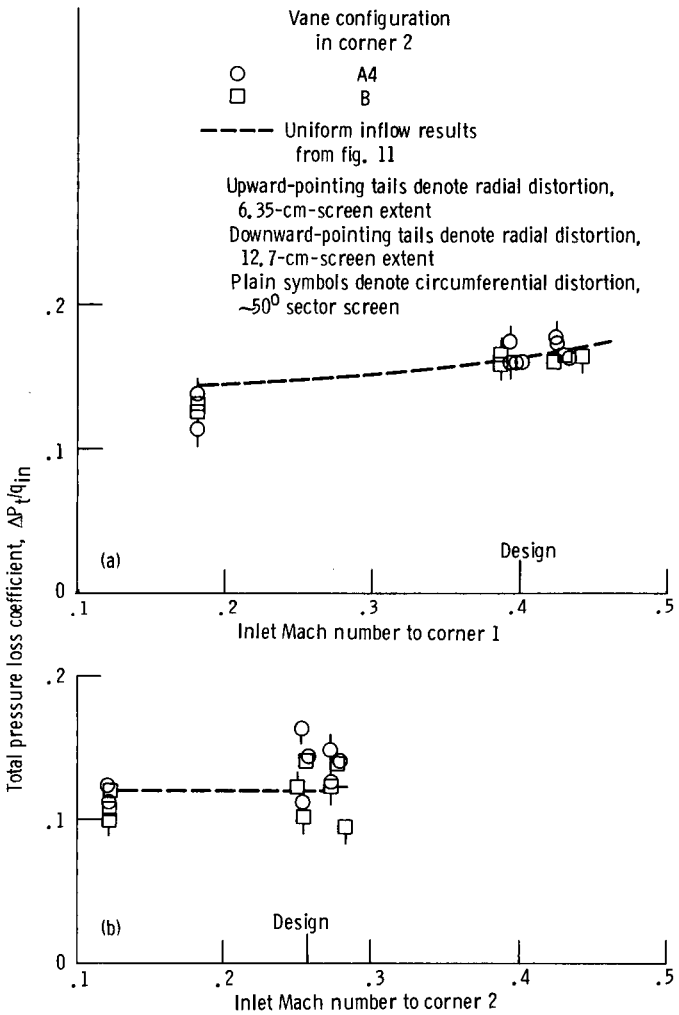

(a) Corner 1 with vanes A10, scoop, and diffuser.
(b) Corner 2.

Figure 13.—Effects of inlet distortion on corner loss coefficients.

The various screen-induced distortions of the inlet flow had little effect on the total pressure loss coefficients (fig. 13). Although some scatter appears in the corner 2 results with distorted inflow, vane design had no consistent effect on corner loss. Some of the reasons behind these responses to inlet distortion are discussed in the next section.

Total Pressure Profiles for Corner 2 with Vane B

Circumferentially averaged pressures.—With corner 2 alone (fig. 14(a)) the loss coefficient $\Delta P_t/q_{in}$ was 0.18. The corner inlet (diffuser exit) total pressure profile was essentially flat except near the wall, where the boundary layer extended to about 25 percent of the flow area (about 13 percent of radius). The ratios of diffuser exit local to room total pressure were about 0.987 in the core flow region and 0.955 near the wall. At the VIGV inlet downstream of vanes B in corner 2 the entire pressure profile shifted to a lower level as expected. Also an additional falloff occurred near the central shaft fairing (figs. 3 and 10), which is the inner flow boundary at this measuring station. The boundary layer extended to about 30 percent of span from the inner wall.

With corner 2 operating downstream of corner 1 (fig. 14(b)) the loss coefficient was 0.127 (table 1), in contrast to 0.18 when corner 2 was operated alone. The loss near the outer and inner (shaft fairing) walls across corner 2 was less when it was downstream of corner 1 as indicated by the reduced difference in total pressure between the diffuser exit (corner 2 inlet) and the VIGV inlet at 10 and 90 percent of span. Losses in the near-wall regions of corner 1 were relatively high, as indicated by the difference in diffuser exit total pressure between figures 14(a) and (b). However, the additional loss experienced in the near-wall regions of corner 2 was reduced because of the relatively lower momentum inflow to these regions.

A similar effect is demonstrated by the radially distorted inflow data of figure 14(c). The difference in diffuser exit pressures between figures 14(a) and (b) indicate relatively large losses in total pressure across the distortion screens. These losses further reduced the momentum of the inflow to corner 2 especially over the outer 60 percent of the flow area. The loss across this region was essentially zero for corner 2 with the tip radial distortions studied. Because of this the overall loss coefficients were reduced to 0.122 with the 6.35-cm distortion screen and to 0.101 with the 12.70-cm distortion screen.

With circumferentially distorted inflow (fig. 14(d)) the overall loss coefficient was 0.139. Here, all the loss across corner 2 appeared to occur over the outer 70 percent of the flow area. However, these total pressures were the result of a circumferential average at each radius. This hid the true circumferential dependence of these corner 2 inlet and exit pressures, as discussed in the following section.

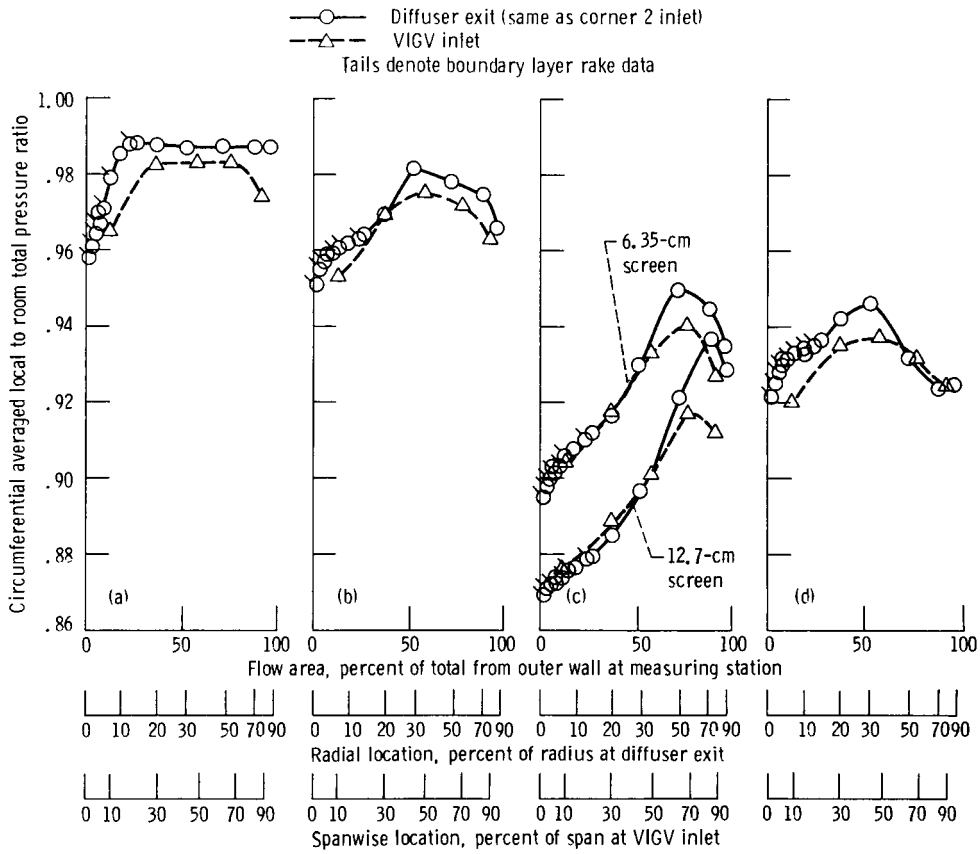

(a) Corner 2 alone. Readings 36 to 40 (of ref. 6); loss coefficient, $\Delta P_t/q_{in}$, 0.180.

(b) Corner 2 with corner 1. Readings 293 to 296; loss coefficient, $\Delta P_t/q_{in}$, 0.127.

(c) Corner 2 with corner 1 and tip radial distortion. Readings 527 to 530 for 6.35-cm screen (loss coefficient, $\Delta P_t/q_{in}$, 0.122) and readings 515 to 518 for 12.70-cm screen (loss coefficient, $\Delta P_t/q_{in}$, 0.101).

(d) Corner 2 with corner 1 and circumferential distortion. Readings 541 to 544; loss coefficient, $\Delta P_t/q_{in}$, 0.139.

Figure 14.—Spanwise variation of circumferentially averaged diffuser exit and VIGV inlet total pressures ratioed to room pressure for corner 2 with vanes B. Nominal airflow, 72.8 kg/sec; nominal corner 2 inlet Mach number, 0.255.

Pressures at particular circumferential locations. —The spanwise variations of total pressure across corner 2 with vanes B at eight circumferential locations for four configurations are shown as parts (a) of figures 15 to 18. Parts (b) of these figures show contour plots of constant pressure drawn from these data. Each figure provides details for one of the four configurations in figure 14. There circumferentially averaged data are presented for design inflow conditions.

For corner 2 alone (fig. 15(a)) the total pressure profiles differed little at the various circumferential locations (identified by θ in degrees) except in the horizontal plane, where θ is either 90° or 270°. The sharp decrease in total pressure measured by the VIGV inlet probe nearest the wall (at 13 percent of flow area or 10 percent of span) at $\theta = 90°$ suggests an upstream flow separation in this region. Visual observation of wool tufts mounted along the inner wall at $\theta = 90°$ indicated a pocket of flow separation from the wall. This pocket was confined in axial extent from about midchord to the trailing edge of vane B. Also, evidence of the corner 2 shaft fairing (with its major axis in the horizontal plane) appears as a relatively greater loss in total pressure over the innermost flow region at θ of 90° and 270°. The contour plot (fig. 15(b)) also shows flow symmetry about a horizontal reference plane.

For corner 2 operating downstream of corner 1 (fig. 16(a)) the losses (proportional to differences in total pressure across the corner) were lower than those for corner 2 alone (fig. 15(a)) at nearly every θ location over the outer 40 percent of the flow area. Comparing these two configurations at $\theta = 90°$ shows several differences. Diffuser exit total pressure dropped sharply near the wall when corner 1 with vanes A10 was upstream of corner 2 (fig. 16(a)). This drop was indicative of an upstream separation from the wall in this region of corner 1. Also, at $\theta = 90°$ the dip in diffuser exit pressure at about 73 percent of the flow area may be the center of a vortex believed to be shed off the inner edge of the corner 1 scoop afterbody (fig. 3). These features are also evident in the contour plots (fig. 16(b)).

On occasion an increase in pressure was indicated at the VIGV inlet over that at the diffuser exit (e.g., see θ of 225° or 315° at 37 percent of flow area from wall, fig. 16(a)). This

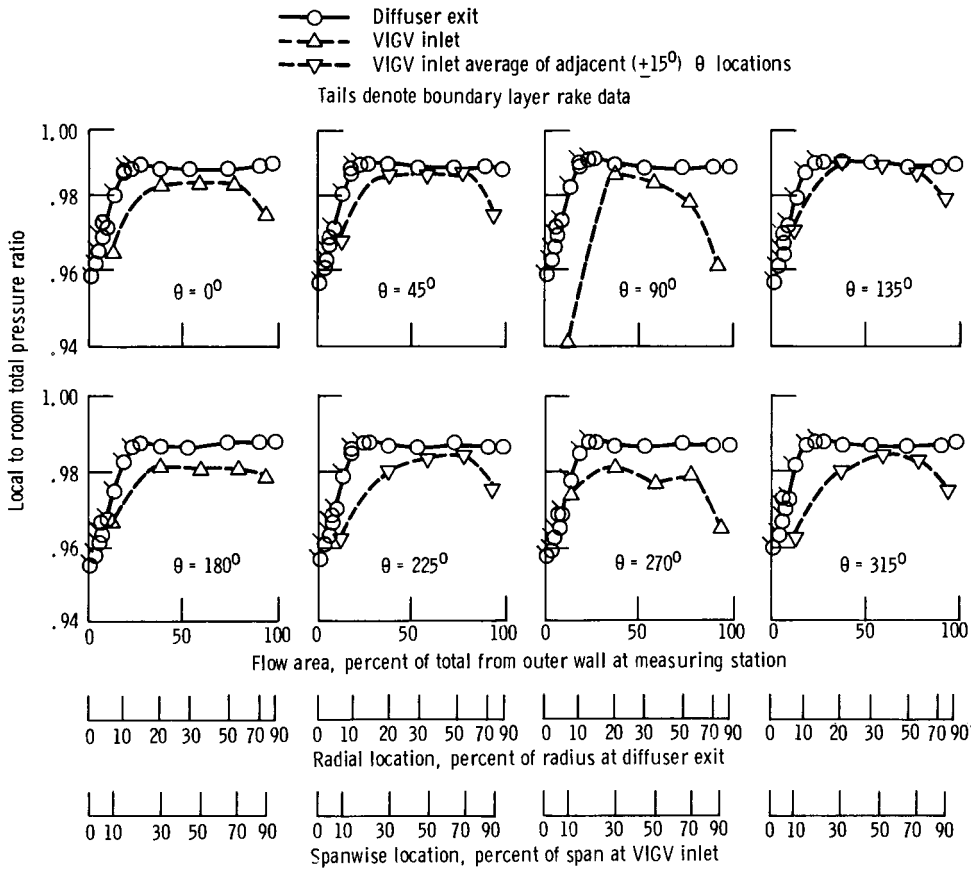

(a)

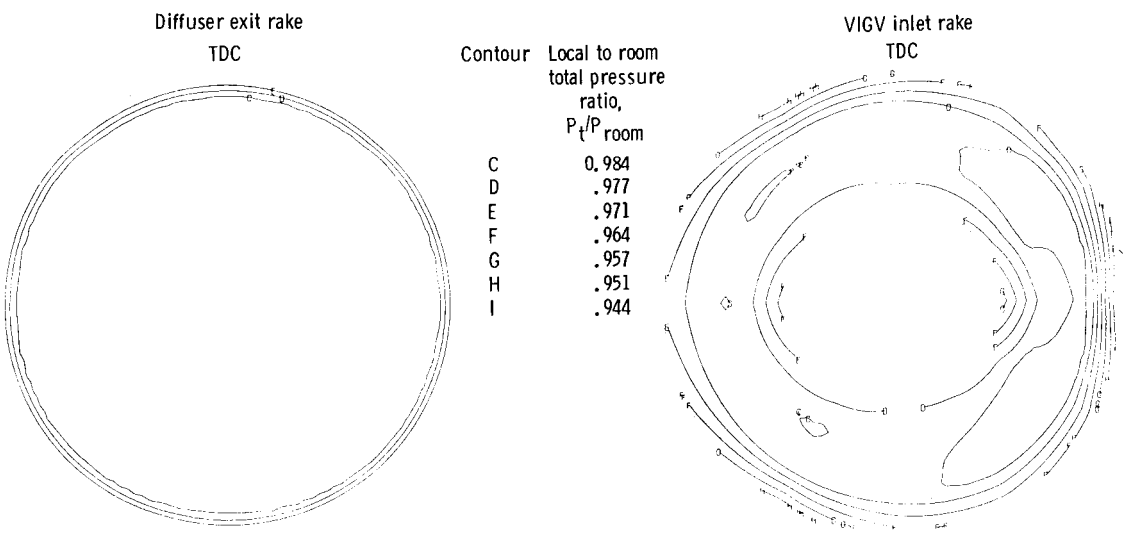

(b)

(a) Spanwise variation at discrete circumferential locations.
(b) Contour plots of constant pressure (looking downstream).

Figure 15.—Local total pressures ratioed to room pressure across corner 2 with vanes B without corner 1 upstream. Airflow, 74.1 kg/sec; corner 2 inlet Mach number, 0.259; readings 36 to 40 (of ref. 6); loss coefficient, $\Delta P_t/q_{in}$, 0.180.

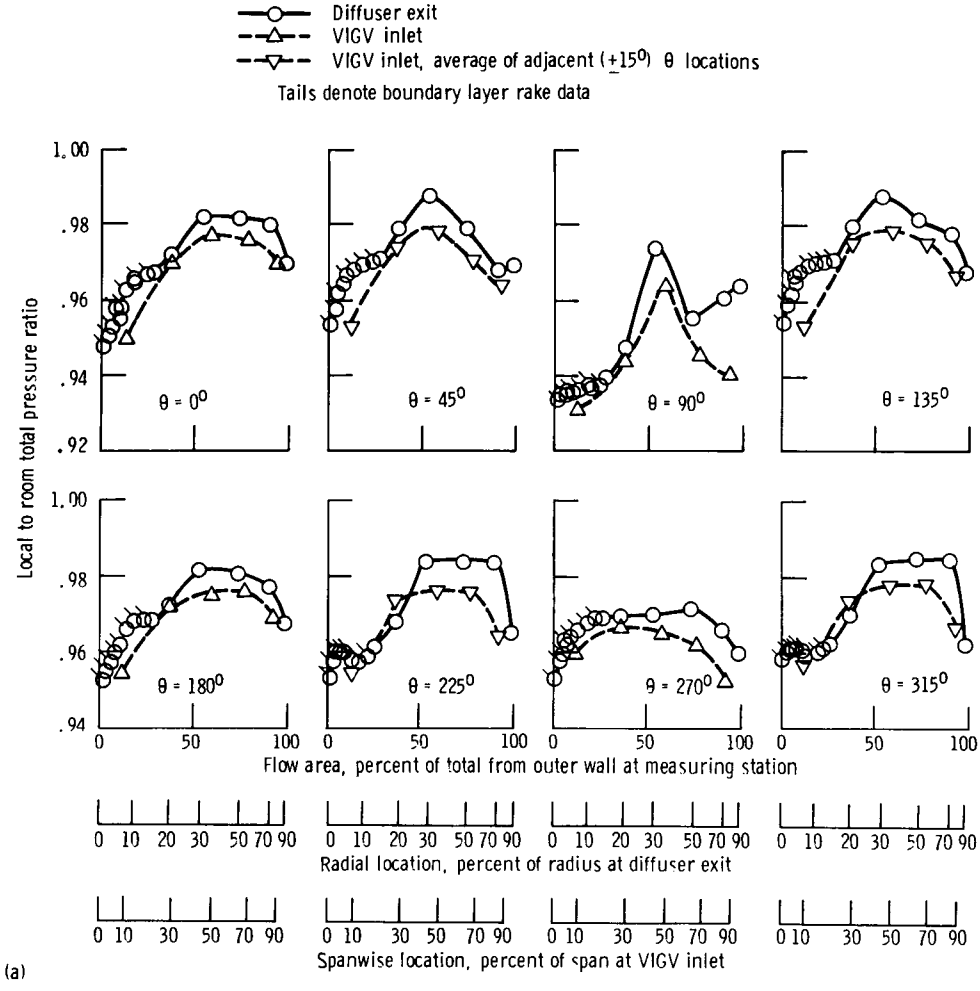

(a)

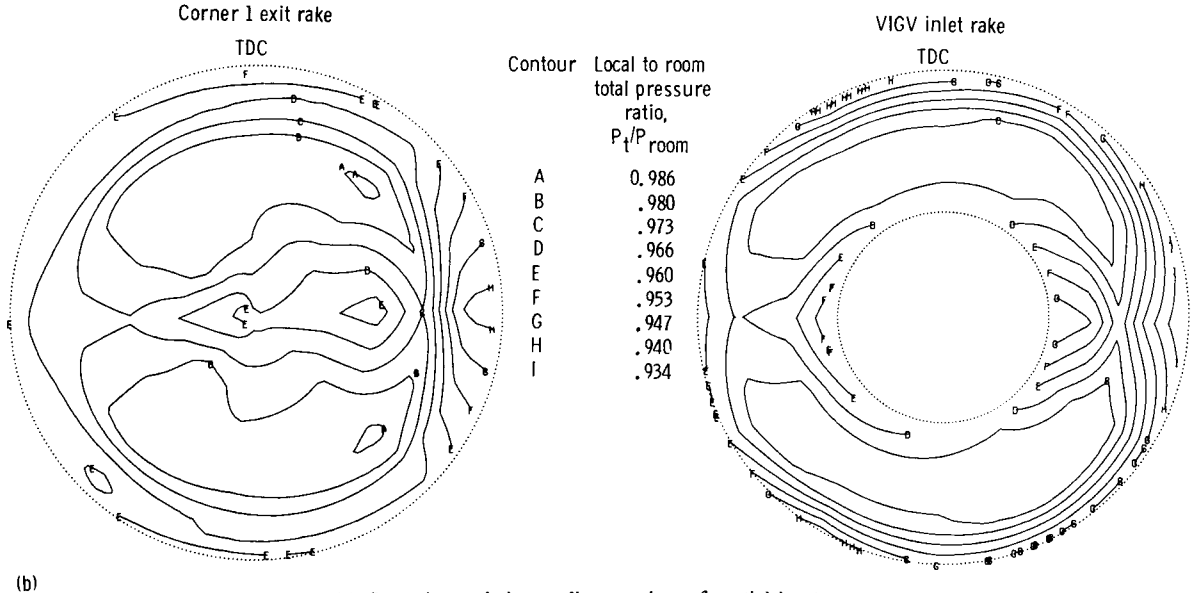

(b)

(a) Spanwise variation at discrete circumferential locations.
(b) Contour plots of constant pressure (looking downstream).

Figure 16.—Local total pressures ratioed to room pressure across corner 2 with vanes B downstream of corner 1 with vanes A10 and scoop. Airflow, 73.1 kg/sec; corner 2 inlet Mach number, 0.255; readings 293 to 296; loss coefficient, $\Delta P_t/q_{in}$, 0.127.

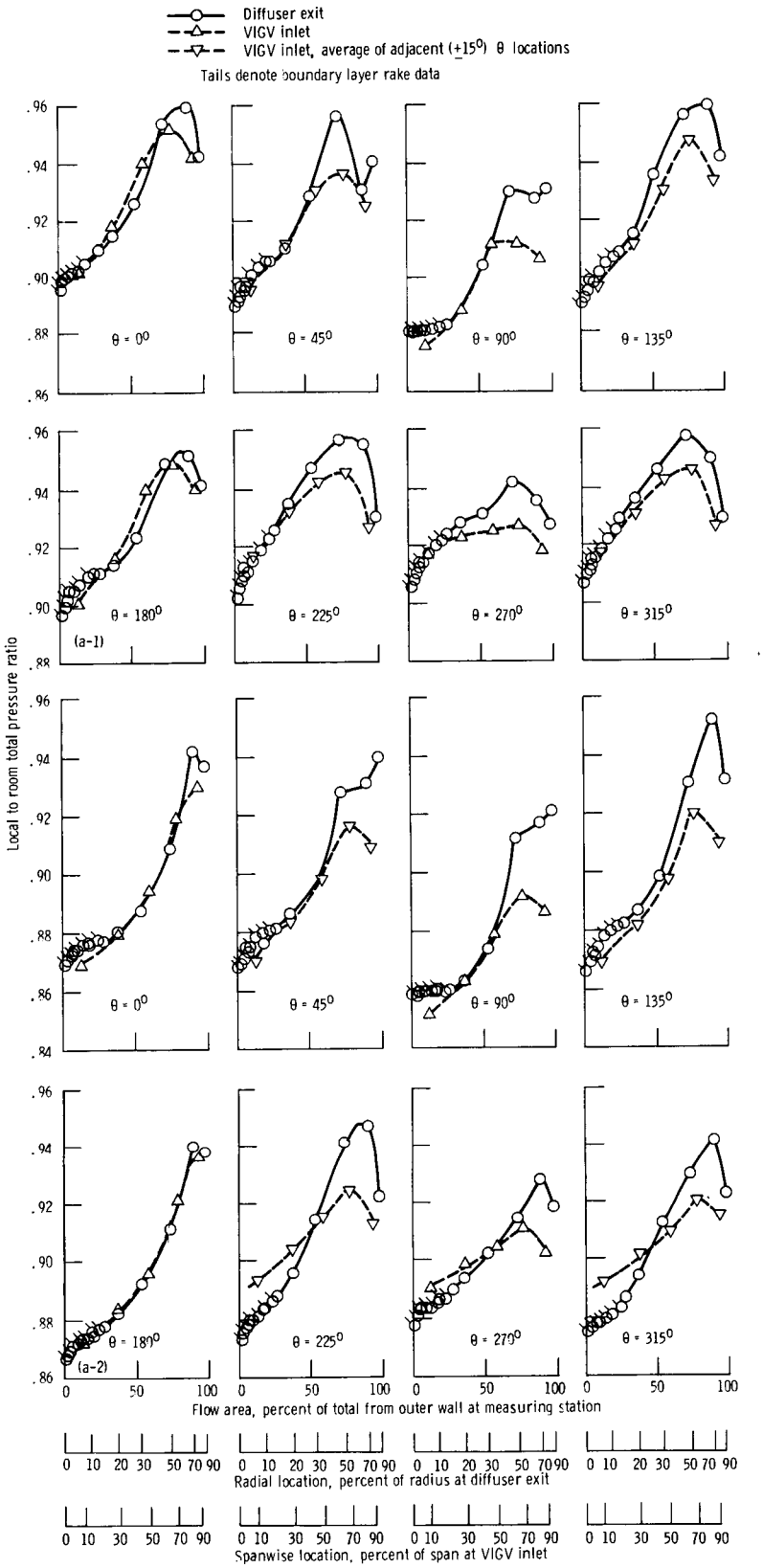

(a-1) Spanwise variation at discrete circumferential locations with 6.35-cm distortion screen. Readings 527 to 530; loss coefficient, $\Delta P_t/q_{in}$, 0.122.
(a-2) Spanwise variation at discrete circumferential locations with 12.70-cm distortion screen. Readings 515 to 518; loss coefficient, $\Delta P_t/q_{in}$, 0.101.

Figure 17.—Local total pressures ratioed to room pressure across corner 2 with vanes B downstream of corner 1 with vanes A10 and scoop. Nominal airflow, 71.8 kg/sec; nominal corner 2 inlet Mach number, 0.252; tip radially distorted inflow.

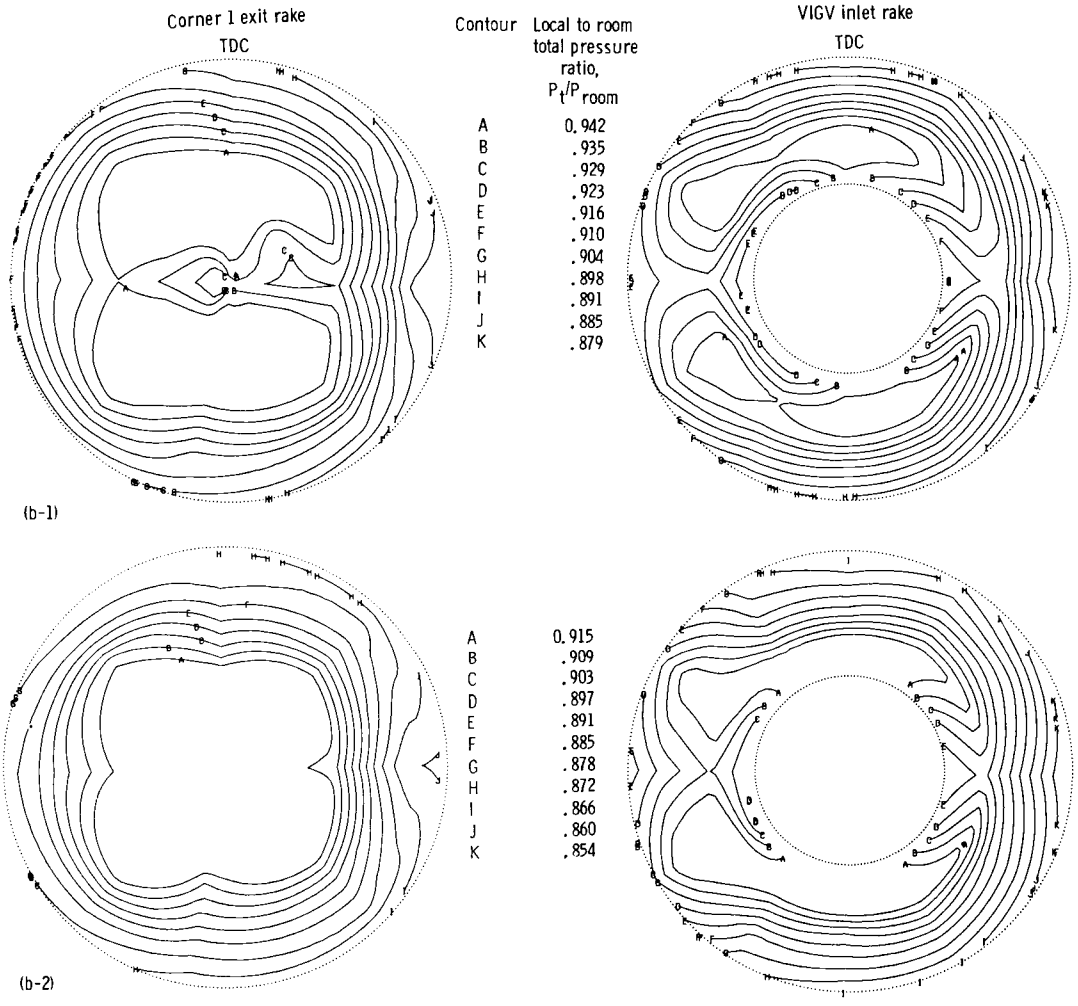

(b-1) Contour plots of constant pressure with 6.35-cm distortion screen. Looking downstream; readings 527 to 530; loss coefficient, $\Delta P_t/q_{in}$, 0.122.
(b-2) Contour plots of constant pressure with 12.70-cm distortion screen. Looking downstream; readings 515 to 518; loss coefficient, $\Delta P_t/q_{in}$, 0.101.

Figure 17.–Concluded.

was attributed to a mismatch in θ or flow area (or both) between these two measuring stations. In other words the stream tube at a particular θ and flow area at the diffuser exit ended up at a different θ or flow area at the VIGV inlet because of flow skewing. Such a skewing was not surprising with the asymmetric scoop fairing in corner 1. More evidence of these apparent pressure increases across corner 2 occurred in the distorted inflow studies of figures 17(a) and 18(a).

With two extents of tip radial distortion imposed upstream of corner 1 (fig. 17(a)) the losses in pressure were near zero at nearly every θ location over the outer half of the flow area. Thus the circumferentially averaged pressures (fig. 14(c)) were similar to those at the eight θ locations with the symmetrically imposed tip radial distortions. Flow symmetry with respect to a horizontal plane is also evident in figure 17(b). Such was not the case with circumferentially imposed distortion, as indicated by the θ-dependent pressure patterns in figure 18.

The screen sector for circumferential distortion was centered at $\theta = 0°$ (fig. 12(c)). The pressure patterns in figure 18(a) were relatively flat there, with nearly zero loss across the corner. Some flow symmetry about $\theta = 0°$ (TDC) is evident at the exit of corner 1 (fig. 18(b)) for about $\pm 45°$. Because the flow was skewed by the circumferentially imposed distortion screen, losses were negative at 45°, 90°, and 315° over the inner 30 percent of the flow area (fig. 18(a)). These results make a significant contribution to the near-zero losses indicated by the circumferentially averaged data of figure 14(d). Away from the distortion screen the pressure data of figure 18 resemble the undistorted inflow data of figure 16, as might be expected.

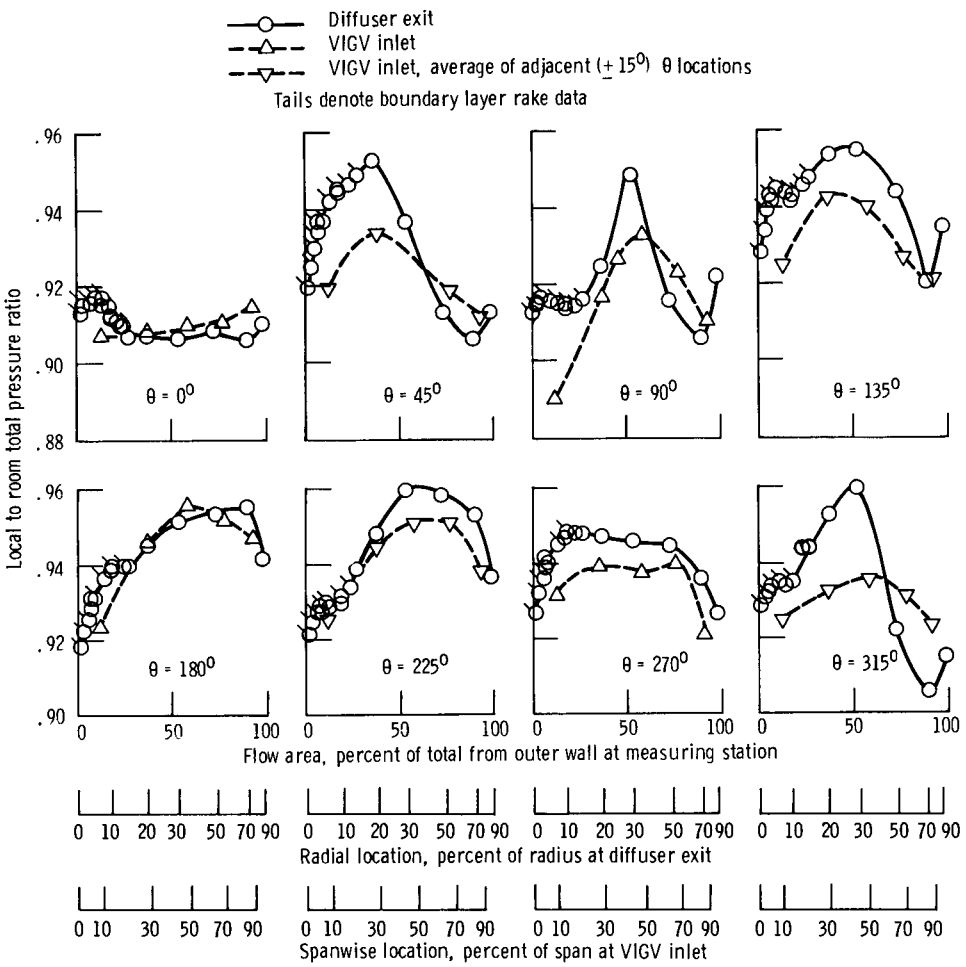

(a)

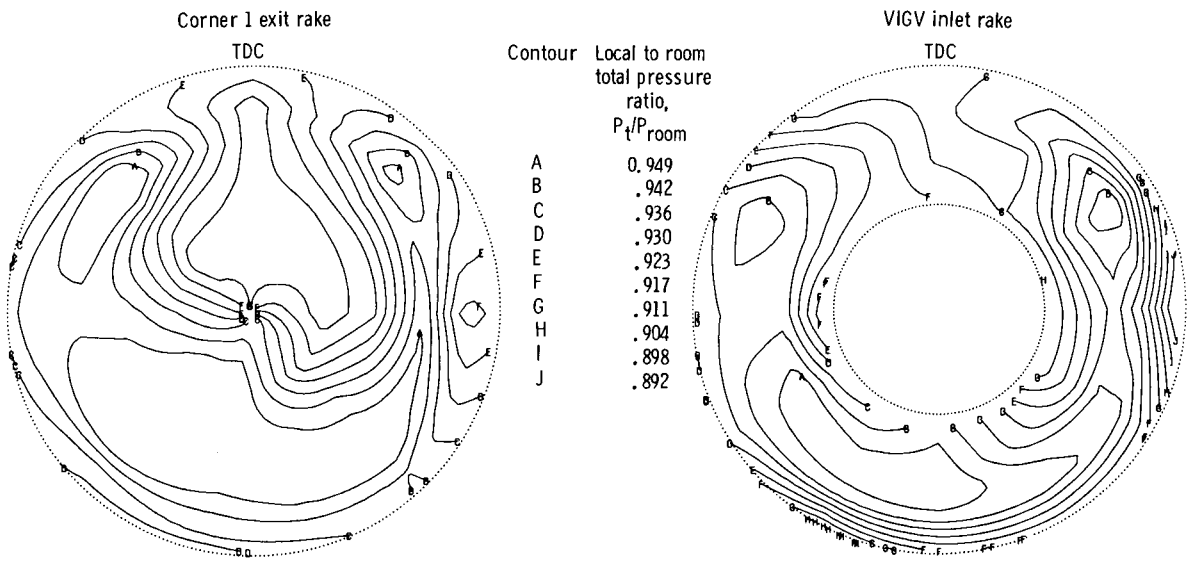

(b)

(a) Spanwise variation at discrete circumferential locations.
(b) Contour plots of constant pressure (looking downstream).

Figure 18.—Local total pressures ratioed to room pressure across corner 2 with vanes B downstream of corner 1 with vanes A10 and scoop. Airflow, 73.3 kg/sec; corner 2 inlet Mach number, 0.256; circumferentially distorted inflow, ~50° sector screen; readings 541 to 544; loss coefficient, $\Delta P_t/q_{in}$, 0.139.

Total Pressure Profiles for Corner 2 with Vane A4

From the study of corner 2 operating alone (ref. 6) the combination of resetting vanes A to $-5°$ and removing the outermost vane (configuration called vane A4) produced the lowest corner loss coefficient. Therefore vane A4 was the only vane A configuration studied in corner 2 operating downstream of corner 1. The presentation and discussion of these data parallel that just completed for vanes B in corner 2.

Circumferentially averaged pressures.—The spanwise variations of circumferentially averaged total pressures across corner 2 with vanes A4 (fig. 19) were nearly the same as those for corner 2 with vanes B (fig. 14). The overall corner loss coefficients for comparable configurations were also nearly the same. From the data for corner 2 alone the minimum difference in local to room total pressure ratio in the core flow region was about 25 percent less across vanes A4 (fig. 19(a)) than across vanes B (fig. 14(a)). This somewhat reflects the relative profile loss coefficients for the two vane designs. More detailed vane wake measurements taken about one-half chord from the vane trailing edge would provide for a more reliable determination of absolute profile loss coefficients. Such data and determinations are reported in reference 11.

The circumferential dependence of inlet and exit pressures across corner 2 with vanes A4 is discussed in the following section.

Pressures at particular circumferential locations.—The spanwise variations of total pressure across corner 2 with vanes A4 at eight circumferential locations for four configurations are shown in figures 20 to 23. Each figure provides details of one of the four configurations in figure 19. There circumferentially averaged data are presented for design inflow conditions. After a brief discussion of the pressure profile difference due to circumferential location, comparisons are made with vanes B.

For corner 2 alone (fig. 20) the total pressure profiles differed little at the various circumferential locations except in the horizontal plane (θ of 90° and 270°) and in the outer

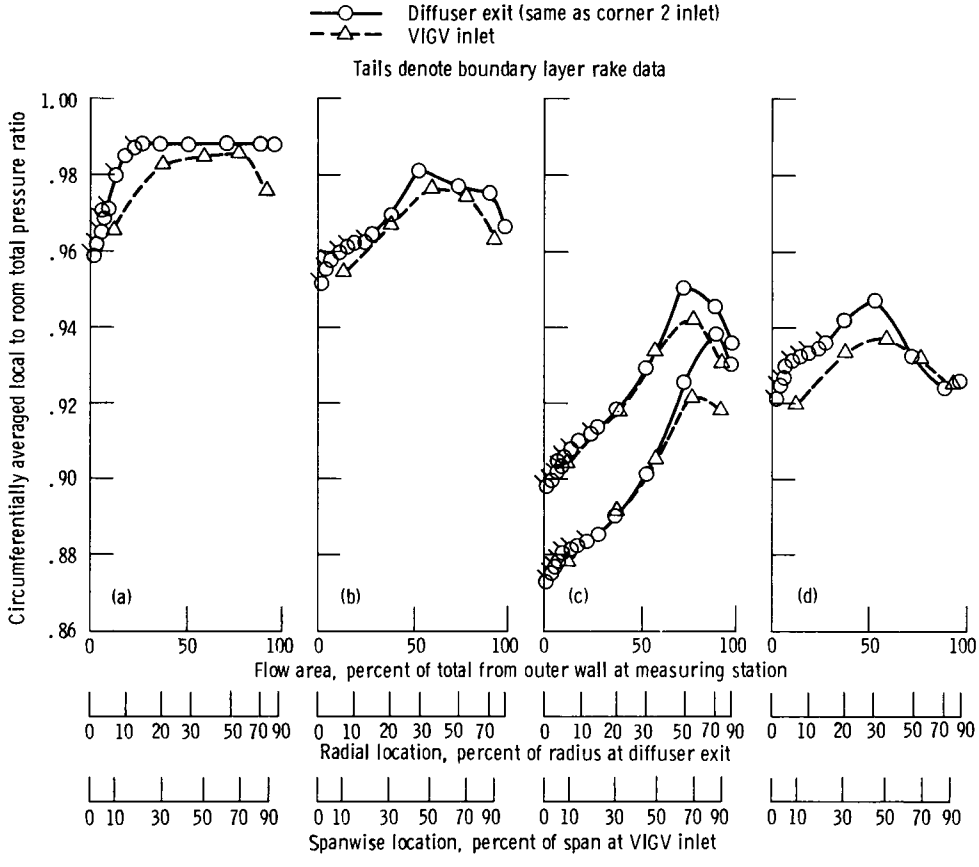

(a) Corner 2 alone. Readings 331 to 338 (of ref. 6) interpolated to 72.9 kg/sec; loss coefficient, $\Delta P_t/q_{in}$, 0.169.

(b) Corner 2 with corner 1. Readings 4 to 16; loss coefficient, $\Delta P_t/q_{in}$, 0.116.

(c) Corner 2 with corner 1 and tip radial distortion. Readings 1241 to 1244 for 6.35-cm screen (loss coefficient, $\Delta P_t/q_{in}$, 0.112) and readings 1224 to 1227 for 12.70-cm screen (loss coefficient, $\Delta P_t/q_{in}$, 0.125); at 5 percent of span data are from boundary layer rakes.

(d) Corner 2 with corner 1 and circumferential distortion. Readings 1258 to 1261; loss coefficient, $\Delta P_t/q_{in}$, 0.142.

Figure 19.—Spanwise variation of circumferentially averaged diffuser exit and VIGV inlet total pressures ratioed to room pressure for corner 2 with vanes A4. Nominal airflow, 72.9 kg/sec; nominal corner 2 inlet Mach number, 0.256.

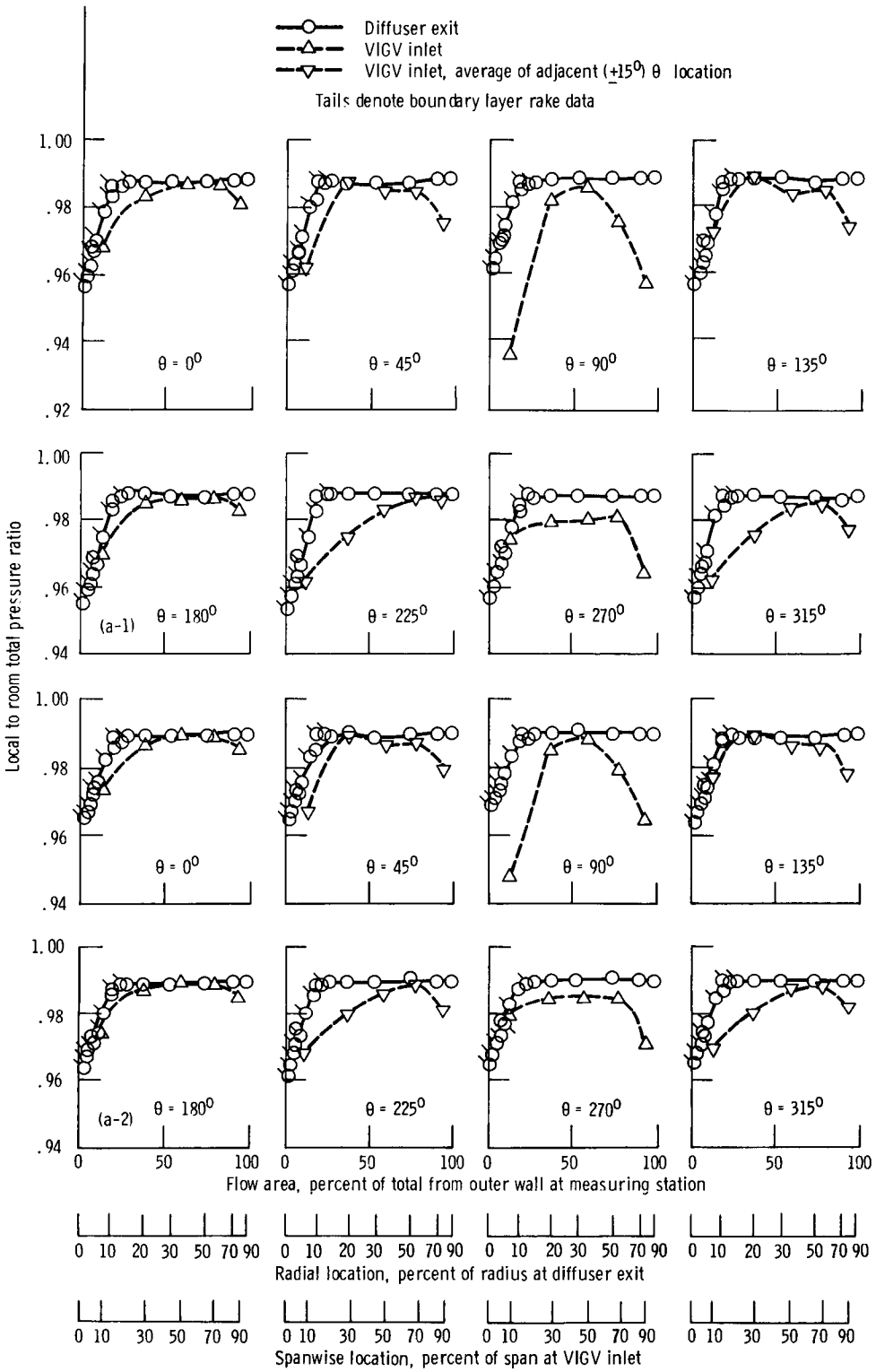

(a-1) Spanwise variations at discrete circumferential locations for airflow of 76.3 kg/sec and corner 2 inlet Mach number of 0.266. Readings 331 to 334 (of ref. 6); loss coefficient, $\Delta P_t/q_{in}$, 0.169.

(a-2) Spanwise variations at discrete circumferential locations for airflow of 69.3 kg/sec and corner 2 inlet Mach number of 0.241. Readings 335 to 338 (of ref. 6); loss coefficient, $\Delta P_t/q_{in}$, 0.170.

Figure 20.—Local total pressures ratioed to room pressure across corner 2 with vanes A4 without corner 1 upstream.

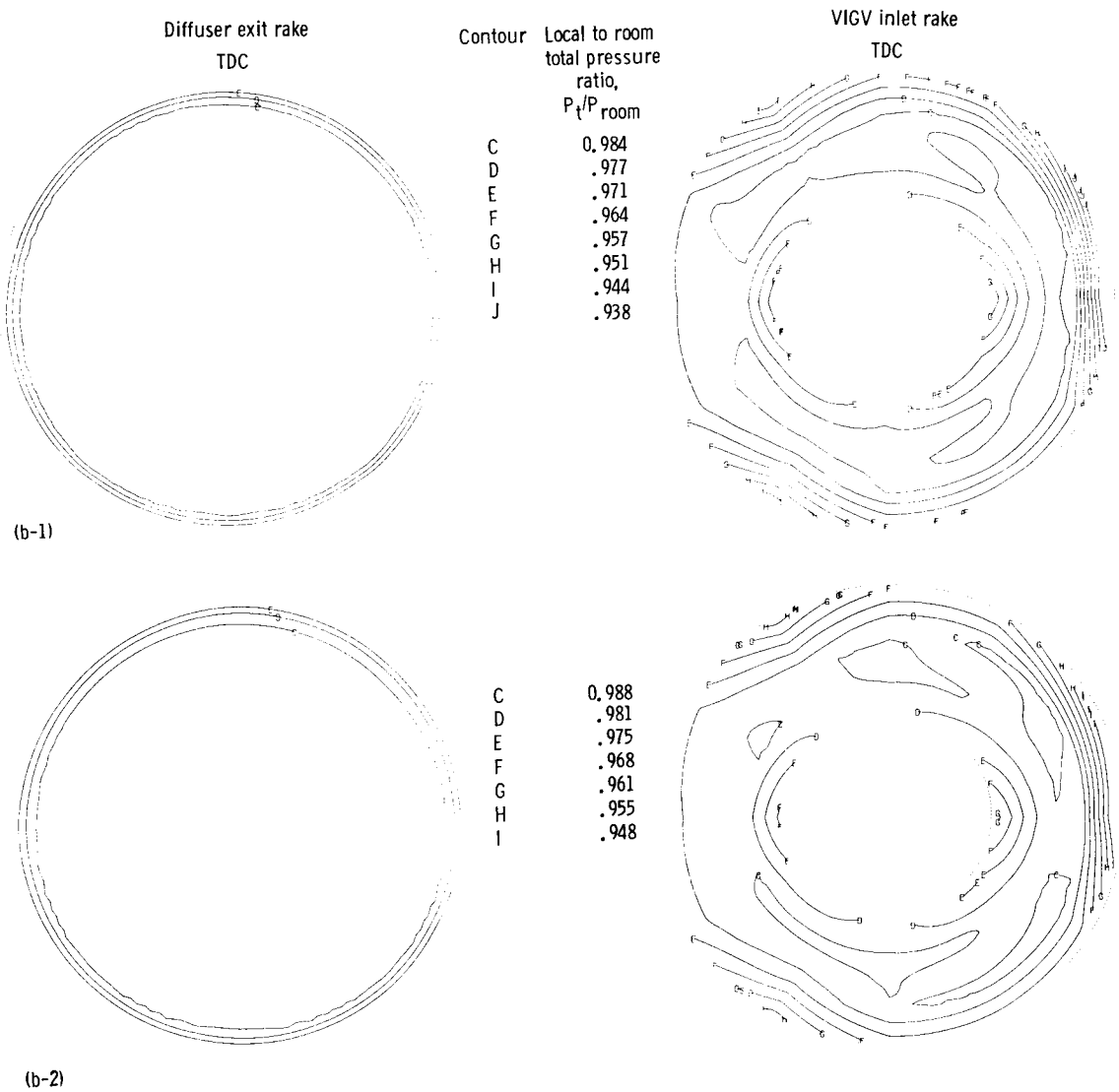

(b-1) Contour plots of constant pressure for airflow of 76.3 kg/sec and corner 2 inlet Mach number of 0.266. Looking downstream; readings 331 to 334 (of ref. 6); loss coefficient, $\Delta P_t/q_{in}$, 0.169.

(b-2) Contour plots of constant pressure for airflow of 69.3 kg/sec and corner 2 inlet Mach number of 0.241. Looking downstream; readings 335 to 338 (of ref. 6); loss coefficient, $\Delta P_t/q_{in}$, 0.170.

Figure 20.—Concluded.

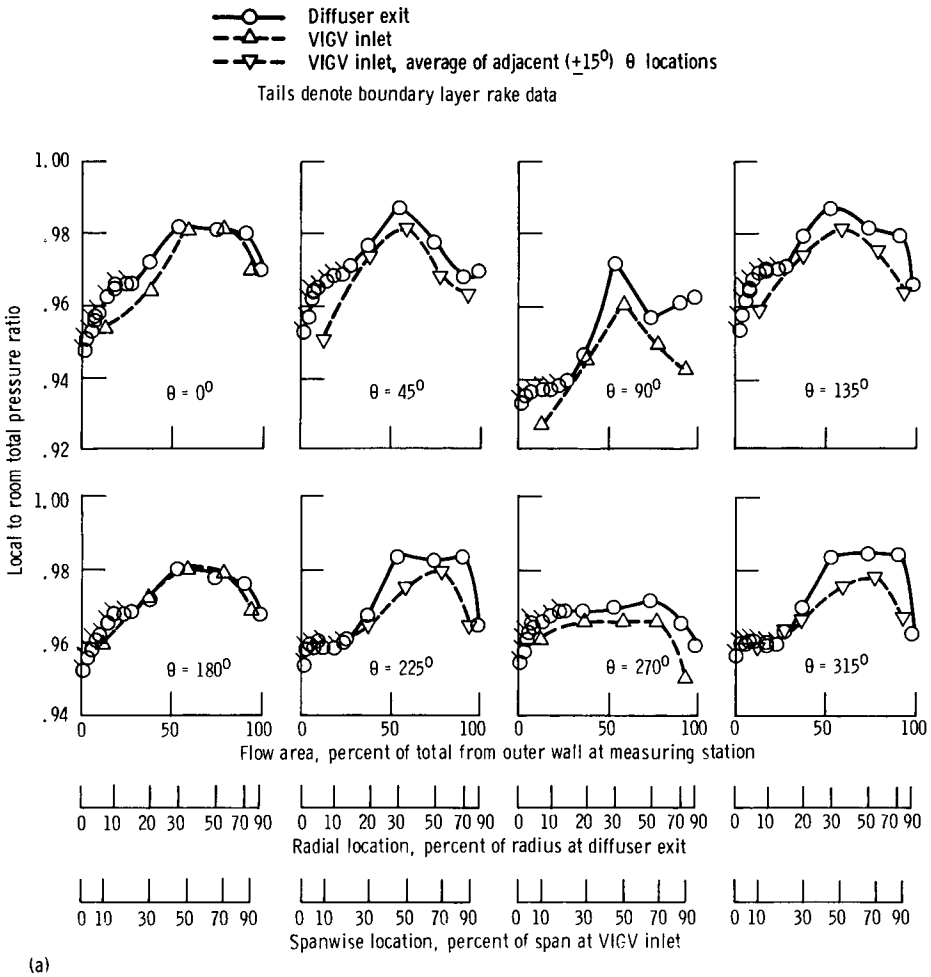

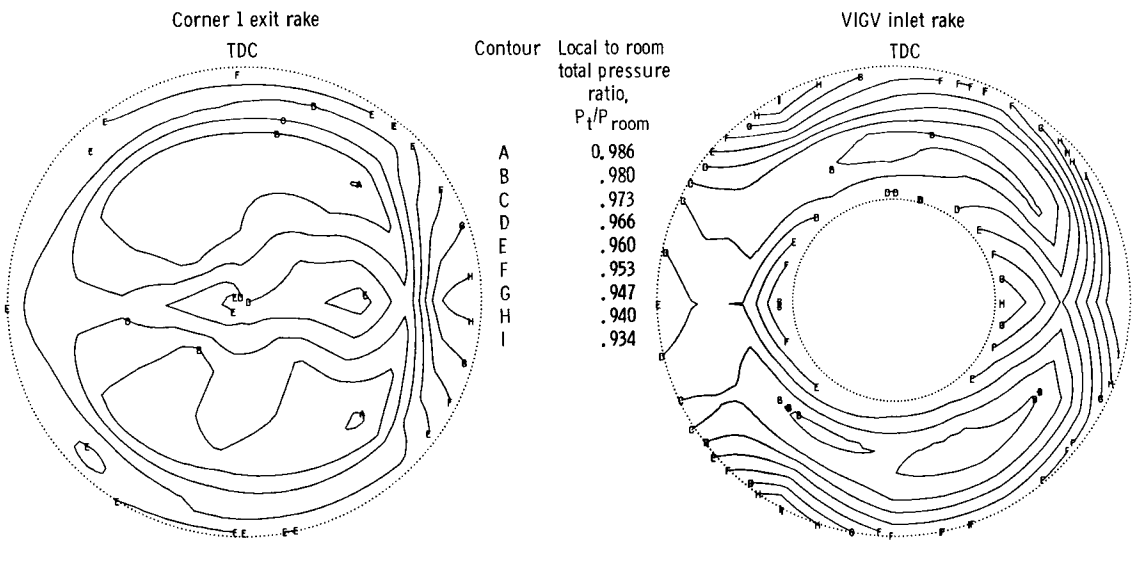

(a) Spanwise variation at discrete circumferential locations.
(b) Contour plots of constant pressure (looking downstream).

Figure 21.—Local total pressures ratioed to room pressure across corner 2 with vanes A4 downstream of corner 1 with vanes A10 and scoop. Airflow, 73.1 kg/sec; corner 2 inlet Mach number, 0.256; readings 4 to 16; loss coefficient, $\Delta P_t/q_{in}$, 0.116.

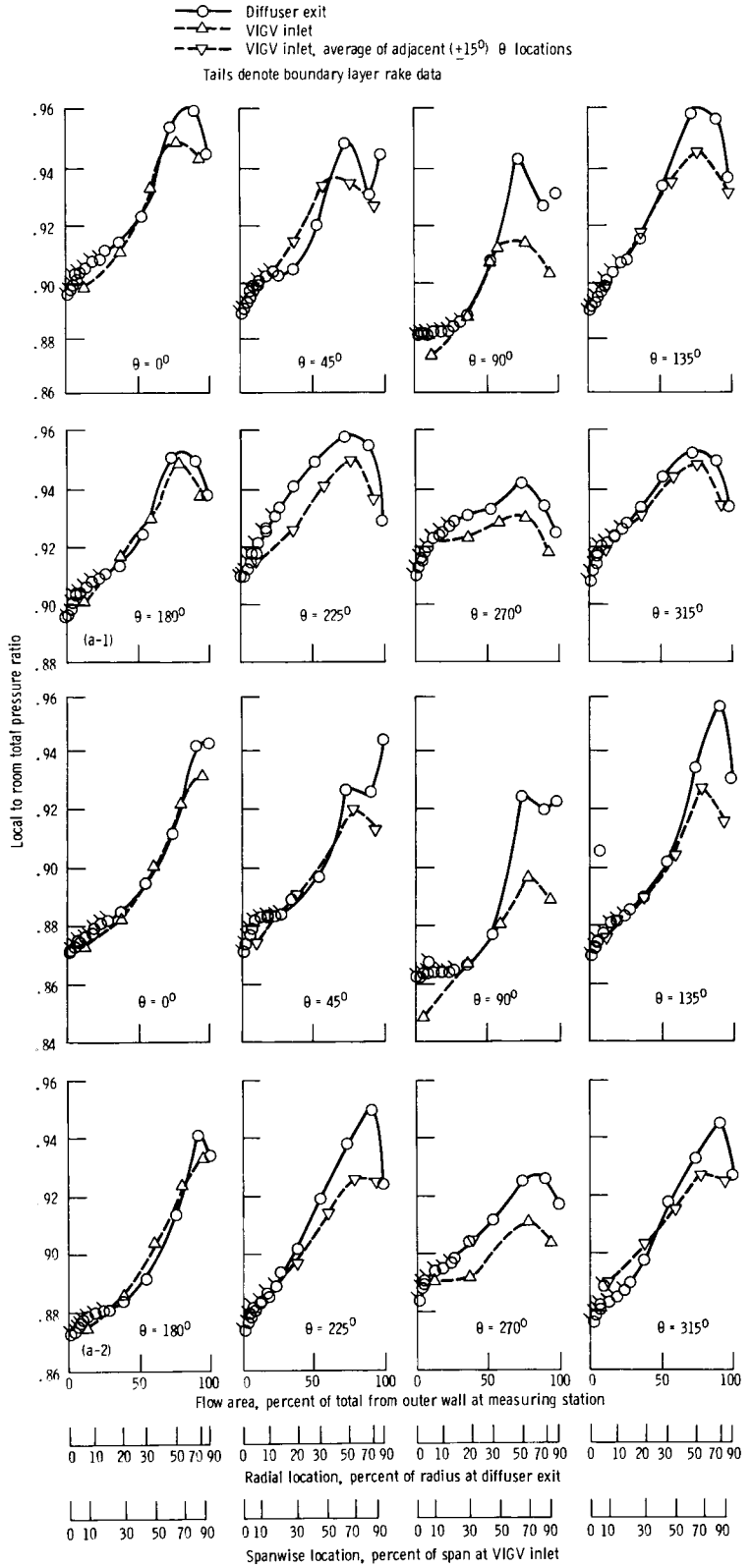

(a-1) Spanwise variations at discrete circumferential locations with 6.35-cm distortion screen. Readings 1241 to 1244; loss coefficient, $\Delta P_t/q_{in}$, 0.112.
(a-2) Spanwise variations at discrete circumferential locations with 12.70-cm distortion screen. Readings 1224 to 1227; loss coefficient, $\Delta P_t/q_{in}$, 0.125.

Figure 22.—Local total pressures ratioed to room pressure across corner 2 with vanes A4 downstream of corner 1 with vanes A10 and scoop. Nominal airflow, 72.3 kg/sec; nominal corner 2 inlet Mach number, 0.254; tip radially distorted inflow.

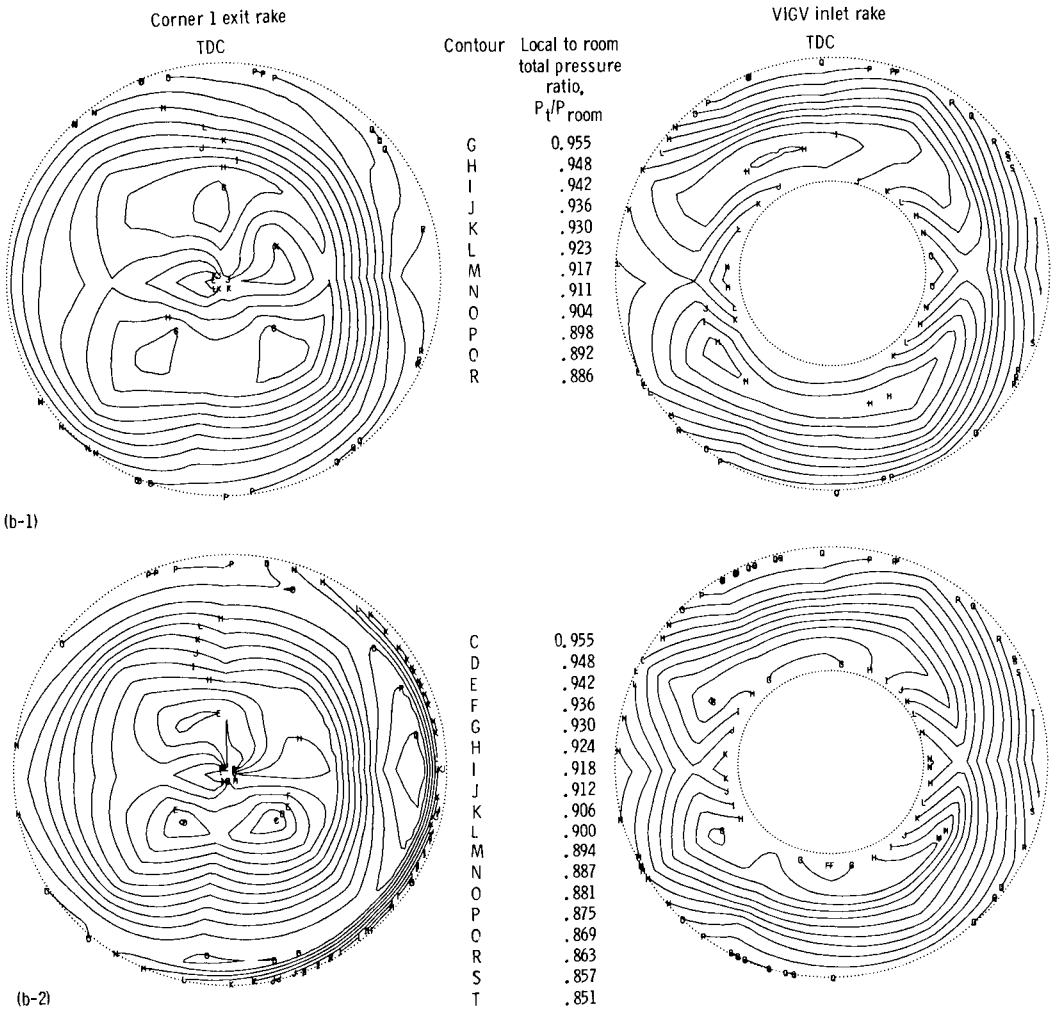

(b-1) Contour plots of constant pressure with 6.35-cm distortion screen. Looking downstream; readings 1241 to 1244; loss coefficient, $\Delta P_t/q_{in}$, 0.112.
(b-2) Contour plots of constant pressure with 12.7-cm distortion screen. Looking downstream; readings 1224 to 1227; loss coefficient, $\Delta P_t/q_{in}$, 0.125.

Figure 22.—Concluded.

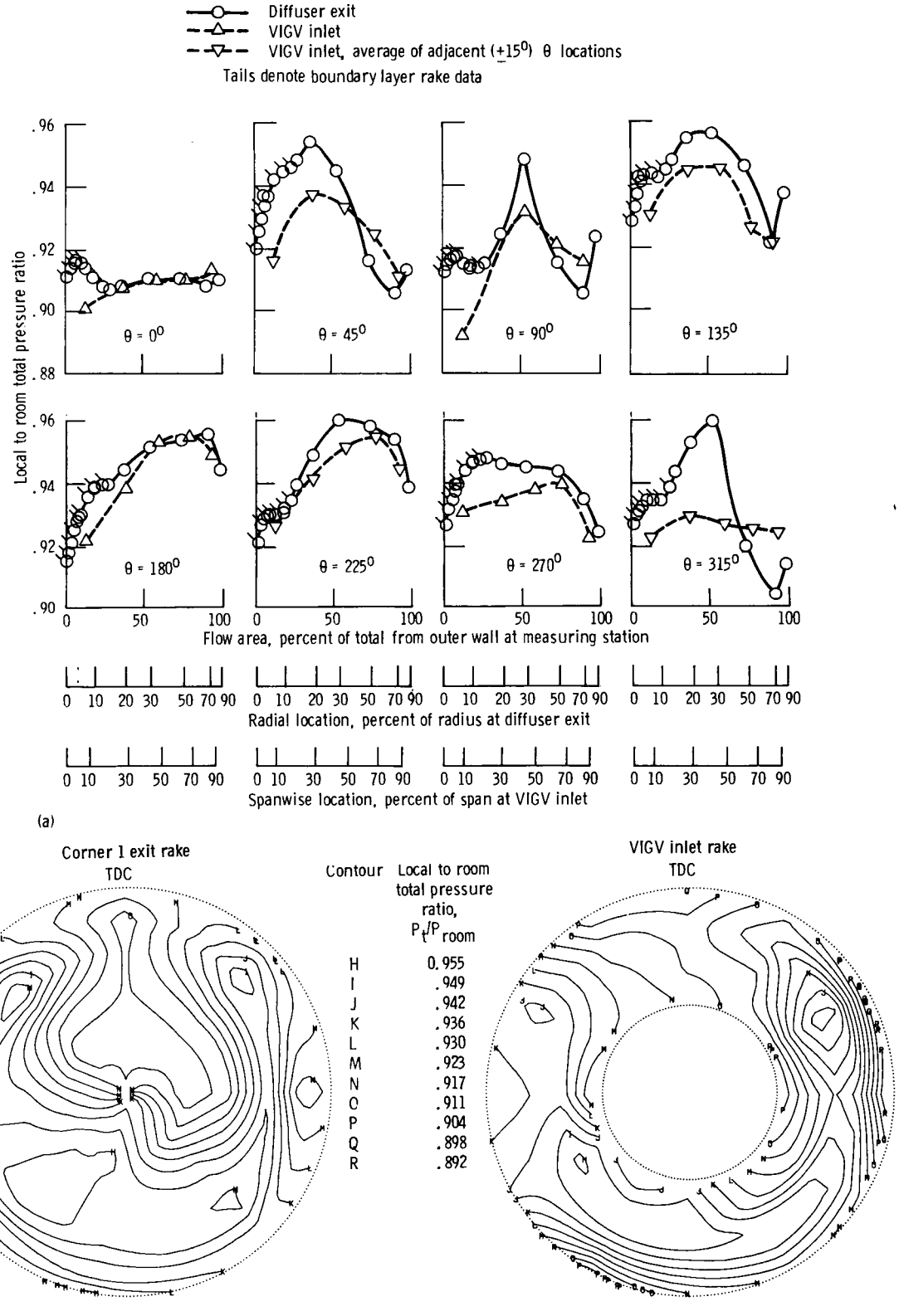

(a) Spanwise variation at discrete circumferential locations.
(b) Contour plots of constant pressure (looking downstream).

Figure 23.—Local total pressures ratioed to room pressure across corner 2 with vanes A4 downstream of corner 1 with vanes A10 and scoop. Airflow, 73.7 kg/sec; corner 2 inlet Mach number, 0.258; circumferentially distorted inflow (~50° sector screen); readings 1258 to 1261; loss coefficient, $\Delta P_t/q_{in}$, 0.142.

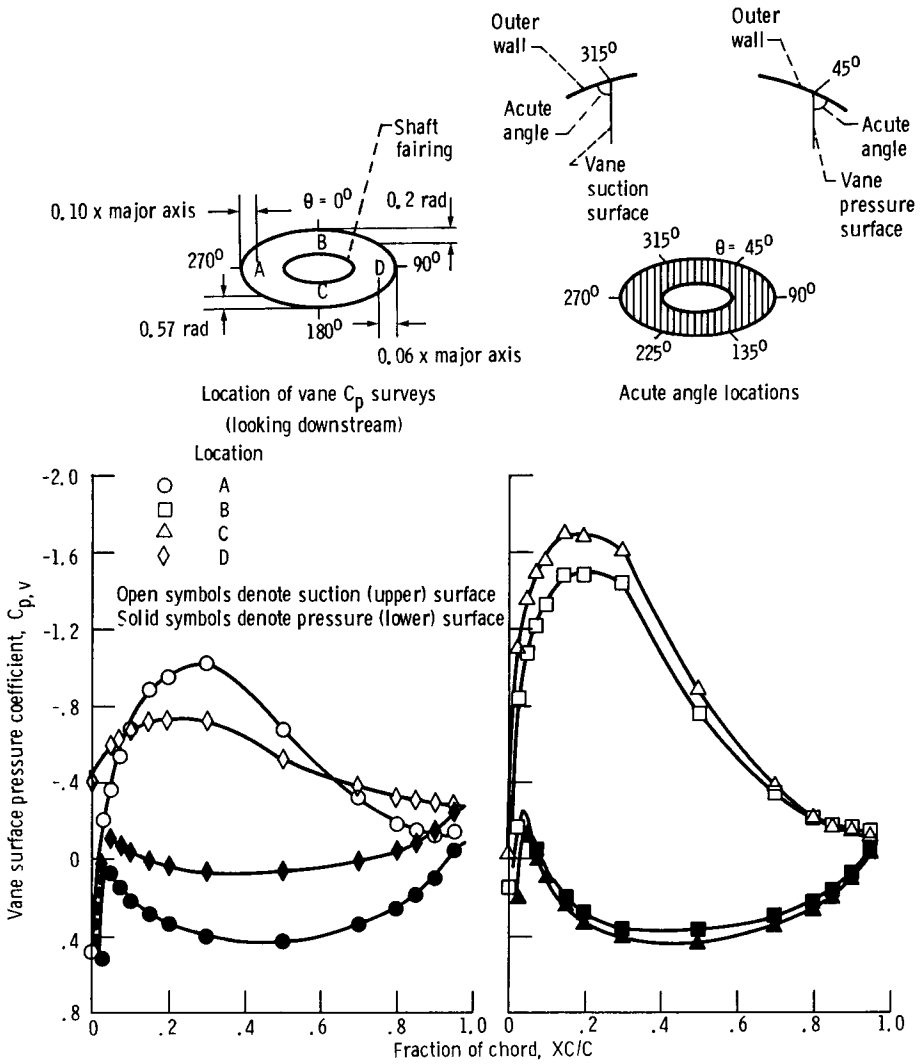

Figure 24.—Vane surface pressure distributions on vanes A4 at four locations in corner 2. Uniform inflow with airflow of 73.1 kg/sec; corner 2 inlet Mach number, 0.256; readings 4 to 16.

θ locations of 225° and 315°. The relatively large reduction in total pressure approaching the outer wall for the VIGV inlet at $\theta = 90°$ indicated flow separation from the wall. At θ of 90° and 270° near the inner wall the horizontal bias of the shaft-fairing centerbody was shown by the relatively greater loss in VIGV inlet total pressure there. At θ of 225° and 315° the boundary layer associated with the outer wall appeared thicker than that at the other locations. At and near these values of θ an acute angle was formed by the intersection of the vane suction (upper) surface and the outer wall, as depicted by the sketches in figure 24. This geometry concentrated the boundary layer flows on the wall and on the vane suction surface. Now the boundary layer growth on the vane suction surface was more rapid than on the pressure surface because of its more adverse chordwise pressure gradient. This is illustrated by the vane surface pressure distributions shown in figure 24 (table 14(d)) at all four instrumented locations. Thus the acute corners formed by the wall and the vane suction surfaces are believed to be more critical flow regions than those formed with the vane pressure (lower) surfaces (sketches in fig. 24). Vane surface pressure distributions are further discussed in a later section so entitled.

For corner 2 operating with corner 1 (fig. 21) the main differences in total pressure profiles at the various circumferential locations occurred at θ of 90° and 270°. The upstream presence of the corner 1 scoop and its afterbody is evident in the reduced total pressures across the corner 2 inlet (diffuser exit) at $\theta = 270°$. The corner 1 scoop also caused a unique corner 2 inlet pressure profile at $\theta = 90°$. The total pressure dip near 50-percent radius at the diffuser exit could reflect a vortex shed off the inner edge of the scoop afterbody, as previously discussed with figure 16. The large dropoff in total pressure at the corner 2 inlet from midradius to the outer wall at $\theta = 90°$ suggests some upstream flow separation from the wall, as previously discussed for this region.

With tip radial distortion imposed upstream of corner 1 the total pressure profiles across corner 2 with vanes A4 (fig. 22) are similar at the various circumferential locations shown. As

expected, the total pressure levels were lower at all θ locations with the 12.70-cm distortion screen (fig. 22(a–2)) than with the 6.35-cm distortion screen (fig. 22(a–1)).

With circumferentially distorted inflow the pressure profiles across corner 2 (fig. 23) were dependent on their θ location as expected. The profiles at θ of 45° and 315° are similar. These locations were symmetrical about the center of the screen sector at $\theta = 0°$. The pressure patterns were relatively flat behind the screen with little additional loss across corner 2 at $\theta = 0°$.

Comparisons of Total Pressure Profiles for Corner 2 with Vanes B and A4

With uniform inflow (fig. 25) vanes A4 had a slight advantage over vanes B in the core region of corner 2 at nearly every θ location. This suggests lower profile losses as previously discussed. Conversely vanes B had a slight advantage over vanes A4 over the outer half span for θ of 225° and 315°. The loading was less with the 28 vanes B than with the 22 vanes A4. Thus the flow in the acute corners formed by vane B suction surfaces and the wall was better able to finish the turn, which resulted in less loss. There appeared to be no significant difference between vanes B and A4 at $\theta = 90°$; upstream outer wall separation was indicated for both cases.

The overall loss coefficients for corner 2 operating downstream of corner 1 were 0.116 for vanes A4 and 0.127 for vanes B. The lower core flow losses with vanes A4 at nearly every θ location slightly outweighed the near-wall loss advantage with vanes B at θ of 225° and 315° when the overall corner loss was evaluated.

With tip radially distorted inflow (figs. 26 and 27) the pressure profiles had similar shapes at each θ location with either vanes A4 or B, but the A4 levels were slightly higher at most locations. The overall corner loss coefficients were mixed. With the 6.35-cm distortion screen the coefficients were 0.112 with vanes A4 and 0.122 with vanes B. With the 12.70-cm distortion screen the coefficients were 0.125 with vanes A4 and 0.101 with vanes B.

With circumferentially distorted inflow the pressure profiles for vanes A4 and B differed little at the various θ locations (fig. 28). This was confirmed by nearly equal values of corner 2 loss coefficients, 0.142 with vanes A4 and 0.139 with vanes B.

In summary, for corner 1 with the scoop installed upstream, corner 2 losses may be lower with the controlled-diffusion vanes (A4) than with the circular-arc vanes (B). Also, only 22 of the A4 vanes are required in contrast to 28 of the B vanes. However, these advantages need to be weighed against the more complex vane A4 cross section in selecting a design for application.

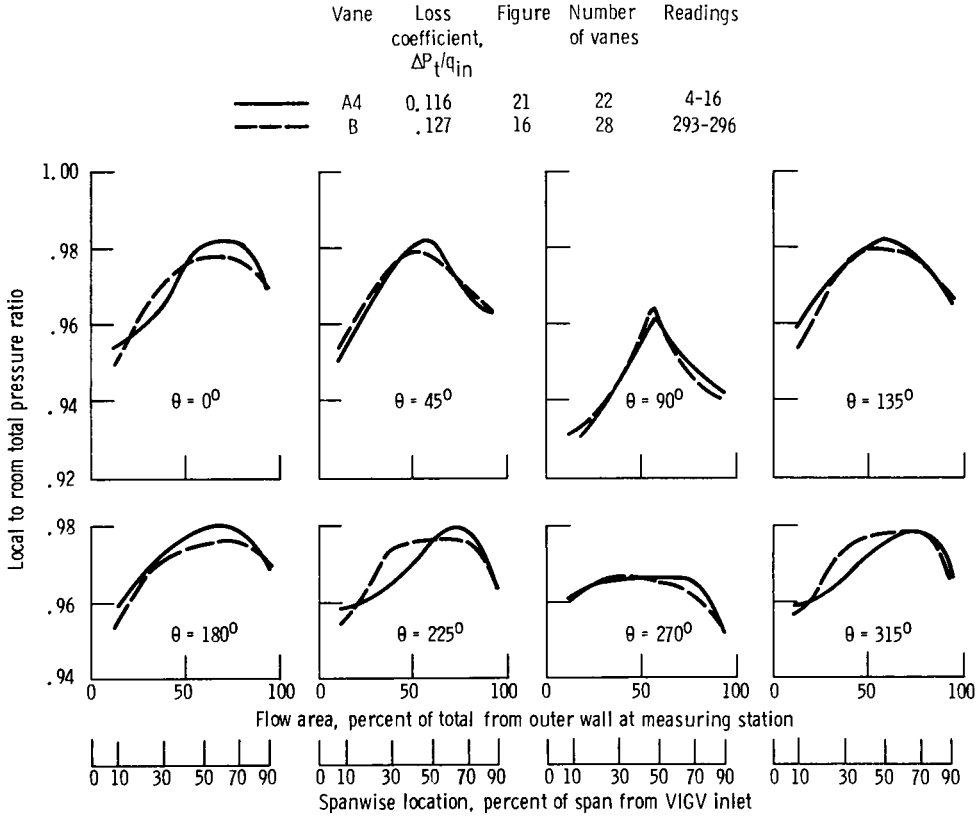

Figure 25.—Comparison of effects of vanes A4 and B in corner 2 with corner 1 upstream on the spanwise variation of VIGV inlet total pressure ratioed to room pressure at eight circumferential locations—uniform inflow. Nominal airflow, 73.1 kg/sec; nominal inlet Mach number, 0.255. (Faired curves from data in figures cited in key.)

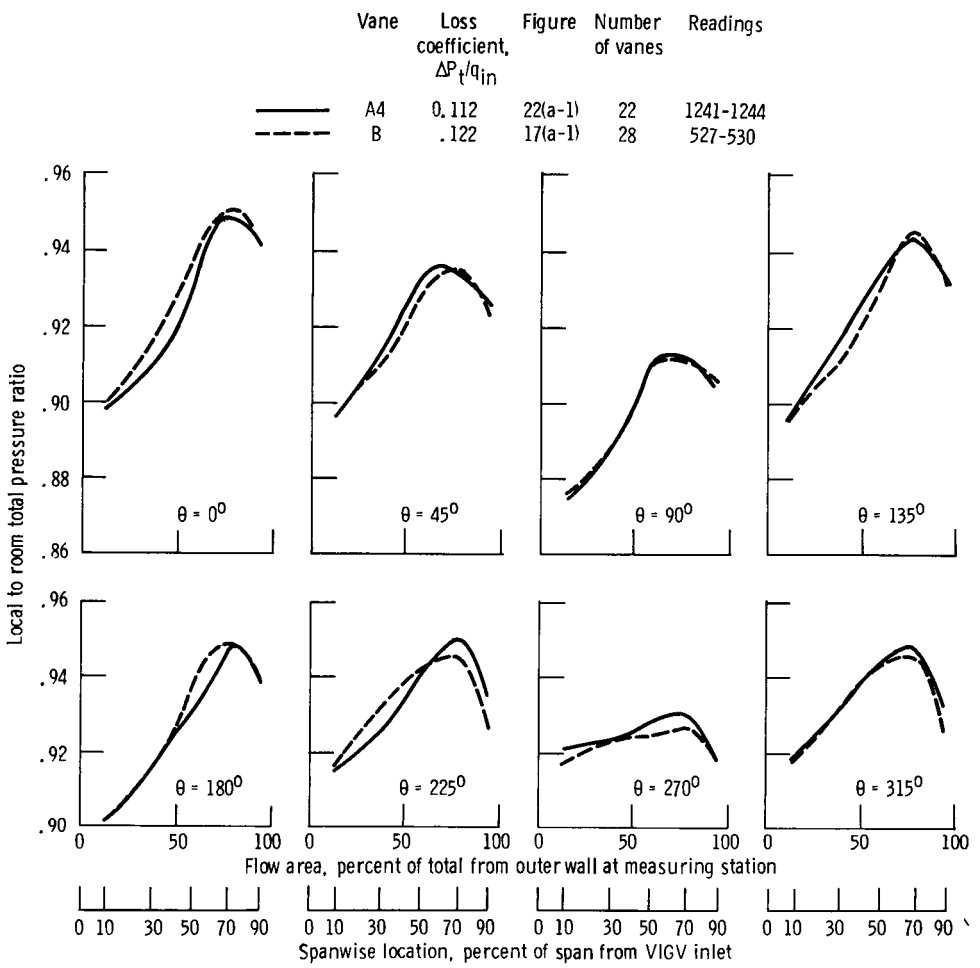

Figure 26.—Comparison of effects of vanes A4 and B in corner 2 with corner 1 upstream on the spanwise variation of VIGV inlet total pressure ratioed to room pressure at eight circumferential locations—tip inflow radially distorted with 6.35-cm screen. Nominal airflow, 72.0 kg/sec; nominal inlet Mach number, 0.253. (Faired curves from data in figures cited in key.)

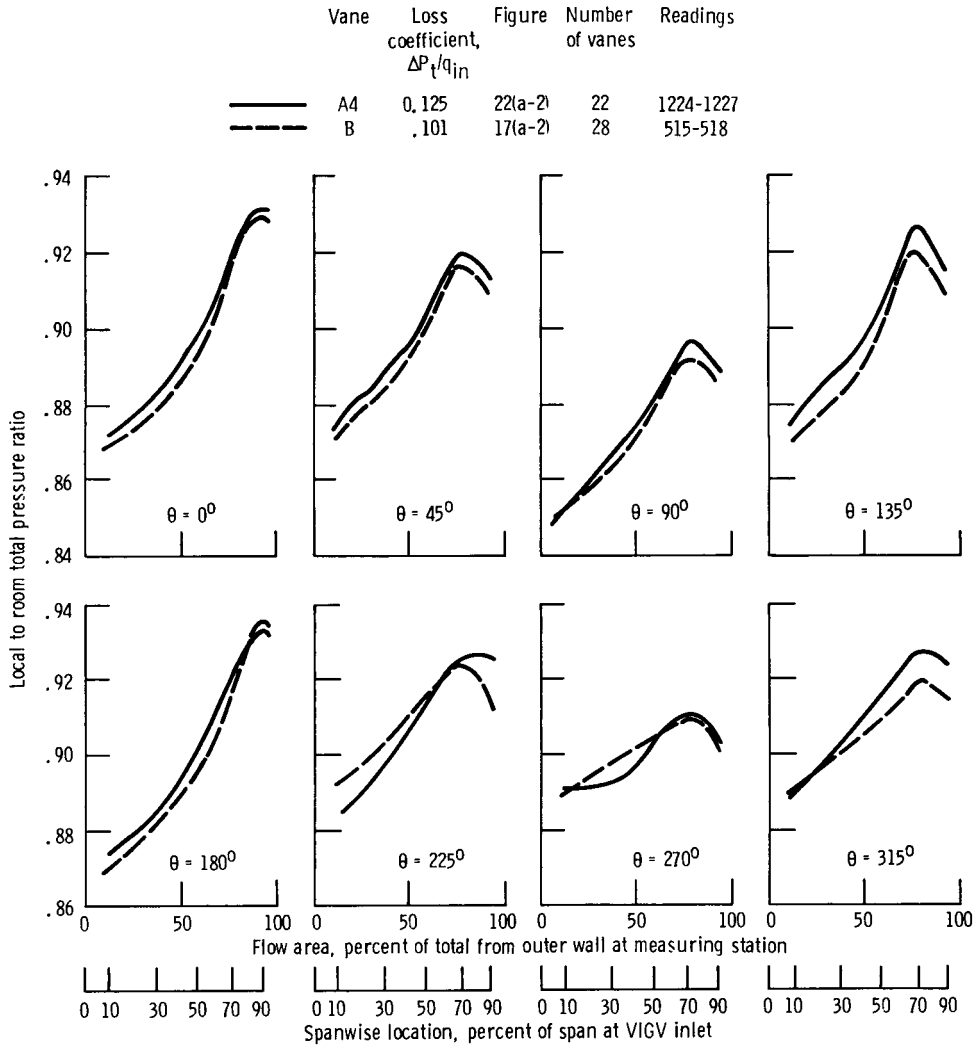

Figure 27.—Comparison of effects of vanes A4 and B in corner 2 with corner 1 upstream on the spanwise variation of VIGV inlet total pressure ratioed to room pressure at eight circumferential locations—tip inflow radially distorted with 12.70-cm screen. Nominal airflow, 72.0 kg/sec; nominal inlet Mach number, 0.253. (Faired curves from data in figures cited in key.)

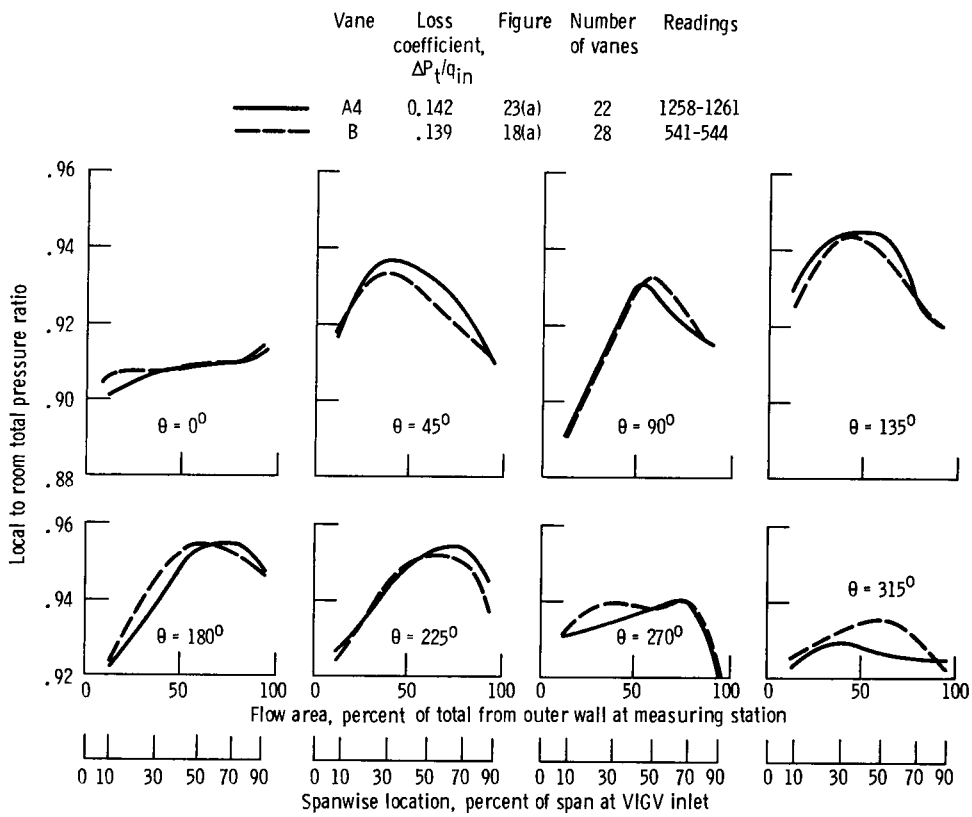

Figure 28.—Comparison of effects of vanes A4 and B in corner 2 with corner 1 upstream on the spanwise variation of VIGV inlet total pressure ratioed to room pressure at eight circumferential locations—inflow circumferentially distorted with ~50° sector screen. Nominal airflow, 73.5 kg/sec; nominal inlet Mach number, 0.257. (Faired curves from data in figures cited in key.)

Circumferential Variation of Pressures Near VIGV's

In this and the following section the character of the flow near the VIGV's is illustrated with typical pressure and Mach number distributions for various configurations of corner 2 operating downstream of corner 1. Such information may be useful in evaluating the design and performance of the tunnel drive fan since it is the next component in the circuit (fig. 1).

With the uniform inflow (fig. 29(a)) the circumferential variation of inlet and exit total pressures ratioed to room pressure across the VIGV's differed little between vanes A4 and B. Also, as expected, the VIGV exit total pressures followed the same pattern and level as the inlet values. The reason is that the VIGV exit probes were located midway between the vanes, not in their wake. The dips in total pressure at 90° and 270° at 50 percent of span reflected the presence of the horizontally biased centerbodies upstream. This was also evident near the walls (at 10 and 90 percent of span) except near the tip, where the 270° dip was replaced by ones about 70° to either side.

With tip radial distortion (fig. 29(b)) the total pressure patterns were generally similar to those for the uniform inflow, but the levels were lower because of the drop across the distortion screen. There was some difference at midspan, where an additional pressure dip occurred at about 200° with the radially distorted inflow. No significant differences were due to vane design.

With circumferentially distorted inflow from an approximately 50° sector screen (fig. 29(c)) the total pressure dip behind the upstream screen sector centered at $\theta = 0°$ was evident at 50 and 90 percent of span. However, at 10 percent of span the pressure pattern was more like those at the same span for either uniform or radially distorted inflow. As before, vane design did not significantly affect the total pressure results.

The VIGV exit static pressure distributions around the circumference (fig. 30) were interpolated from the inner and outer wall taps. Generally static pressure differed little across the span at any θ location. The circumferential variation was also small, and the difference due to vane design was negligible. Only the pressure levels differed as a direct result of the different inflow conditions. From the total and static pressure distributions at the VIGV exit (figs. 29 and 30) local Mach numbers were determined.

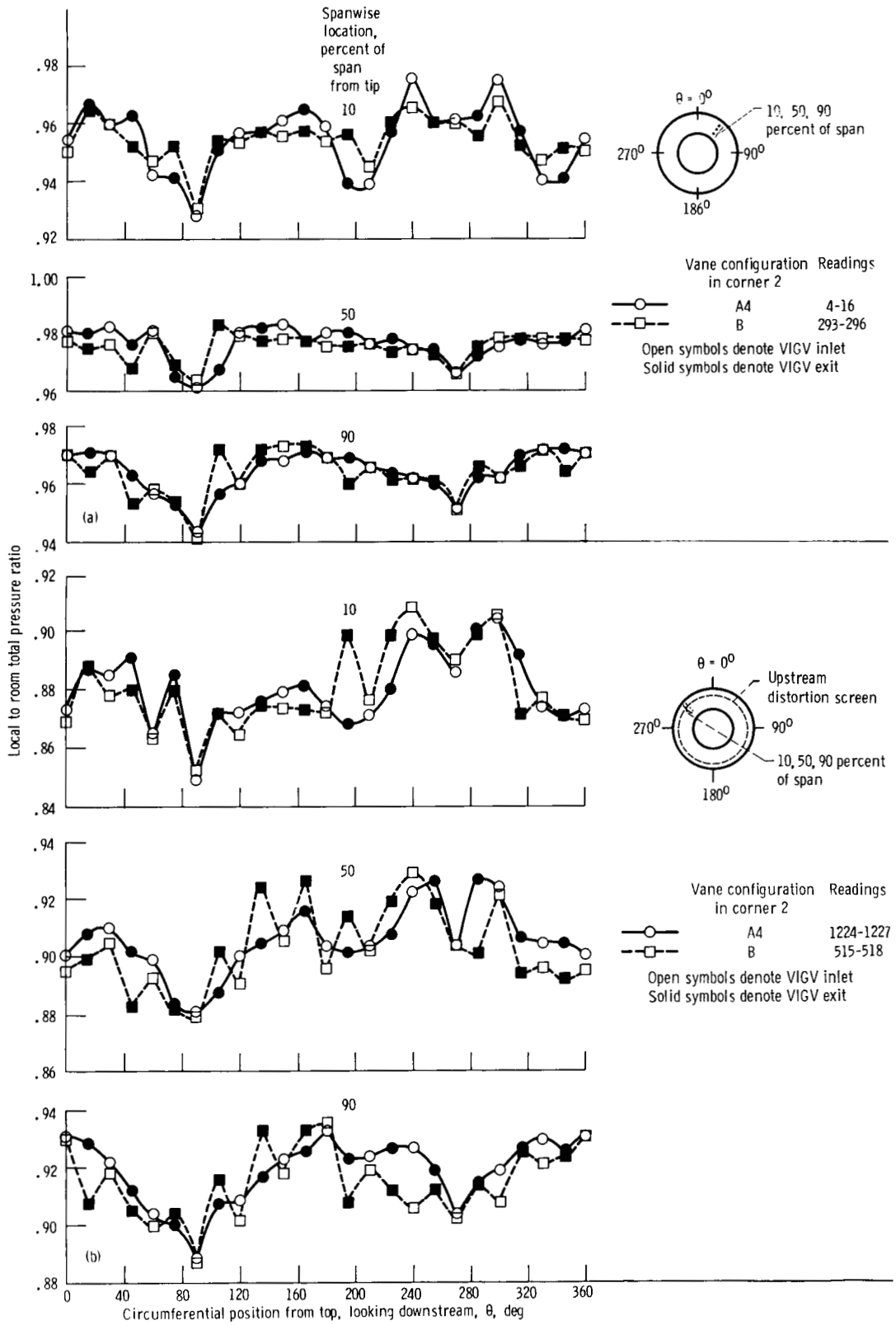

(a) Uniform inflow.
(b) Tip inflow radially distorted with 12.70-cm screen.

Figure 29.—Circumferential variation of VIGV inlet and exit total pressures ratioed to room pressure at three spanwise locations. Corner 1 with vane A10 plus corner 2 with either vanes A4 or B; nominal airflow, 73.0 kg/sec; nominal corner 1 inlet Mach number, 0.395.

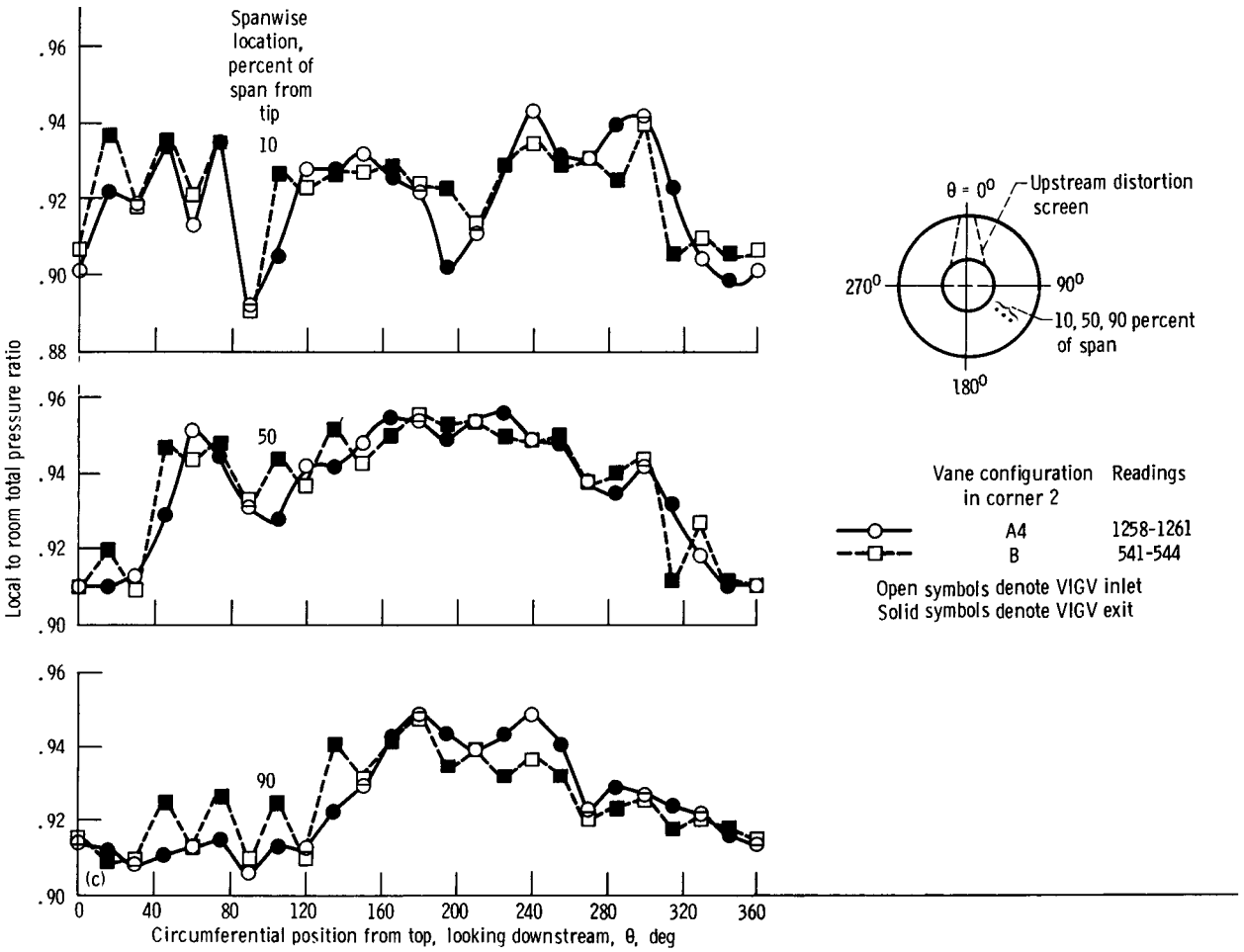

(c) Inflow circumferentially distorted with ~50° sector screen.

Figure 29.—Concluded.

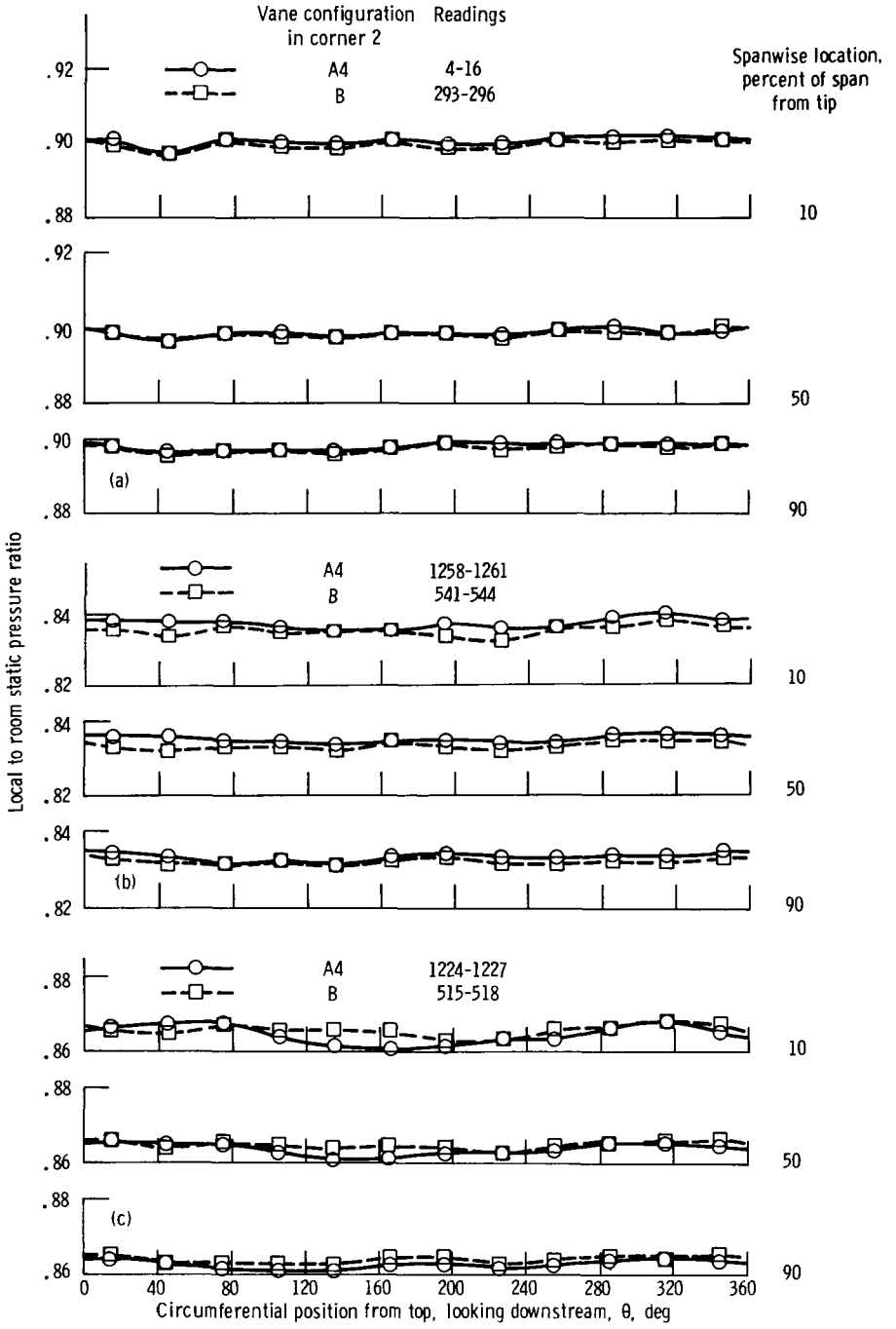

(a) Uniform inflow.
(b) Tip inflow radially distorted with 12.70-cm screen.
(c) Inflow circumferentially distorted with ~50° sector screen.

Figure 30.—*Circumferential variation of* VIGV *exit static pressure ratioed to room pressure for three inflow conditions to corner 1 with effects of* corner 2 vane design indicated. Nominal airflow, 73.0 kg/sec; nominal corner 1 inlet Mach number, 0.395.

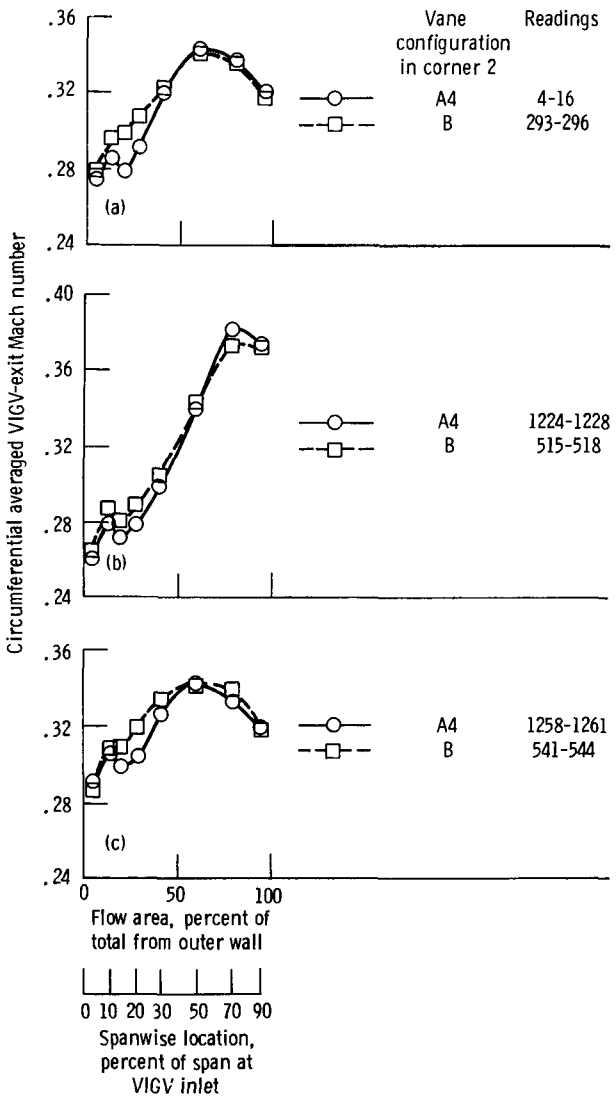

(a) Uniform inflow.
(b) Tip inflow radially distorted with 12.70-cm screen.
(c) Inflow circumferentially distorted with ~50° sector screen.

Figure 31.—Spanwise variation of circumferentially averaged VIGV exit Mach number for three inflow conditions to corner 1 with vanes A10 plus corner 2 with either vanes A4 or B. Nominal airflow, 73.0 kg/sec; nominal corner 1 inlet Mach number, 0.395.

VIGV Exit Mach Number Profiles

The circumferentially averaged Mach number profiles were nearly the same with either vanes A4 or B in corner 2 irrespective of the inflow condition (fig. 31). Also, there was little difference between the uniform inflow and the small-sector circumferentially distorted inflow. The maximum spanwise difference in Mach number in either figure 31(a) or (c) was from about 0.28 near the tip (outer wall) to about 0.34 near midspan. For the proposed tunnel drive fan with a design tip speed of 221 m/sec (724 ft/sec) this maximum difference in fan inlet Mach number resulted in a maximum change in inlet air angle of about 4°. With the 12.70-cm tip radial distortion screen (fig. 31(b)) the maximum difference in inlet air angle at design fan speed was about 7° from the outer to the inner wall.

Although the circumferentially averaged Mach number profiles were nearly the same with uniform inflow or with small-sector circumferentially distorted inflow with either vane design, both θ location and vane design differences are evident in figures 32(a) and (c). With uniform inflow (fig. 32(a)) the spanwise extremes varied less with θ location for vanes B than for vanes A4. With circumferentially distorted inflow (fig. 32(c)) the regions nearest the screen wake (θ of 15° and 315°) had less spanwise Mach number variation with vanes A4 than with vanes B. However, at $\theta = 195°$ vanes B had less of a Mach number gradient than vanes A4. We believe the effects of such differences on tunnel drive fan performance to be small.

The largest differences in VIGV exit Mach number profiles due to θ location or vane design occurred for tip radial distortion with the 12.70-cm screen (fig. 32(b)). Near the outer wall at $\theta = 195°$ the Mach number was about 0.23 with vanes A4 but 0.33 with vanes B. An opposite trend with about half the magnitude change occurred at $\theta = 315°$. Again we believe these local differences due to θ location and vane design to be insignificant in terms of expected fan performance.

To conclude this section on VIGV exit Mach number profiles, let us consider the effects of resetting the aft part of the VIGV $\pm 10°$ for uniform inflow with vanes A4 in corner 2 (fig. 33). The faired data for the 0° reset of the VIGV's are also indicated. In general the VIGV reset had little effect on the Mach number profiles. The maximum change in Mach number from a reset of $\pm 10°$ was about 0.04 near the outer wall at $\theta = 195°$. At some θ locations reset had little effect on Mach number. The effect on inlet air angle was much greater, of course. Assuming no separation of flow from the surfaces of the VIGV's with reset, the change in inlet air angle would directly follow the amount of reset in degrees. Such changes in inlet air angle to the fan will affect its useful range of operation between wide-open-throttle and fan-stall flow rates. This is why, of course, such VIGV reset capability is provided.

Static Pressure Distributions on Walls and Fairings

The axial distributions of wall static pressure around the configuration of corner 1 (with vanes A10) coupled to corner 2 (with either vanes A4 or B) at design inflow conditions are described here for the different parts of the assembly. This section indicates the general behavior of the flow along the walls and illustrates the detail contained in the tables.

Upstream of corner 1.—Generally the local static to room pressure patterns were the same for all inflow conditions with either vanes A4 or vanes B in corner 2 (fig. 34). However, the overall levels were lower with inlet distortion. Because the loss in total pressure from stations 1 to 20 was minimal, these static pressure patterns indicated flow acceleration along

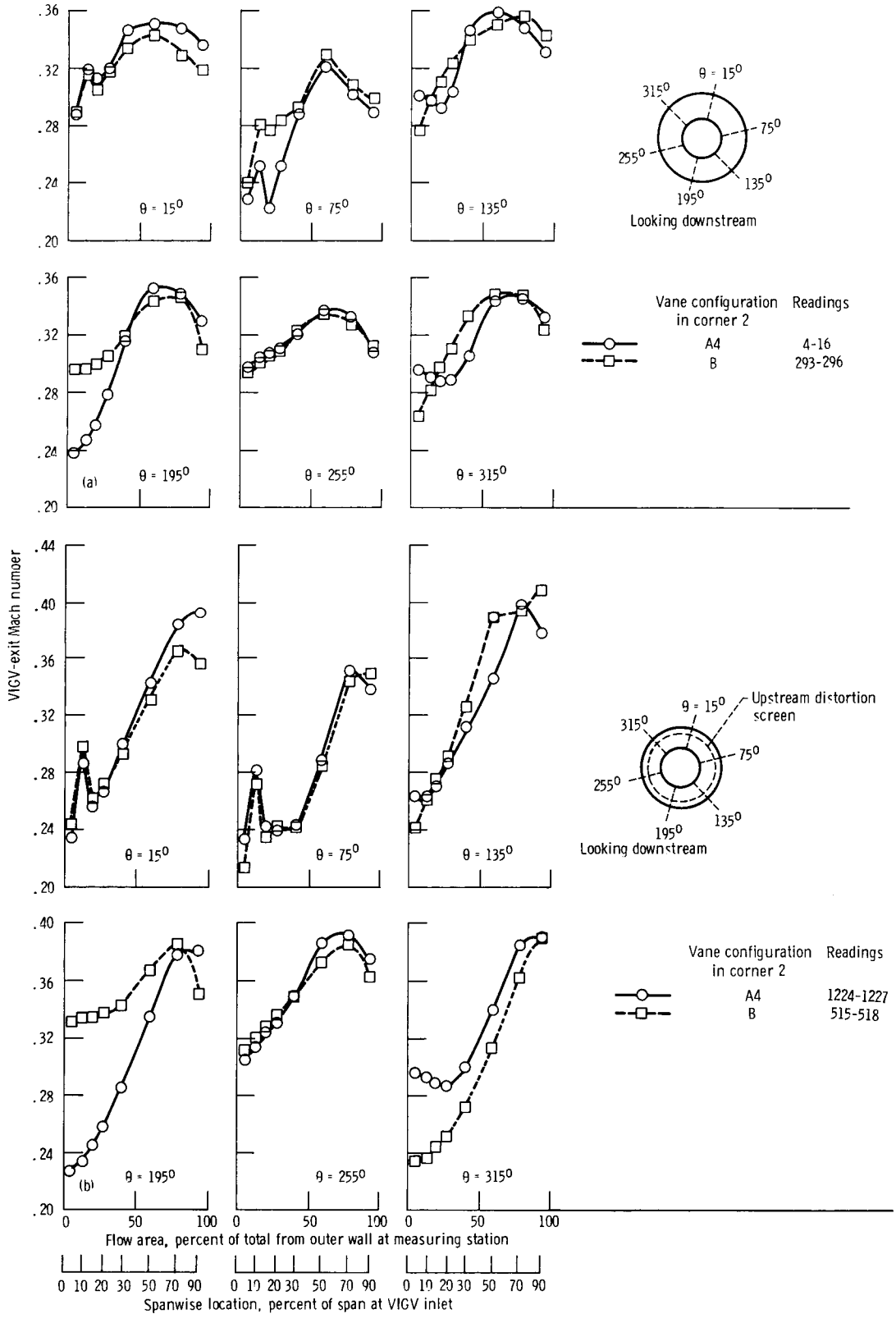

(a) Uniform inflow.
(b) Tip inflow radially distorted with 12.70-cm screen.

Figure 32.—Spanwise variation of VIGV exit Mach number at six circumferential locations. Corner 1 with vanes A10 plus corner 2 with either vanes A4 or B. Nominal airflow, 73.0 kg/sec; nominal corner 1 inlet Mach number, 0.395.

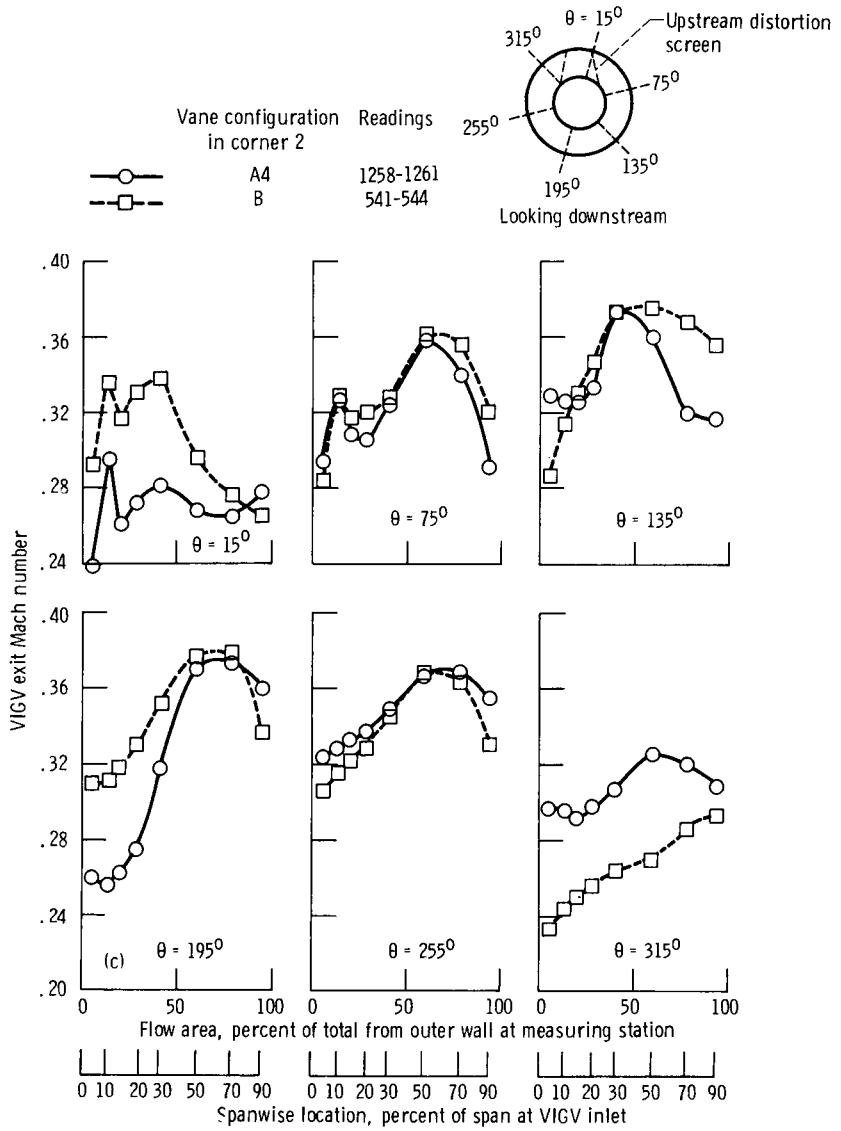

(c) Inflow circumferentially distorted with ~50° sector screen.

Figure 32.—Concluded.

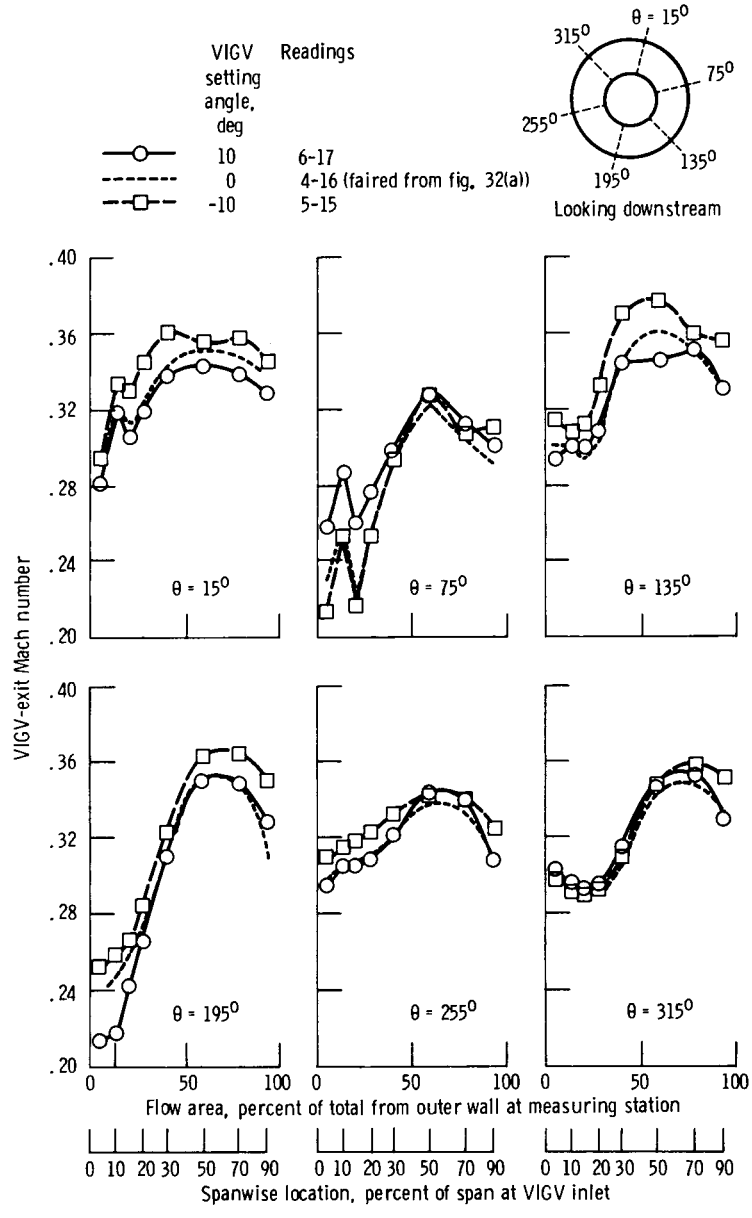

Figure 33.—Effects of VIGV setting angle on the spanwise variation of VIGV exit Mach number at six circumferential locations. Corner 1 with vanes A10 plus corner 2 with vanes A4. Nominal airflow, 72.9 kg/sec; nominal corner 1 inlet Mach number, 0.395; uniform inflow.

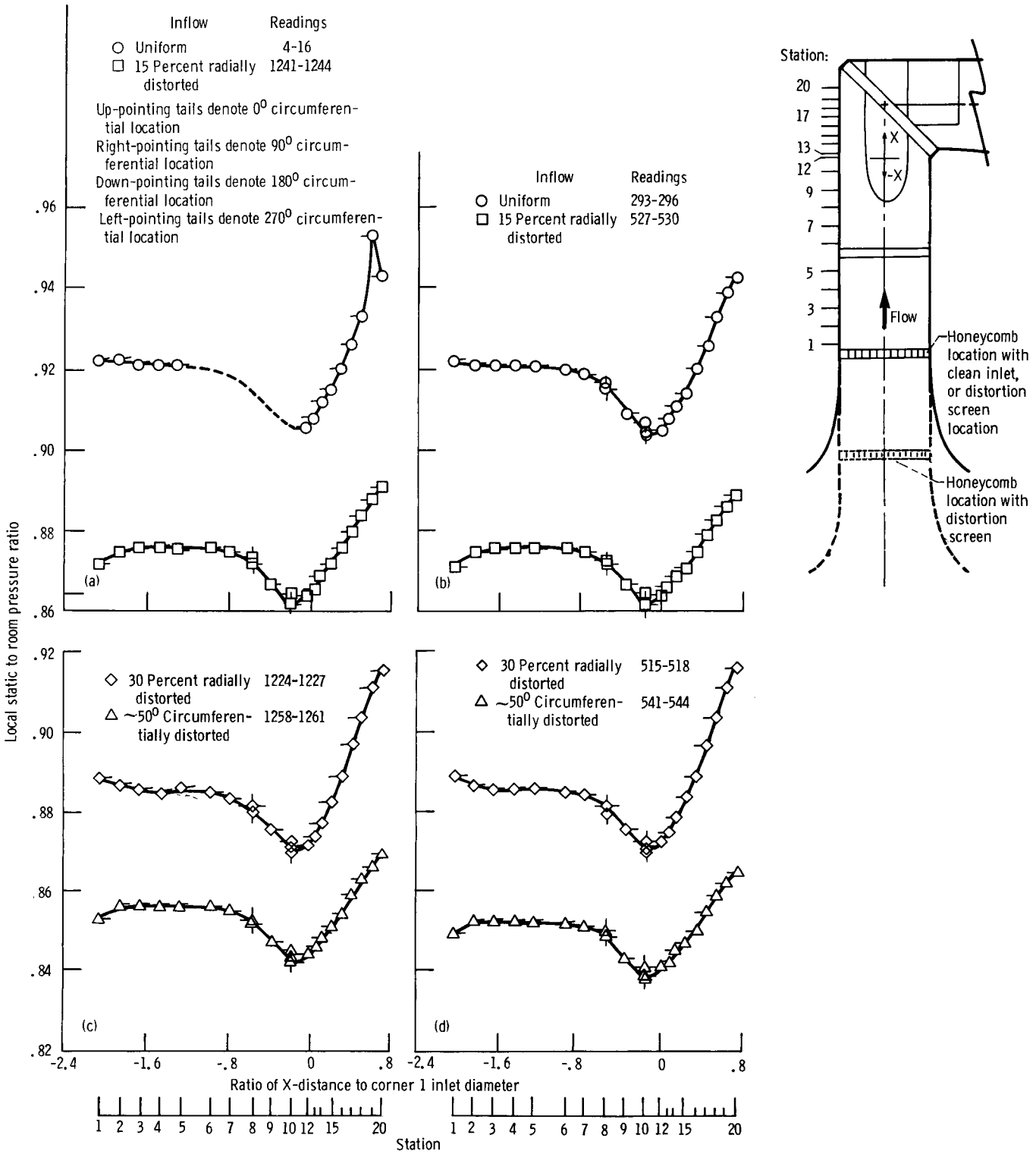

(a) Vanes A4 in corner 2, comparing uniform and 15-percent radially distorted inflow.
(b) Vanes B in corner 2, comparing uniform and 15-percent radially distorted inflow.
(c) Vanes A4 in corner 2, comparing 30-percent radially distorted and ~50° circumferentially distorted inflow.
(d) Vanes B in corner 2, comparing 30-percent radially distorted and ~50° circumferentially distorted inflow.

Figure 34.—Axial wall static pressure distribution upstream of corner 1 (with vanes A10) with and without inlet distortion. Nominal airflow, 72.7 kg/sec; nominal corner 1 inlet Mach number, 0.395 (station 12).

the tunnel walls starting at about one-half centerbody diameter upstream of the centerbody. This continued and was the same for all θ's until the maximum centerbody thickness was reached at about station 10. From there the measurements along the outer wall ($\theta = 270°$) indicated a flow deceleration to velocity levels at station 20 that were lower than those at station 1. As discussed in reference 4 the simulated scoop and its afterbody fairing in corner 1 blocks and thus slows some of the flow near the outer wall. Since the total oncoming flow rate does not change, some of this outer flow must be diverted inward. For undistorted, or uniform, inlet flow approximate flow Mach numbers along the outer wall ($\theta = 270°$) calculated from the local static to room pressure ratios shown were 0.35, 0.38, and 0.29 at stations 1, 10, and 20, respectively.

Crossleg diffuser and inlet to corner 2.—In the diffuser section (fig. 35), stations 34 to 47, the wall static pressure patterns with uniform inlet flow were similar irrespective of the vane design in corner 2 as expected. The circumferential variation in the diffuser flow was slight but consistent, with higher static pressures along $\theta = 270°$ than along $\theta = 90°$. This trend was also apparent with distorted inflow.

Except for $\theta = 270°$ pressures in the inlet section to corner 2 (fig. 35), stations 48 to 53, were relatively constant because of the constant duct diameter. At $\theta = 270°$ the wall pressures continued to increase throughout the corner inlet. This was caused by the blockage effects of the centerbody, which had its major axis along $\theta = 270°$ (fig. 10). Aft of this centerbody at station 53 the pressure at $\theta = 270°$ returned approximately to its preblockage level at station 48.

The corner 2 inlet pressure patterns changed little with various types of inlet distortion. However, an overall level shift occurred in the ratios because of a reduction in wall pressures that was comparable to the total pressure reduction across the distortion screens (figs. 14 and 19).

Downstream of corner 2.—Along the outer wall, at $\theta = 270°$ and for stations 57 to 60 just downstream of the corner vanes, the wall pressures were a little higher with vanes B in the corner than with vanes A4, for both uniform and distorted inflow conditions (fig. 36). With uniform inflow total pressures along the outer wall at $\theta = 270°$ were essentially the same with either vanes B or A4 (figs. 16(a) and 21(a)). Thus the higher wall pressures downstream of vanes B indicated a slightly slower flow in this region with vanes B. Since the physical flow areas were the same, apparently the vane and wall boundary layers caused slightly less blockage in the stream with vanes B. Similar trends were noted with distorted inflow. However, from stations 61 to 75 the difference due to vane design was negligible with or without distorted inflow. At station 79, near the VIGV's, the wall pressures at θ of 0° and 90° were nearly equal to but consistently lower than those at θ of 180° and 270°, which were also nearly equal. This slight flow skewness appeared irrespective of inflow conditions, but its cause was not readily apparent.

Corner 2 shaft fairing.—The static pressures for the corner 2 shaft fairing centerbody at $\theta = 270°$ matched those along the outer wall at the same θ (fig. 37), as expected. At $\theta = 90°$ and for stations 54 to 60 the centerbody pressures were close to the total pressure values for comparable inflow conditions (figs. 16 to 18 and 21 to 23). This suggested a stagnation of the oncoming flow. Just ahead of the vanes (stations 54 to 57) and along the top and bottom of the fairing (θ of 0° and 180°) static pressures were relatively low for all cases. This reflected the accelerating flow caused by blockage at the maximum fairing thickness (see end view in fig. 37 sketch). The top and bottom pressures on the fairing showed a sharp decline from stations 63 to 78. Again this reflected accelerating flow caused by the increasing blockage as the drive fan centerbody was encountered. Its maximum diameter occurred near station 78. The fairing pressures from stations 54 to 78 were nearly equal at θ of 0° and 180°, indicative of flow symmetry about the horizontal plane.

Cascade inlet plane to corner 2.—The local static to room pressure ratio distribution around the cascade inlet plane as a function of circumferential location is shown in figure 38. The horizontal scale is double valued to illustrate the data symmetry about the horizontal plane. Uniform inflow data for corner 2 alone (from ref. 6) are presented (figs. 38(a) and (b)) for a convenient reference to the other parts of the figure. The total pressures in the cascade inlet plane of corner 2 without corner 1 upstream were essentially constant around the circumference (see diffuser exit values in figs. 15(a) and 20(a)). Thus the static pressure patterns in figures 38(a) and (b) can be used to infer velocity and flow patterns. The cascade inlet flow was more uniform around the duct with vanes A4 in corner 2 than with vanes B (fig. 38(b)). With vanes B the flow has been skewed so that less is in the outer half ($180° < \theta < 360°$) and more is in the inner half ($0° < \theta < 180°$). However, the skewing was not large since the maximum variation in inlet Mach number was from about 0.263 at $\theta = 270°$ to about 0.293 at $\theta = 90°$. The maximum static pressure occurred at $\theta = 270°$ for either vane design. As indicated in reference 6, this may be attributed to being in the wake of the downstream edge of the shaft fairing (see sketch in fig. 37). The pressure patterns where corner 2 is preceded by corner 1 (fig. 38(c)) were similar to those for corner 2 alone.

With distorted inflow imposed ahead of corner 1 (figs. 38(d) to (f)) the flow shifted slightly more from the outer to the inner half. But as with uniform inflow this shift was somewhat less with vanes A4 than with vanes B, except for the 12.70-cm radial distortion, where the reverse occurred. Circumferential distortion (fig. 38(f)) resulted in less horizontal symmetry than for the other inflow conditions. Lower pressures or more flow appeared over the central part of the lower elliptical cross section than over the upper part. This seemed a reasonable shift when the location of the circumferential distortion screen was considered (see fig. 12(c)).

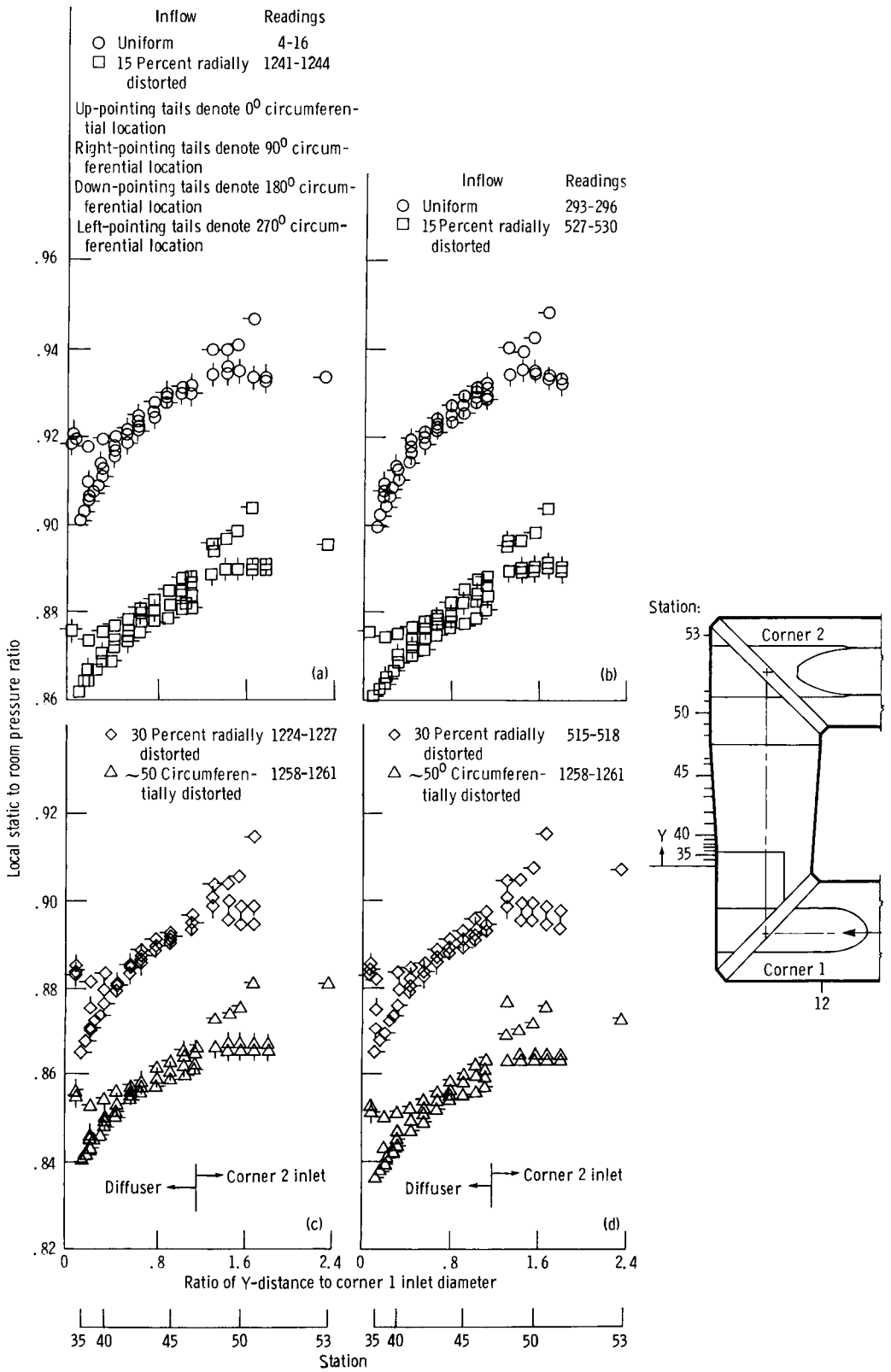

(a) Vanes A4 in corner 2, comparing uniform and 15-percent radially distorted inflow.
(b) Vanes B in corner 2, comparing uniform and 15-percent radially distorted inflow.
(c) Vanes A4 in corner 2, comparing 30-percent radially distorted and ~50° circumferentially distorted inflow.
(d) Vanes B in corner 2, comparing 30-percent radially distorted and ~50° circumferentially distorted inflow.

Figure 35.—Axial wall static pressure distribution on crossleg diffuser and corner 2 inlet with and without inlet distortion. Nominal airflow, 72.8 kg/sec; nominal corner 1 inlet Mach number, 0.395 (station 12).

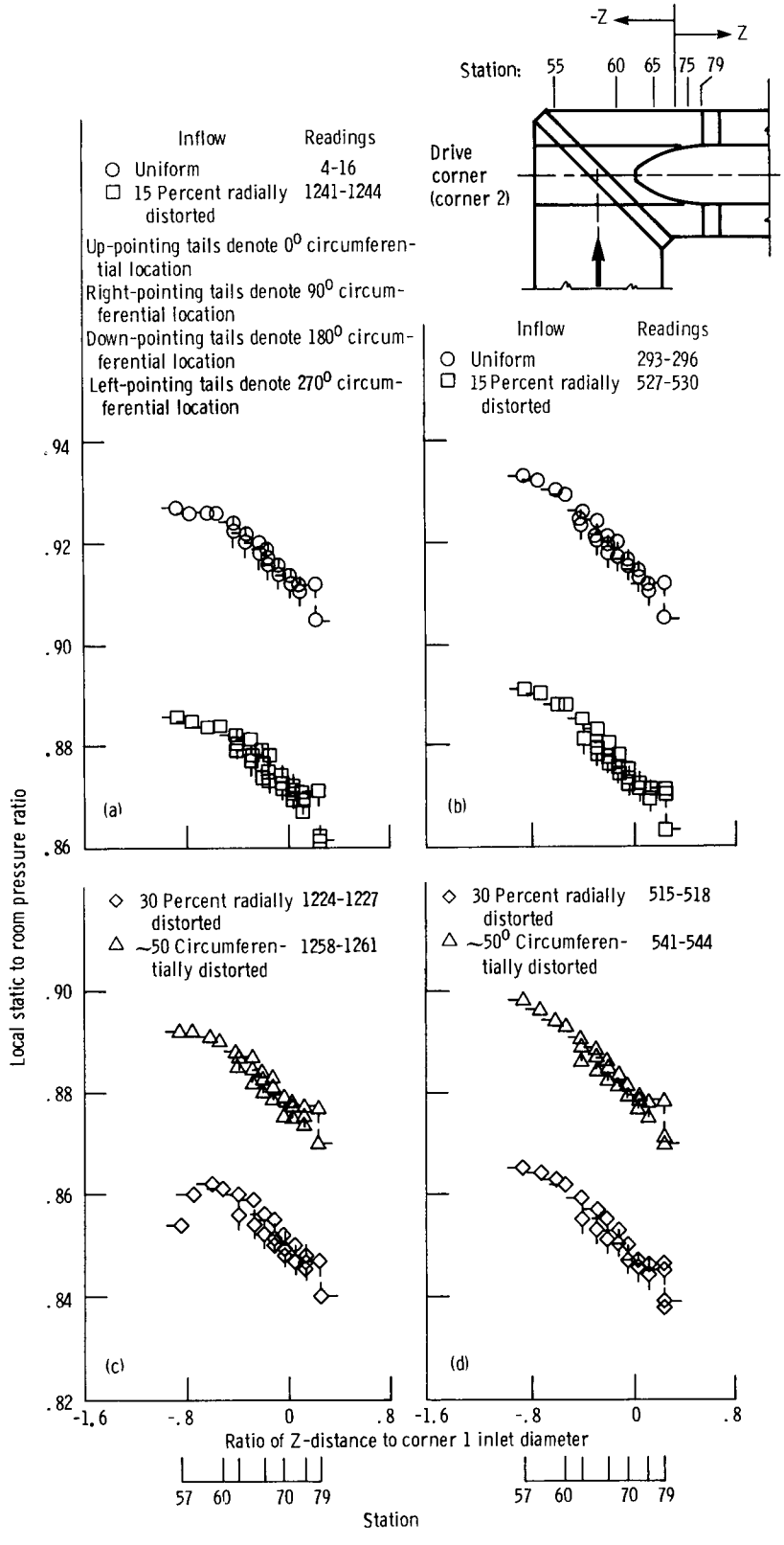

(a) Vanes A4 in corner 2, comparing uniform and 15-percent radially distorted inflow.
(b) Vanes B in corner 2, comparing uniform and 15-percent radially distorted inflow.
(c) Vanes A4 in corner 2, comparing 30-percent radially distorted and ~50° circumferentially distorted inflow.
(d) Vanes B in corner 2, comparing 30-percent radially distorted and ~50° circumferentially distorted inflow.

Figure 36.—Axial wall static pressure distribution on corner 2 outlet with and without inlet distortion. Nominal airflow, 72.8 kg/sec; nominal corner 1 inlet Mach number, 0.395 (station 12).

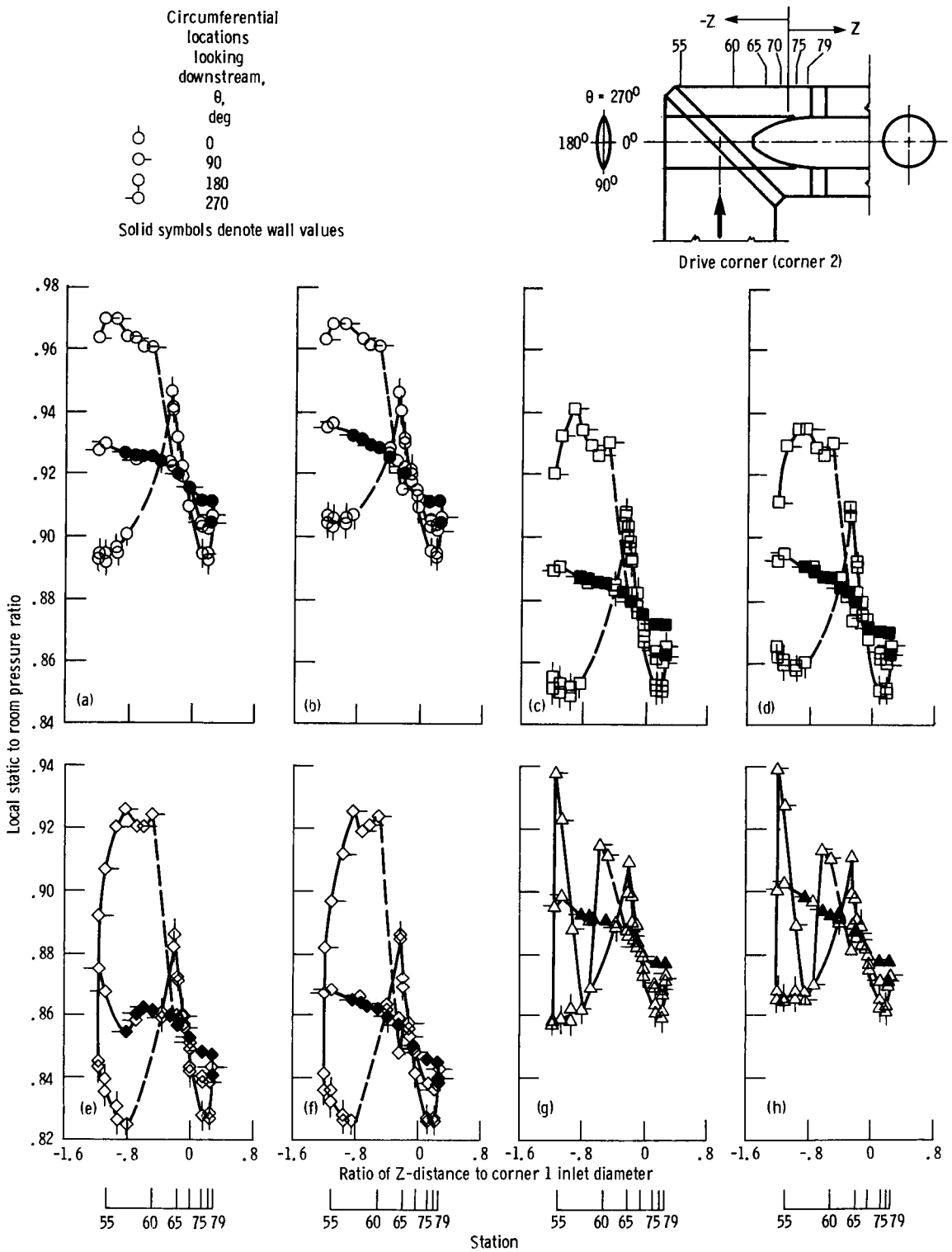

(a) Vanes A4 in corner 2, uniform inflow (readings 4 to 16).
(b) Vanes B in corner 2, uniform inflow (readings 293 to 296).
(c) Vanes A4 in corner 2, 15-percent radial distortion (readings 1241 to 1244).
(d) Vanes B in corner 2, 15-percent radial distortion (readings 527 to 530).
(e) Vanes A4 in corner 2, 30-percent radial distortion (readings 1224 to 1227).
(f) Vanes B in corner 2, 30-percent radial distortion (readings 575 to 578).
(g) Vanes A4 in corner 2, ~50° circumferential distortion (readings 1258 to 1261).
(h) Vanes B in corner 2, ~50° circumferential distortion (readings 541 to 544).

Figure 37.—Axial static pressure distribution on corner 2 shaft fairing and adjacent walls with and without inlet distortion. Nominal airflow, 72.8 kg/sec; nominal corner 1 inlet Mach number, 0.395 (station 12).

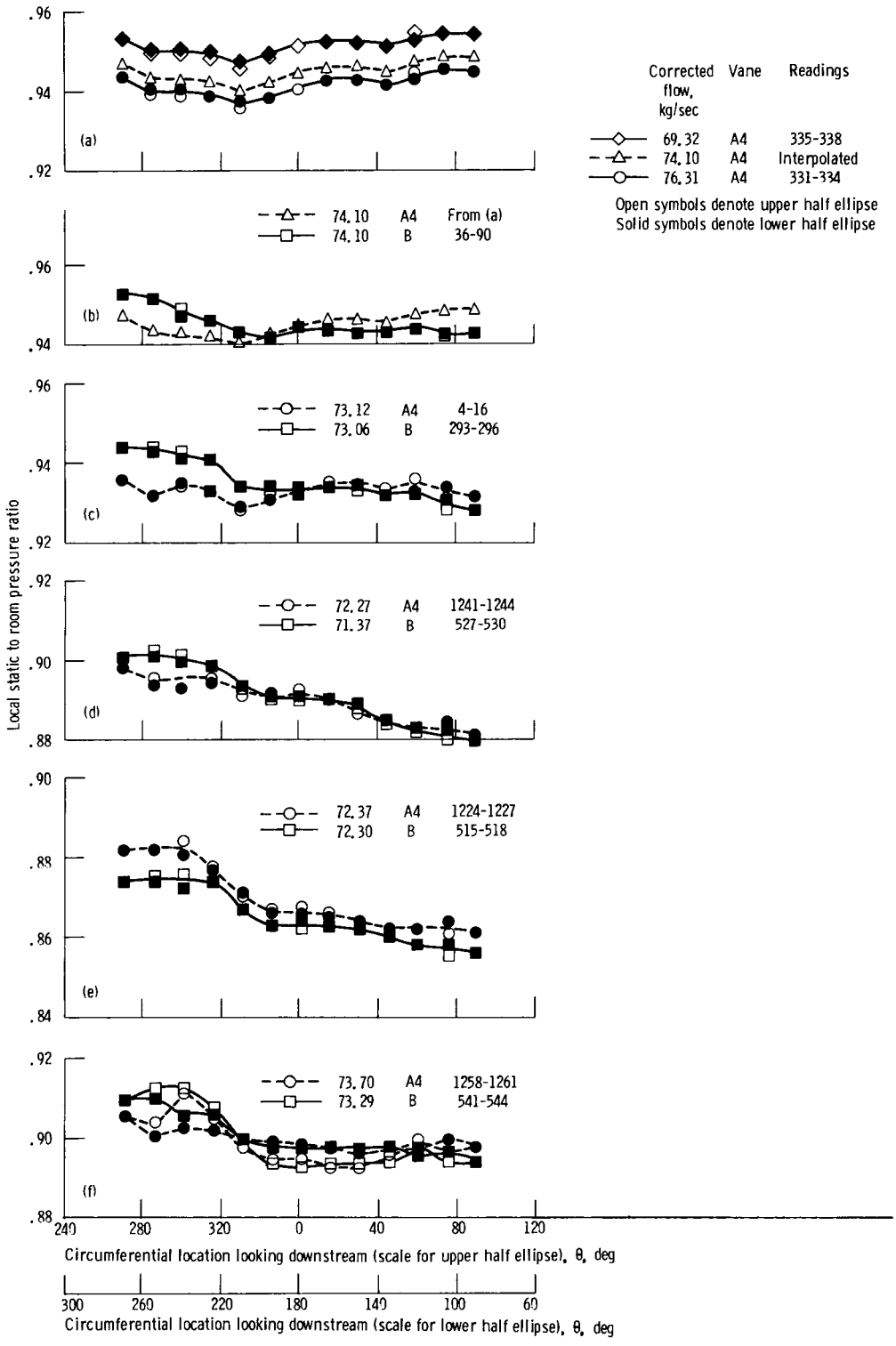

(a) Uniform inflow to corner 2 alone with vanes A4 (ref. 6).
(b) Uniform inflow to corner 2 alone with vanes B (ref. 6).
(c) Uniform inflow to corner 1 plus corner 2.
(d) Inflow radially distorted with 6.35-cm screen.
(e) Inflow radially distorted with 12.70-cm screen.
(f) Inflow circumferentially distorted with ~50° sector screen.

Figure 38.—Effects of various upstream conditions and vane design in corner 2 on static pressure distribution around cascade inlet plane to corner 2. Nominal inlet Mach number to corner 2, 0.255.

Vane Surface Pressure Distributions

Some of the surface pressure data for vanes B and A4 operating in corner 2 with corner 1 upstream are shown in figures 39 to 42. Only data behind the central pair of vanes are shown, but all the data are contained in tables 7 and 21 for vanes B and tables 14 and 28 for vanes A4. Comparisons are made with similar data from an isolated corner 2 (ref. 6). The effects of imposed flow distortion upstream of corner 1 are also shown.

Vanes B.—With uniform inflow neither corner 1 nor the radius from the wall locations above or below the shaft fairing had a significant effect on the pressure distributions (figs. 39(a) and 40(a)). The strong adverse pressure gradient on the upper (suction) surface near the trailing edge actually started near 80 percent of chord, although nearly 90 percent of chord had been predicted. The boundary layer on this surface was likely to separate before the trailing edge, resulting in somewhat higher two-dimensional or profile losses than with a non-separated layer. Other than the premature separation on the suction surface the remaining pressure distribution patterns agreed reasonably well with predictions, especially for the measurement location above the shaft fairing (fig. 39(a)).

With distorted inflow sizable differences occurred in pressure distribution between the above-shaft location at 0.2 radius from the wall (fig. 39(b)) and the below-shaft location at 0.57 radius (fig. 40(b)). The 0.2-radius-from-the-wall location was well within the low total pressure region behind the various distortion screens as shown in figures 17 and 18 for $\theta = 0°$. In this region the inlet Mach numbers were only about 0.15 based on the static pressures from figure 37 and the total pressures from figures 17 and 18. The resulting pressure distributions show less-negative pressures on the upper surface and more-positive pressures on the lower surface than with uniform inflow. Below the shaft fairing at 0.57 radius from the wall the total pressures ahead of the vanes were relatively high (figs. 17 and 18 for $\theta = 180°$) with resulting inlet Mach numbers of about 0.30 in contrast to a design value of about 0.26. This resulted in lower than design surface pressures on the upper surface of the vanes (fig. 40(b)).

Vanes A4.—With uniform inflow again neither corner 1 nor the radius from the wall locations above or below the shaft fairing had a significant effect on the pressure distributions (figs. 41(a) and 42(a)). These pressures agreed well with those predicted by the analysis code of reference 8 for the vane A design (ref. 4) operating at a setting angle 5° less than design. On the upper surface near the trailing edge the pressure data show no signs of significant boundary layer separation. The two-dimensional or profile losses are thus likely to be less for vanes A4 than for vanes B. Such is shown to be true in references 5 and 11.

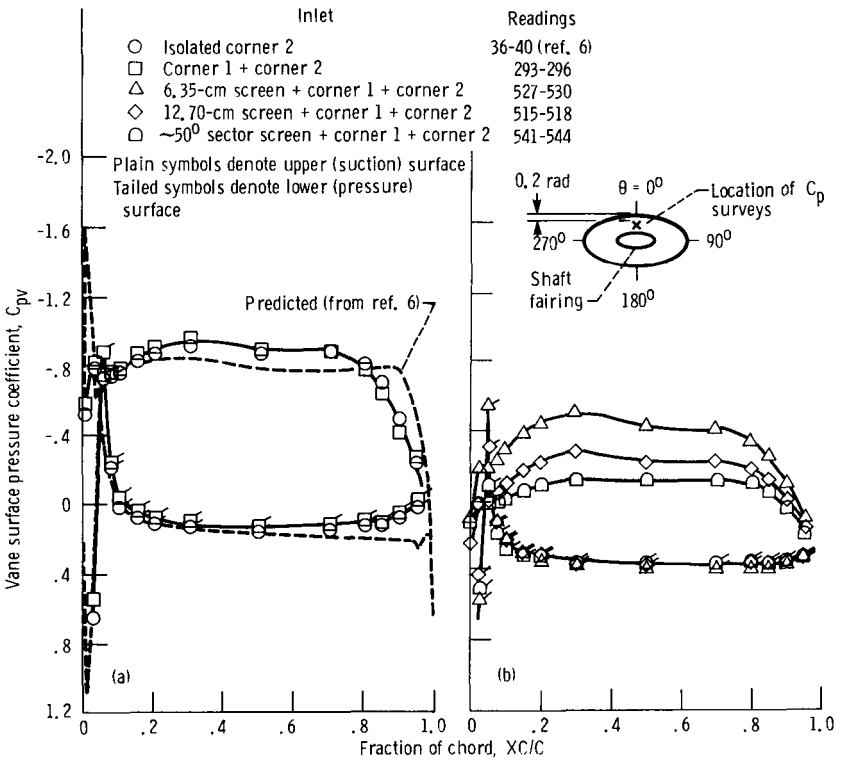

(a) Uniform inflow.
(b) Distorted inflow.

Figure 39.—Vane surface pressure distributions on vanes B in corner 2, near-wall region of central vanes at 0.2 radius from wall above shaft fairing, with and without inlet distortion. Nominal airflow, 72.8 kg/sec; nominal corner 2 inlet Mach number, 0.26.

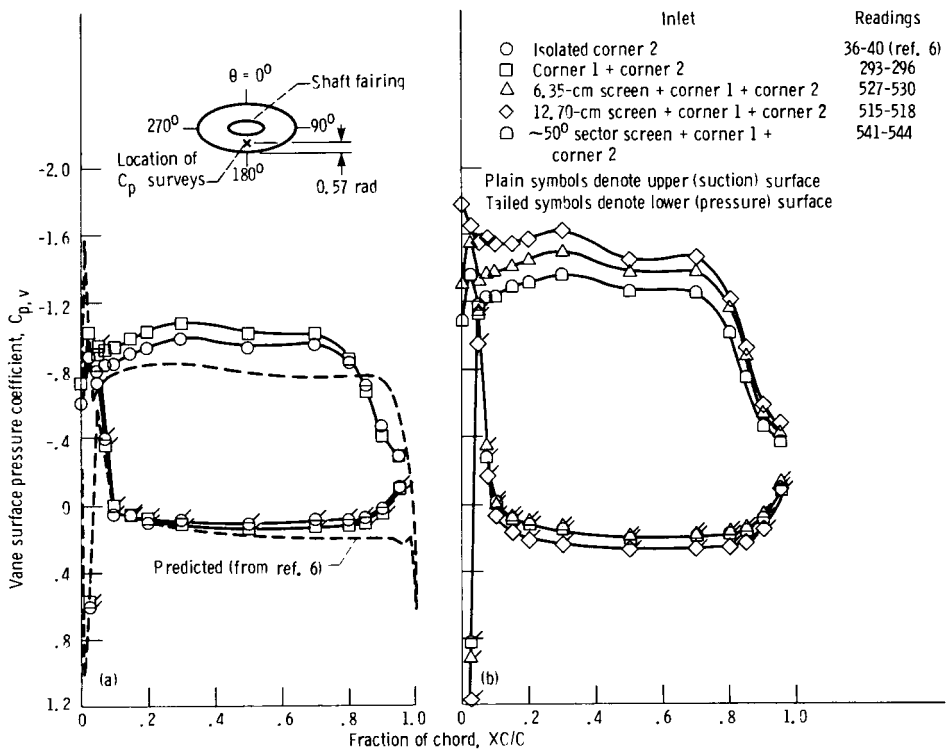

(a) Uniform inflow.
(b) Distorted inflow.

Figure 40.—Vane surface pressure distributions on vanes B in corner 2, midspan region of central vanes at 0.57 radius from wall below shaft fairing, with and without inlet distortion. Nominal airflow, 72.8 kg/sec; nominal corner 2 inlet Mach number, 0.26.

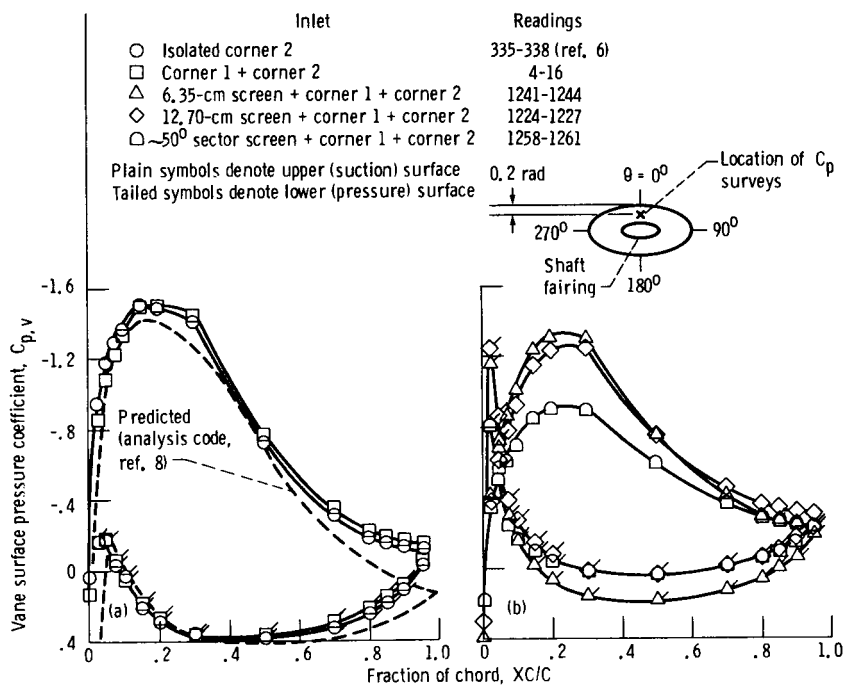

(a) Uniform inflow.
(b) Distorted inflow.

Figure 41.—Vane surface pressure distributions on vanes A4 in corner 2, near-wall region of central vanes at 0.2 radius from wall above shaft fairing, with and without inlet distortion. Nominal airflow, 72.2 kg/sec; nominal corner 2 inlet Mach number, 0.25.

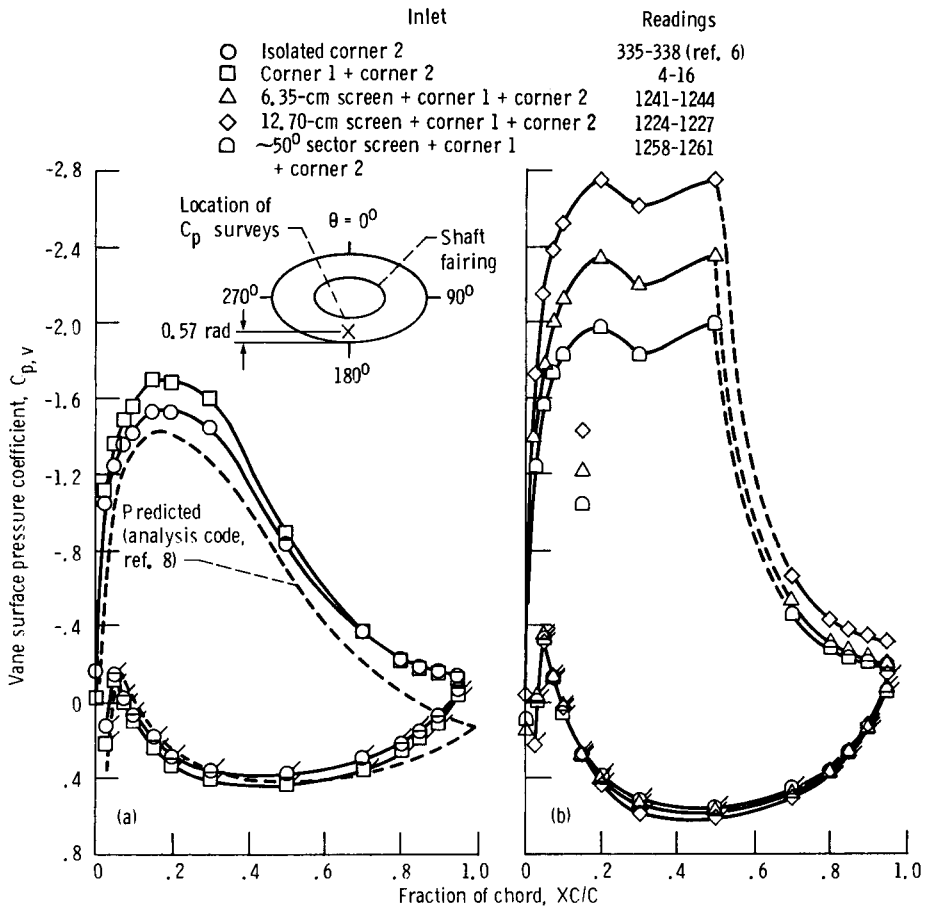

(a) Uniform inflow.
(b) Distorted inflow.

Figure 42.—Vane surface pressure distributions on A4 vanes in corner 2, midspan region of central vanes at 0.57 radius from wall below shaft fairing, with and without inlet distortion. Nominal airflow, 72.2 kg/sec; nominal corner 2 inlet Mach number, 0.25.

With distorted inflow the surface pressure trends for vanes A4 were very similar to those previously discussed for vanes B. This is reasonable since their inlet conditions were about the same, as seen by comparing figures 22 and 23 with 17 and 18.

Summary of Results

For the high-speed corner 1 with exhaust scoop coupled to a diffuser and then to the fan-drive corner 2 with drive-shaft fairing, operating at near-design corner inlet Mach numbers of about 0.4 (to corner 1) and 0.26 (to corner 2), the following principal results were obtained:

1. The total pressure loss coefficient was about 0.16 for corner 1 with a controlled-diffusion vane design (vanes A10) and about 0.12 for corner 2 with either a controlled-diffusion vane design (vanes A4) or a circular-arc vane design (vanes B).

2. The corner 2 loss coefficient depended on whether corner 2 was preceded by corner 1 or not. At the same corner inlet Mach number the loss coefficient was about 25 percent lower with corner 1 upstream. This was due to lower losses near the outer wall of corner 2, which in turn resulted from the lower momentum inflow to this region caused by the near-wall losses of corner 1.

3. Fewer controlled-diffusion vanes (A4) than circular-arc vanes (B) are needed in corner 2—only 22 of vanes A4 in contrast to 28 of vanes B. However, the A4 vane shape is more complex.

4. Expected inlet flow distortions to corner 1 were simulated with radial and circumferential screen sections upstream of that corner. Their effects on the loss coefficients for either corner 1 or 2 were small and differed little with vane design.

National Aeronautics and Space Administration
Lewis Research Center
Cleveland, Ohio 44135, November 24, 1986

Appendix A
Symbols

A	area, cm^2
A_{ex}	area at corner 1 exit, cm^2
ΔA_{ex}	incremental area for rake element at exit, cm^2
A_{in}	area at corner 1 inlet, cm^2
ΔA_{in}	incremental area for rake elements at inlet, cm^2
A_s	cross-sectional area of scoop at corner 1 inlet, cm^2
C	vane chord, cm
$C_{p,V}$	vane surface static pressure coefficient
$C_{p,w}$	wall static pressure coefficient
D	diameter, cm
d_n	nozzle plate diameter, cm
M	Mach number
M_{in}	Mach number at corner inlet
N	station
P_n	standard-day-corrected nozzle total pressure, N/cm^2
P_{room}	room pressure, N/cm^2
P_s	standard-day-corrected static pressure, N/cm^2
$P_{s,in}$	standard-day-corrected static pressure at corner 1 inlet, N/cm^2
$P_{s,V}$	standard-day-corrected vane surface static pressure, N/cm^2
$P_{s,X}$	standard-day-corrected wall static pressure at X location, N/cm^2
P_t	standard-day-corrected total pressure, N/cm^2
$P_{t,ex}$	area-averaged, standard-day-corrected exit total pressure, N/cm^2
$P_{t,i}$	individual rake element standard-day-corrected total pressure, N/cm^2
$P_{t,in}$	area-averaged standard-day-corrected inlet total pressure, N/cm^2
$\Delta P_t/q_{in}$	loss coefficient for corner 2
q_{in}	standard-day-corrected velocity head, N/cm^2
R	gas constant
T_n	standard-day-corrected nozzle total temperature, K
T_t	standard-day-corrected total temperature, K
V	distance from corner 1, cm
W	airflow, kg/sec
X	axial distance from corner 1 inlet, cm
XC/C	fraction of vane chord in chordwise direction
Y	axial distance from corner 1 exit, cm
Z	axial distance from corner 2 exit, cm
γ	ratio of specific heats, 1.40
θ	circumferential location from top dead center (clockwise looking downstream), deg

Appendix B
Equations

Airflow

$$W = 0.04044 \frac{P_n}{T_n} \frac{\pi}{4} d_n^2 \tag{B1}$$

Overall Inlet Total Pressure

$$P_{t,in} = \frac{\sum_{i=1}^{64} \Delta A_{in} P_{t,i}}{A_{in}} \tag{B2}$$

Overall Exit Total Pressure

$$P_{t,ex} = \frac{\sum_{i=1}^{64} \Delta A_{ex} P_{t,i}}{A_{ex}} \tag{B3}$$

Loss Coefficient

$$\frac{P_{t,in} - P_{t,ex}}{q_{in}} = \frac{\Delta P_t}{q_{in}} \tag{B4}$$

Wall Static Pressure Coefficient

$$\frac{P_{t,\text{in}} - P_{s,X}}{q_{\text{in}}} = C_{p,w} \tag{B5}$$

Vane Surface Static Pressure Coefficient

$$\frac{P_{s,v} - P_{s,\text{in}}}{q_{\text{in}}} = C_{p,V} \tag{B6}$$

Mach Number

$$\frac{M}{(1 + 0.2M^2)^3} = \frac{W}{(A - A_s)P_t}\sqrt{\frac{RT_t}{\gamma}} \tag{B7}$$

Velocity Head

$$q_{\text{in}} = 0.7P_{s,\text{in}}M_{\text{in}}^2 \tag{B8}$$

Average Inlet Static Pressure

$$P_{s,\text{in}} = P_{t,\text{in}}\left(1 + \frac{M_{\text{in}}^2}{5}\right)^{-3.5} \tag{B9}$$

References

1. Chamberlin, R.: The Altitude Wind Tunnel (AWT)—A Unique Facility for Propulsion System and Adverse Weather Testing. AIAA Paper 85-0314, Jan. 1985.
2. Blaha, B.; and Shaw, R.J.: The NASA Altitude Wind Tunnel: Its Role in Advanced Icing Research and Development. AIAA Paper 85-0090, Jan. 1985.
3. Abbott, J.M., et al.: Analytical and Physical Modeling Program for the NASA Lewis Research Center's Altitude Wind Tunnel (AWT). AIAA Paper 85-0379, Jan. 1985.
4. Moore, R.D.; Boldman, D.R.; and Shyne, R.J.: Experimental Evaluation of Two Turning Vane Designs for High-Speed Corner of 0.1-Scale Model of NASA Lewis Research Center's Proposed Altitude Wind Tunnel. NASA TP-2570, 1986.
5. Gelder, T.F., et al.: Wind Tunnel Turning Vanes of Modern Design. AIAA Paper 86-0044, Jan. 1986.
6. Boldman, D.R.; Moore, R.D.; and Shyne, R.J.: Experimental Evaluation of Two Turning Vane Designs for Fan Drive Corner of 0.1-Scale Model of NASA Lewis Research Center's Proposed Altitude Wind Tunnel. NASA TP-2646, 1987.
7. Sanz, J. M.: Improved Design of Subcritical and Supercritical Cascades Using Complex Characteristics and Boundary Layer Correction. NASA CR-168166, 1983.
8. McFarland, E.R.: A Rapid Blade-to-Blade Solution for Use in Turbomachinery Design. J. Eng. Gas Turbines Power, vol. 106, no. 2, Apr. 1984, pp. 376–382.
9. Shapiro, A. H.: The Dynamics and Thermodynamics of Compressible Fluid Flow. Vol. 1, Ronald Press Co., 1953, p. 85.
10. Ciepluch, C.C., et al.: Progress in the Lewis Research Center Altitude Wind Tunnel (AWT) Modeling Program. AIAA Paper 86-0757, Mar. 1986.
11. Moore, R.D., et al.: Detailed Flow Surveys of Turning Vanes Designed for a 0.1-Scale Model of NASA Lewis Research Center's Proposed Altitude Wind Tunnel. NASA TP-2680, 1987.

TABLE 1.—OVERALL PERFORMANCE BASED ON RAKE MEASUREMENTS IN CORNERS 1 AND 2 WITH VANES B IN CORNER 2—UNIFORM INFLOW

Parameter	Reading						
	313-316	301-304	297-300	293-296	317-320	309-312	305-308
Airflow, kg/sec	81.19	78.49	75.31	73.04	68.45	56.21	35.38
Mach number:							
Corner 1 inlet	0.447	0.430	0.410	0.396	0.368	0.296	0.182
Diffuser exit	0.285	0.275	0.263	0.255	0.238	0.194	0.121
VIGV:							
Inlet	0.331	0.323	0.307	0.300	0.275	0.218	0.133
Exit	0.355	0.347	0.329	0.322	0.294	0.233	0.142
Total pressure, N/cm^2:							
Corner 1 inlet	10.411	10.398	10.369	10.357	10.322	10.250	10.178
Diffuser exit	10.199	10.195	10.189	10.188	10.180	10.161	10.144
VIGV:							
Inlet	10.131	10.131	10.131	10.131	10.131	10.131	10.131
Exit	10.131	10.128	10.130	10.127	10.131	10.129	10.131
Total pressure loss, N/cm^2:							
Corner 1 with diffuser	0.212	0.203	0.180	0.169	0.142	0.088	0.033
Corner 2	0.067	0.064	0.058	0.056	0.048	0.030	0.013
VIGV	0.001	0.003	0.002	0.004	0.001	0.002	0
Total pressure loss coefficient:							
Corner 1 with diffuser	0.167	0.171	0.165	0.166	0.159	0.149	0.145
Corner 2	0.123	0.124	0.123	0.127	0.125	0.115	0.122
VIGV	0.001	0.004	0.002	0.006	0.001	0.005	0.002
Room pressure, N/cm^2	10.566	10.545	10.503	10.490	10.421	10.317	10.207

TABLE 8.—OVERALL PERFORMANCE BASED ON RAKE MEASUREMENTS IN CORNERS 1 AND 2 WITH VANES A4 IN CORNER 2—UNIFORM INFLOW

Parameter	Reading								
	38–41	22–25	18–21	4–16	5–15	6–17	34–37	30–33	26–29
Airflow, kg/sec	81.16	78.37	75.21	73.10	73.03	72.77	68.61	56.23	35.35
Mach number:									
Corner 1 inlet	0.447	0.430	0.410	0.397	0.396	0.395	0.369	0.296	0.182
Diffuser exit	0.285	0.275	0.263	0.256	0.255	0.254	0.239	0.194	0.121
VIGV:									
Inlet	0.331	0.324	0.306	0.300	0.299	0.300	0.276	0.219	0.133
Exit	0.354	0.346	0.326	0.320	0.333	0.320	0.293	0.233	0.142
Total pressure, N/cm^2:									
Corner 1 inlet	10.406	10.394	10.364	10.355	10.352	10.354	10.319	10.250	10.178
Diffuser exit	10.195	10.193	10.186	10.183	10.183	10.183	10.176	10.161	10.144
VIGV:									
Inlet	10.131	10.131	10.131	10.131	10.131	10.131	10.131	10.131	10.131
Exit	10.127	10.125	10.124	10.127	10.135	10.120	10.129	10.130	10.130
Total pressure loss, N/cm^2:									
Corner 1 with diffuser	0.210	0.201	0.179	0.172	0.168	0.170	0.143	0.089	0.034
Corner 2	0.064	0.061	0.054	0.052	0.052	0.052	0.045	0.029	0.012
VIGV	0.005	0.007	0.008	0.004	−0.004	0.011	0.003	0.002	0.002
Total pressure loss coefficient:									
Corner 1 with diffuser	0.166	0.170	0.165	0.168	0.165	0.168	0.160	0.150	0.147
Corner 2	0.116	0.120	0.115	0.116	0.117	0.118	0.115	0.112	0.117
VIGV	0.006	0.009	0.011	0.007	−0.005	0.017	0.005	0.004	0.012
Room pressure, N/cm^2	10.559	10.545	10.503	10.490	10.483	10.490	10.428	10.317	10.200

TABLE 15.—OVERALL PERFORMANCE BASED ON RAKE MEASUREMENTS IN CORNERS 1 AND 2 WITH VANES B IN CORNER 2—DISTORTED INFLOW

Parameter	12.70-cm tip radial distortion			6.35-cm tip radial distortion			~50° Sector circumferential distortion		
	Reading								
	519–522	515–518	511–514	523–526	527–530	532–536	545–548	541–544	537–540
Airflow, kg/sec	80.11	72.28	35.30	77.07	71.36	35.26	78.72	73.27	35.41
Mach number:									
Corner 1 inlet	0.441	0.388	0.182	0.423	0.387	0.182	0.431	0.397	0.183
Diffuser exit	0.283	0.254	0.121	0.272	0.250	0.121	0.276	0.256	0.121
VIGV:									
Inlet	0.331	0.300	0.132	0.324	0.301	0.132	0.321	0.298	0.130
Exit	0.363	0.330	0.143	0.353	0.326	0.142	0.346	0.328	0.140
Total pressure, N/cm^2:									
Corner 1 inlet	10.386	10.339	10.171	10.376	10.337	10.170	10.397	10.358	10.174
Diffuser exit	10.182	10.176	10.143	10.193	10.184	10.142	10.203	10.194	10.144
VIGV:									
Inlet	10.131	10.131	10.131	10.131	10.131	10.131	10.131	10.131	10.131
Exit	10.163	10.158	10.136	10.150	10.146	10.133	10.131	10.161	10.132
Total pressure loss, N/cm^2:									
Corner 1 with diffuser	0.203	0.163	0.029	0.182	0.153	0.029	0.194	0.164	0.030
Corner 2	0.051	0.044	0.011	0.062	0.052	0.010	0.072	0.062	0.012
VIGV	−0.031	−0.027	−0.004	−0.018	−0.015	−0.001	0.001	−0.030	0
Total pressure loss coefficient:									
Corner 1 with diffuser	0.164	0.166	0.125	0.159	0.157	0.126	0.163	0.160	0.131
Corner 2	0.094	0.101	0.108	0.124	0.122	0.098	0.139	0.139	0.120
VIGV	−0.039	−0.041	−0.027	−0.025	−0.023	−0.009	0.001	−0.044	−0.002
Room pressure, N/cm^2	11.566	11.303	10.345	11.145	10.986	10.276	11.028	10.903	10.269

TABLE 22.—OVERALL PERFORMANCE BASED ON RAKE MEASUREMENTS IN CORNERS 1 AND 2 WITH VANES A4 IN CORNER 2—DISTORTED INFLOW

Parameter	12.70-cm tip radial distortion			6.35-cm tip radial distortion			~50° Sector circumferential distortion		
	Reading								
	1232–1235	1224–1227	1228–1231	1236–1239	1241–1244	1246–1249	1254–1257	1258–1261	1250–1253
Airflow, kg/sec	77.64	72.35	33.34	77.56	72.25	35.26	79.22	73.68	35.41
Mach number:									
Corner 1 inlet	0.425	0.393	0.182	0.425	0.393	0.182	0.434	0.400	0.183
Diffuser exit	0.273	0.254	0.121	0.273	0.254	0.121	0.278	0.258	0.121
VIGV:									
Inlet	0.326	0.303	0.132	0.326	0.304	0.133	0.324	0.301	0.132
Exit	0.353	0.329	0.143	0.352	0.328	0.142	0.353	0.322	0.140
Total pressure, N/cm^2:									
Corner 1 inlet	10.401	10.363	10.177	10.407	10.356	10.175	10.402	10.362	10.176
Diffuser exit	10.195	10.203	10.151	10.206	10.180	10.143	10.205	10.196	10.144
VIGV:									
Inlet	10.131	10.131	10.131	10.131	10.131	10.131	10.131	10.131	10.131
Exit	10.149	10.149	10.137	10.151	10.139	10.134	10.149	10.122	10.129
Total pressure loss, N/cm^2:									
Corner 1 with diffuser	0.206	0.160	0.026	0.201	0.175	0.032	0.197	0.166	0.032
Corner 2	0.064	0.072	0.020	0.075	0.049	0.011	0.073	0.064	0.013
VIGV	−0.018	−0.017	−0.005	−0.020	−0.007	−0.002	−0.017	0.010	0.002
Total pressure loss coefficient:									
Corner 1 with diffuser	0.177	0.159	0.113	0.173	0.174	0.138	0.163	0.160	0.137
Corner 2	0.126	0.163	0.192	0.148	0.112	0.111	0.140	0.142	0.124
VIGV	−0.024	−0.026	−0.032	−0.026	−0.011	−0.013	−0.022	0.014	0.012
Room pressure, N/cm^2	11.455	11.269	10.338	11.131	10.979	10.276	11.028	10.903	10.269

1. Report No.	2. Government Accession No.	3. Recipient's Catalog No.
NASA TP-2681		

4. Title and Subtitle	5. Report Date
Experimental Evaluation of Turning Vane Designs for High-Speed and Coupled Fan-Drive Corners of 0.1-Scale Model of NASA Lewis Research Center's Proposed Altitude Wind Tunnel	May 1987
	6. Performing Organization Code: 505-62-3A

7. Author(s)	8. Performing Organization Report No.
Thomas F. Gelder, Royce D. Moore, Rickey J. Shyne, and Donald R. Boldman	E-3218
	10. Work Unit No.

9. Performing Organization Name and Address	11. Contract or Grant No.
National Aeronautics and Space Administration Lewis Research Center Cleveland, Ohio 44135	13. Type of Report and Period Covered: Technical Paper

12. Sponsoring Agency Name and Address	14. Sponsoring Agency Code
National Aeronautics and Space Administration Washington, D.C. 20546	

15. Supplementary Notes

Data tables are included as a microfiche supplement.

16. Abstract

Two turning vane designs were experimentally evaluated for the fan-drive corner (corner 2) coupled to an upstream diffuser and the high-speed corner (corner 1) of the 0.1-scale model of NASA Lewis Research Center's proposed Altitude Wind Tunnel. For corner 2 both a controlled-diffusion vane design (vane A4) and a circular-arc vane design (vane B) were studied. The corner 2 total pressure loss coefficient was about 0.12 with either vane design. This was about 25 percent less loss than when corner 2 was tested alone. Although the vane A4 design has the advantage of 20 percent fewer vanes than the vane B design, its vane shape is more complex. The effects of simulated inlet flow distortion on the overall losses for corner 1 or 2 were small.

17. Key Words (Suggested by Author(s))	18. Distribution Statement
Wind tunnel turning vanes Cascades Guide vanes Corner flows	Unclassified – unlimited STAR Category 09

19. Security Classif. (of this report)	20. Security Classif. (of this page)	21. No of pages	22. Price*
Unclassified	Unclassified	53	A04

*For sale by the National Technical Information Service, Springfield, Virginia 22161

NASA-Langley, 1987